ANALYSIS AND DESIGN OF A NEW TYPE OF COUPLER AND PHASE SHIFTER BASED ON SEMI-ELLIPTICAL EDGE-COUPLED STRUCTURE

LO YEW CHIONG

DOCTOR OF PHILOSOPHY IN ENGINEERING

LEE KONG CHIAN FACULTY OF ENGINEERING AND SCIENCE
UNIVERSITI TUNKU ABDUL RAHMAN

APRIL 2019

ANALYSIS AND DESIGN OF A NEW TYPE OF COUPLER AND PHASE SHIFTER BASED ON SEMI-ELLIPTICAL EDGE-COUPLED STRUCTURE

By

LO YEW CHIONG

A thesis submitted to the Department of Electrical and Electronics Engineering,
Lee Kong Chian Faculty of Engineering and Science,
Universiti Tunku Abdul Rahman,
in partial fulfillment of the requirements for the degree of
Doctor of Philosophy in Engineering
April 2019

ABSTRACT

ANALYSIS AND DESIGN OF A NEW TYPE OF COUPLER AND PHASE SHIFTER BASED ON SEMI-ELLIPTICAL EDGE-COUPLED STRUCTURE

Lo Yew Chiong

The analysis and design of wideband directional coupler and phase shifter using semi-elliptical edge-coupled structure are presented. The structures consist of two semi-elliptical patches on the top layer and an elliptical defected ground plane on the bottom layer to increase the coupling coefficient and operating bandwidth.

The proposed structure is modelled as a four-port device. Two of the ports are open circuited for the case of phase shifter. The coupling coefficient can be expressed in terms of even and odd mode characteristic impedances. For phase shifter design, the amount of phase shift can be controlled by changing the coupling coefficient. Even and odd mode analysis is carried out and sets of design graphs are formulated to facilitate the design of the directional coupler and phase shifter on substrate with dielectric constant of 2.2 and 3.38. Using the design graphs, the physical dimensions of the directional coupler and the phase shifter can be obtained. An approximate equation is also formulated to estimate the center frequency of the device.

For the case of directional coupler, designs are made with coupling factor, *C* of 10dB ± 1 dB. The reflection coefficient, insertion loss, coupling, and isolation

are first simulated. The designs are fabricated on Rogers RT/Duroid 5880 and RO4003C with different substrate thicknesses and tested using a vector network analyser. The fabricated couplers have a reflection coefficient of better than -18 dB, isolation of better than 22 dB, and insertion loss of less than 1 dB. The proposed coupler design exhibits wideband characteristics, with a bandwidth ratio of 2.4.

For the case of phase shifter, designs are made with coupling factor, C of 5 dB and 6 dB. The reflection coefficient, insertion loss, and differential phase shift are first simulated and the designs are fabricated on Rogers RT/Duroid 5880 and RO4003C with different substrate thicknesses. The bandwidth ratio are approximately 2.4 and 2.1 for coupling of 5 dB and 6 dB, respectively. The phase shifts are $80 \pm 3^{\circ}$ and $97.5 \pm 3.5^{\circ}$ for coupling of 5 dB and 6 dB, respectively. All phase shifters have reflection coefficient better than -10 dB, and insertion loss better than 1 dB throughout the operating frequency range. These results show that the proposed design exhibits wideband characteristics with low phase ripple. The proposed structure is compact, simple, easy to fabricate and low cost.

ACKNOWLEDGEMENTS

I wish to express my greatest gratitude to Prof. Dr. Chung Boon Kuan and Prof. Dr. Lim Eng Hock for their guidance and valuable advices throughout the entire period of this research project. Their trust and endless support, both theoretically and practically, had made this project a memorable one.

Special thanks is extended to UTAR and MMU for providing lab facilities that are needed for simulations and measurements during the research, and also the access to online databases to get all the important literatures.

APPROVAL SHEET

This thesis entitled '**ANALYSIS AND DESIGN OF A NEW TYPE OF COUPLER AND PHASE SHIFTER BASED ON SEMI-ELLIPTICAL EDGE-COUPLED STRUCTURE**' was prepared by LO YEW CHIONG and submitted as partial fulfillment of the requirement for the degree of Doctor of Philosophy in Engineering at Universiti Tunku Abdul Rahman.

Approved by:

____
(Prof. Dr. Chung Boon Kuan) Date:……………..
Supervisor
Department of Electrical and Electronic Engineering
Lee Kong Chian Faculty of Engineering and Science
Universiti Tunku Abdul Rahman

____
(Prof. Dr. Lim Eng Hock) Date:……………..
Co-supervisor
Department of Electrical and Electronic Engineering
Lee Kong Chian Faculty of Engineering and Science
Universiti Tunku Abdul Rahman

LEE KONG CHIAN FACULTY OF ENGINEERING AND SCIENCE

UNIVERSITI TUNKU ABDUL RAHMAN

Date: 10 April 2019

SUBMISSION OF THESIS

It is hereby certified that **LO YEW CHIONG** (ID No: **09UED09158**) has completed this thesis entitled "**ANALYSIS AND DESIGN OF A NEW TYPE OF COUPLER AND PHASE SHIFTER BASED ON SEMI-ELLIPTICAL EDGE-COUPLED STRUCTURE**" under the supervision of Prof. Dr. Chung Boon Kuan (Supervisor) from the Department of Electrical and Electronic Engineering, Lee Kong Chian Faculty of Engineering and Science (LKC FES), and Prof. Dr. Lim Eng Hock (Co-Supervisor) from the Department of Electrical and Electronic Engineering, Lee Kong Chian Faculty of Engineering and Science (LKC FES).

I understand that University will upload softcopy of my thesis in pdf format into UTAR Institutional Repository, which may be made accessible to UTAR community and public.

Yours truly,

____

(LO YEW CHIONG)

DECLARATION

I hereby declare that the thesis is based on my original work except for citations and quotations which have been duly acknowledged. I also declare that it has not been previously and concurrently submitted for any other degree or award at UTAR or other institutions.

(LO YEW CHIONG)

Date: 10 April 2019

TABLE OF CONTENTS

LIST OF TABLES

LIST OF FIGURES

CHAPTER 1

INTRODUCTION

1.1 Introduction to Directional Coupler and Phase Shifter

Directional couplers are passive devices widely used in microwave circuits and subsystems. They allow a certain portion of microwave power to be coupled to the secondary port in a preferred direction. They are used to sample power for amplitude control and used in power splitting and combining. Directional couplers are commonly found in amplifiers, balanced mixers, microwave instruments, modulators and antenna beam-forming networks (Pozar, 2011).

The electrical symbol of directional coupler is shown in Figure 1.1. Power is supplied to port 1 (input port) and the coupled signal appears at port 3 (coupled port). The remaining of the input power will be delivered to port 2 (through port), and ideally, no power is delivered to port 4 (isolated port).

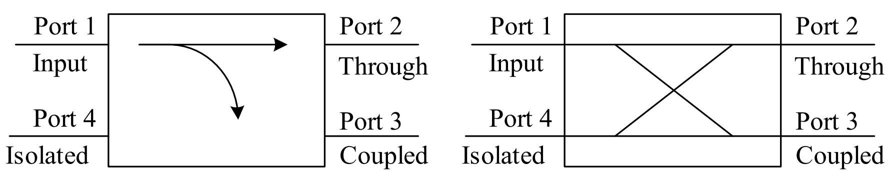

Figure 1.1: The common symbols used for directional couplers.

The general characteristics of a coupler include insertion loss (L), coupling factor (C), isolation (I), and directivity (D), which can be defined by (1.1):

$$L = 10\log\left(P_1 / P_2\right) \tag{1.1a}$$

$$C = 10\log\left(P_1 / P_3\right) \tag{1.1b}$$

$$I = 10\log\left(P_1 / P_4\right) \tag{1.1c}$$

$$D = 10\log\left(P_3 / P_4\right) \tag{1.1d}$$

The earliest form of directional coupler is introduced by Affel of A.T.T., Co in 1922 (Cohn and Levy, 1984), followed by the works by Alford (1941) and Pistolkors and Neumann (1941). Bethe hole coupler is one of the earliest waveguide directional coupler, constructed by coupling one waveguide to another through a single hole between the two waveguides. Subsequently, coupled waveguides with two or more holes (Mumford, 1947; Riblet, 1947), slot (Riblet, 1952) and multi-apertures (Levy, 1968; Levy, 1983) were introduced.

Directional couplers are also implemented on parallel-coupled TEM lines of single section (Oliver, 1954), multiple sections (Barnett et al., 1955; Shimizu and Hones 1958; Cristal and Young, 1965) and tandem configuration (Monteath, 1955). This is the point where even and odd mode analysis is first applied to study the properties of the coupled lines. The exact formulas are derived for coplanar strips (Cohn, 1955) and broadside coupled strips (Cohn, 1960) between two ground planes. Offset broadside coupled strips are later introduced (Shelton, 1966; Shelton and Mosko, 1966) to allow the implementation of multisection broadside coupled structure. Tapered TEM couplers are also introduced (Tresselt, 1966; Kammler, 1969) in order to improve the performance and widen the bandwidth of the coupler. Branch line couplers were introduced (Kyhl, 1947; Lomer and Crompton, 1957) to realize tight coupling between the coupled lines.

Microstrip couplers are gaining attention due to the widespread use of microstrip lines in microwave circuits. Microstrip coupler has the advantage of easy integration with microwave circuit on a single substrate. However, due to inhomogeneous medium, the inequality of the even and odd mode propagation velocities degrades the directivity of the coupler. Compensation techniques are introduced to equalize the modal phase velocities (Podell, 1970; Sheleg and Spielman, 1974; Paolino, 1978; Kajfez, 1978; March, 1982; Dydyk, 1990). In order to achieve tight coupling, narrow gap width between coupled lines is required. The solution is first proposed by Lange (1969) and a few variations of Lange's design were also published (Waugh and LaCombe, 1972; Paolino, 1976; Ho and Moser, 1981).

Phase shifters are passive device used to provide a constant phase shift over a frequency range. They are used in many modern microwave systems such as electronic beam-scanning phased arrays, modulators, microwave measurement and instrumentation systems, and many other industrial applications.

Phase shifters can be considered as a four-port network, which consists of the main line and the reference line, as shown in Figure 1.2. The main line produces a phase shift of Φ, while the reference line produces a phase shift of Φ_r. The differential phase shift, ΔΦ between the two lines is $\Delta\Phi = \Phi - \Phi_r$. One of the basic requirements of phase shifter is to produce a constant ΔΦ over a wide frequency range, at the same time maintain low insertion loss between the input and output ports of the main line.

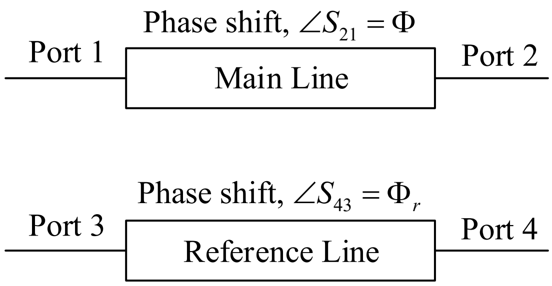

Figure 1.2: Circuit schematic of differential phase shifter.

One of the earliest design of phase shifter is the Schiffman differential phase shifter, constructed based on coupled stripline structure (Schiffman, 1958). It consist of a folded edge-coupled section and another reference transmission line. In order to increase the bandwidth and lower the phase deviation, phase shifters which consist of cascaded multiple sections are later introduced (Schiffman, 1966; Shelton and Mosko, 1966; Schiek and Kohler, 1977). Continuous tapered coupled section is also proposed by Tresset (1968) to increase the performance of broadband phase shifter. In order to equalize the even and odd mode phase velocities when implemented on microstrip technology, Taylor and Prigel (1976) introduced a wiggling technique to design a broadband edge-coupled phase shifter. Ahn and Wolff (2002) introduced an asymmetric ring-hybrid phase shifter which is built without using coupled lines. The phase shift is tuned by the terminating impedances. With the advancement in microwave integrated circuit technology, switched phase shifters are introduced (Eom, 2004; Jin et al., 2006; Cheng et al., 2006) to deliver a wide range of phase shift from a single device. However, this type of phase shifters usually has limited bandwidth and suffers from high insertion loss.

1.2 Coupled Lines Circuits and Their Characteristics

Coupling occurred when two unshielded transmission lines are placed in close proximity due to the interaction of electromagnetic fields. The coupling strength depends on the physical dimensions of the structure, the operating frequency, the mode of propagation, and the direction of propagation of the primary power (Mongia et al., 2007). These lines are referred to as coupled transmission lines, and generally consists of two or more transmission lines in close proximity. Figure 1.3 shows a few examples of coupled transmission lines, which includes edge coupled and broadside coupled transmission line.

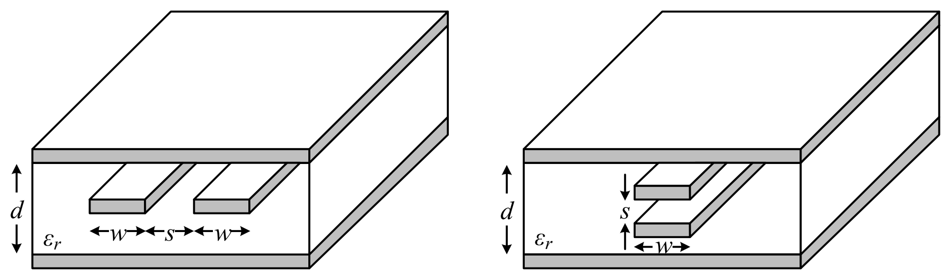

(a) (b)

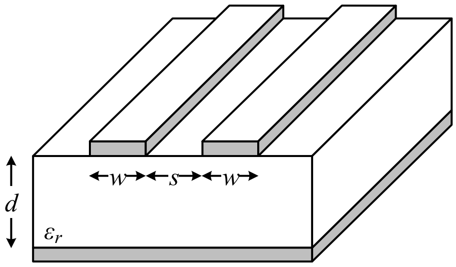

(c)

Figure 1.3: Coupled transmission lines. (a) Coupled stripline (edge coupled), (b) Coupled stripline (broadside coupled), and (c) Coupled microstrip line.

For stripline structure, the coupled transmission lines are assumed to operate in the TEM mode. This assumption is only approximately valid for microstrip line due to nonhomogeneous dielectric media.

The symmetric coupled line structures shown in Figure 1.3 support two modes: the even and odd mode. For TEM propagation, the electrical characteristic can be determined from the capacitances between the lines and the velocity of propagation on the line, as shown in Figure 1.4. The capacitance between the two conductors is represented by C_{12}, and the capacitance between a conductor to ground is represented by C_{11} and C_{22}, respectively.

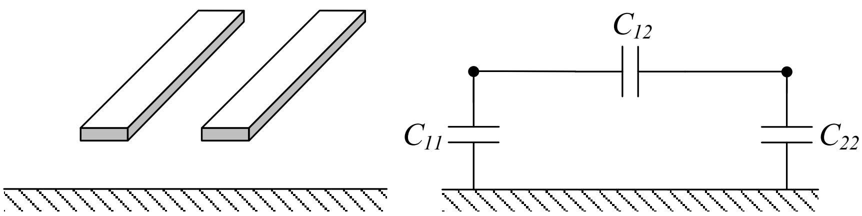

Figure 1.4: Coupled transmission line and the equivalent capacitance network.

The coupled lines are excited with even and odd mode signals. In even mode excitation where the currents in the conductors are in the same direction and equal in amplitude, the electric field has even symmetry at the center of the coupled line. The equivalent circuit is shown in Figure 1.5(a) where C_{12} is effectively an open circuit. The capacitance of either line to ground is $C_e = C_{11} = C_{22}$. The characteristic impedance for the even mode, Z_{0e} is given by:

$$Z_{0e} = \sqrt{\frac{L}{C_e}} = \frac{\sqrt{LC_e}}{C_e} = \frac{1}{v_p C_e} \tag{1.2}$$

where $v_p = c / \sqrt{\varepsilon_r}$ is the phase velocity of propagation.

In the odd mode excitation, currents in the conductors are in the opposite direction and equal in amplitude. The electric field pattern is illustrated in Figure 1.5(b), where the middle of C_{12} can be represented by a virtual ground plane. The capacitance between either conductor and ground can be expressed as $C_o = C_{11} + 2C_{12} = C_{22} + 2C_{12}$. The odd mode characteristic impedance, Z_{0o} is

$$Z_{0o} = \frac{1}{v_p C_o} \tag{1.3}$$

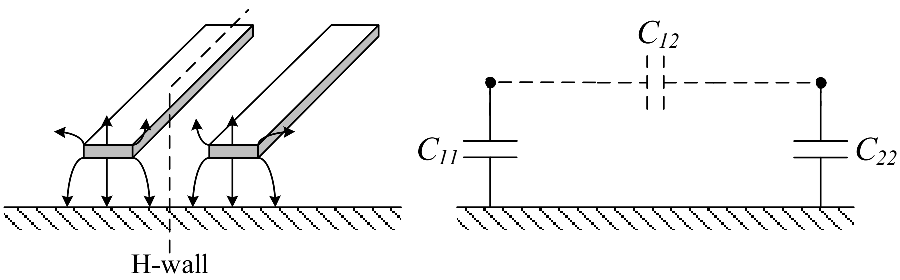

(a)

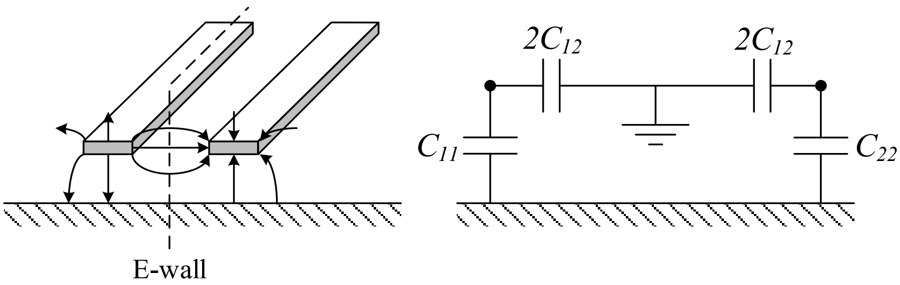

(b)

Figure 1.5: Even and odd mode excitations and their equivalent capacitance networks. (a) Even mode and (b) Odd mode.

For TEM coupled lines, the capacitance per unit length of the line can be determined by techniques such as conformal mapping (Howe, 1974). For quasi-TEM line such as microstrip, the results can be obtained either numerically (Pozar, 2011) or approximated by quasi-static techniques by Mongia et al. (2007). From (Mongia et al., 2007), the even and odd mode phase velocities are given by

$$v_{pe} = \frac{c}{\sqrt{\varepsilon_{re}}} \tag{1.4}$$

$$v_{po} = \frac{c}{\sqrt{\varepsilon_{ro}}} \tag{1.5}$$

where $\varepsilon_{re} = C_e/C_{0e}$ and $\varepsilon_{ro} = C_o/C_{0o}$ are the even and odd mode effective dielectric constant, respectively. C_{0e} and C_{0o} are the free space even and odd mode capacitance of either line. Using (1.4), (1.5) and the expression of ε_{re} and ε_{ro}, the even and odd mode impedances for quasi-TEM line can be expressed as:

$$Z_{0e} = \frac{1}{c\sqrt{C_e C_{0e}}} \tag{1.6}$$

$$Z_{0o} = \frac{1}{c\sqrt{C_o C_{0o}}} \tag{1.7}$$

Applying even and odd mode analysis to a pair of coupled line, it can be shown by Pozar (2011) that if

$$Z_0 = \sqrt{Z_{0e} Z_{0o}} \tag{1.8}$$

then the input impedance, Z_i = Z_0 and all ports are matched. The coupling coefficient, C can be defined as

$$C = \frac{Z_{0e} - Z_{0o}}{Z_{0e} + Z_{0o}} \tag{1.9}$$

From Equation (1.8) and (1.9), the even and odd mode characteristic impedances can be expressed as

$$Z_{0e} = Z_0 \sqrt{\frac{1+C}{1-C}} \tag{1.10}$$

$$Z_{0o} = Z_0 \sqrt{\frac{1-C}{1+C}} \tag{1.11}$$

If the characteristic impedance, Z_0 and the coupling factor, C are specified, the required even and odd mode characteristic impedances can be calculated from (1.10) and (1.11).

1.3 Research Objectives and Motivation

The existing designs of coupled line directional couplers and phase shifters suffer from several limitations, such as limited bandwidth and high phase deviation (phase shifter). The requirement of narrow gap width between coupled lines and the use of multilayer structure increase the difficulty in fabrication. Therefore, the first objective is to explore new structure and configuration for the design of directional coupler and phase shifter. The structure shall be simple, easy to fabricate and exhibit wideband performance. To meet this objective, a new structure consists of semi-elliptical coupled lines and a defected ground plane is proposed.

The second objective is to analyze and design the wideband directional coupler and phase shifter based on the proposed structure. Electromagnetic simulation software is used to optimize the performance of the structure and analyze its characteristics. Using the analysis, sets of design graphs are generated to facilitate the design of the proposed coupler and phase shifter.

The final objective is to fabricate the proposed design and verify their performance experimentally. To meet this objective, a number of couplers and phase shifters are fabricated on materials with different dielectric constants and substrate thicknesses. Their performance parameters are measured using a vector network analyzer and compared to the simulation results.

1.4 Thesis Overview

This thesis consists of 5 chapters. The first chapter gives an introduction on directional coupler and phase shifter, and an overview on the coupled line circuits and their characteristics. The research objectives and motivation are explained in the later part of the same chapter.

Chapter 2 gives a survey on the different types of directional couplers and phase shifters designs documented in the literatures, together with their advantages and disadvantages. The preferred characteristics of directional coupler and phase shifter design are also discussed.

Chapter 3 reports on a novel directional coupler design based on semi-elliptical lines and a defected ground plane. The chapter explains the design technique of the proposed structure and contains design graphs for materials with dielectric constant of 2.2 and 3.38 to facilitate the design of the directional coupler. It also contains the simulation and measurement results of the proposed design.

Chapter 4 focuses on the design of wideband phase shifter based on the similar semi-elliptical lines and a defected ground plane. Design graphs are also included to facilitate the design of the proposed phase shifter. Theoretical analysis is performed and series of simulations are carried out to characterize the phase shifter. The measurement results are also documented in the later part of the chapter.

Chapter 5 gives a summary of the work and reports conclusions. It also gives some recommendations for future work.

CHAPTER 2

DESIGN OF DIRECTIONAL COUPLERS AND PHASE SHIFTERS

2.1 Introduction

In this chapter, several designs of the directional couplers and phase shifters available in the open literature are studied. The design process is briefly summarized and the design is reviewed in terms of design complexity, ease of fabrication, physical sizes, along with their performance such as operating bandwidth and phase stability (for the case of phase shifter). Each design has their advantages and disadvantages, which will be discussed in the following sections.

2.2 Design of Directional Couplers

Edge-coupled directional couplers such as stripline couplers and microstrip couplers are backward-wave couplers. The coupling strength for these types of couplers is determined by the difference between the even and odd mode characteristic impedance. Since it is difficult to obtain large impedance difference, tight coupling is difficult to realize unless extremely small spacing between the coupled lines is used (Pozar, 2001).

Multisection coupled-line coupler is introduced by Wu et al. (2013) to realize tight coupling. The design consists of two coupled-line sections which are symmetry along the horizontal and vertical axes. Due to its symmetry nature, the even and odd analysis method (Reed and Wheeler, 1956; Yeung, 2001) is used to analyse the proposed structure. The coupler is designed by first determining the required coupling coefficient, *k* and the center frequency. The even and odd mode characteristic impedances of the first section, Z_{e1} and Z_{o1}, together with the electrical length of the second section, θ_2, are chosen. The electrical length θ_1 is assumed to be 90º. The corresponding even and odd mode characteristic impedances of the second section, Z_{e2} and Z_{o2}, are then calculated. The electrical parameters are then converted to physical parameters and the design can be optimized using commercial simulation software. The advantages of the design are high directivity and tight coupling coefficient while maintaining reasonable gap width, making the structure practical to realize on a printed circuit board (PCB). However, this design shows limited bandwidth (bandwidth ratio less than 1.6 : 1). Cascaded multiple sections also increases the size and design complexity of the circuit.

When tight coupling is required, branch-line couplers, Lange couplers, and tandem couplers can also be used. Branch-line couplers suffer from limited bandwidth due to the quarter-wave requirement. In order to increase the bandwidth of branch-line coupler, multisection design (Levy and Lind, 1968) is proposed. However, higher number of coupled sections requires higher characteristic impedance, making it difficult to realize on planar structure. Tang et al. (2014) introduced a multisectional branch line coupler to increase the bandwidth and lower the required impedances of the transmission lines. At the same time, defected ground structure (Tang et al., 2006) is used to further increase the characteristic impedances of the transmission line, making it more practical to realize on PCB. Although the proposed design achieved a fractional bandwidth of more than 70%, the size of the coupler increased considerably.

Lange (1969) introduced a design which uses multiple conductors in interdigital configuration to increase the mutual capacitances between the lines and therefore results in higher coupling. In this design, each of the coupled-line is divided into two lines, and arranged in an interdigital manner with alternate conductors connected together at the ends. The mutual capacitance increases considerably as the number of adjacent line increases. Ou (1975) and Presser (1978) presented the design of interdigital coupler with an arbitrary even number of conductor, N. The design equations are written in terms of even and odd mode impedances of a pair of coupled lines. For a given value of characteristic impedance (Z_0), number of conductors (N), and coupling coefficient (k), the design equation can be written as:

$$k = \frac{(N-1)(1-R^2)}{(N-1)(1+R^2)+2R} \tag{2.1}$$

$$Z = \frac{Z_{0o}}{Z_0} = \frac{\sqrt{R\left[(N-1)+R\right]\left[(N-1)R+1\right]}}{(1+R)} \tag{2.2}$$

$$R = \frac{Z_{0o}}{Z_{0e}} \tag{2.3}$$

where Z_{0o} and Z_{0e} are the odd and even mode characteristic impedances.

Equation (2.1) to (2.3) will be used to determine the even and odd mode characteristic impedances, which can be used later to determine the physical parameters of the lines including the dimension and spacing between them. These equations are approximate equations assuming that the mode of propagation along the structure is TEM. An improved version was proposed by Kajfez, et. al (1978) taking into account unequal velocities for even and odd mode. Design graph which consists of different values of *s/h* and *w/h* are computed for substrate with dielectric constant, $\varepsilon_r = 10$ and $N = 4$ conductors to facilitate the design of the directional coupler.

Han et al. (2009) improved the accuracy for the synthesis of a four line interdigitated coupler by defining two new mode admittances. A design graph is generated to represent the relation between the two mode admittances and the physical dimensions of the coupled lines.

Kemp et al. (1983) introduced a tandem Lange coupler configuration to realize tight coupling and extend the bandwidth of typical Lange coupler. The typical coupling is 3 dB and the achievable bandwidth is approximately 3 : 1. Another multisection tandem coupler is proposed by Cho et al. (2005), where the coupler is realized with N sections of parallel-coupled microstrip line. The design does not require high impedance lines. Therefore, narrow line width limitation of Lange couplers is eliminated. The number of coupled sections can be increased to lower the required coupling coefficient, maintaining a practical gap width for PCB implementation. However, the operating bandwidth is limited to 3.6 – 5.5 GHz (bandwidth ratio of 1.5 : 1).

Tang et al. (2013) presented a modified tandem coupler with short circuited coupled lines and asymmetrical feeding. Compared to the couplers presented by Hindin and Rosenzweig (1968), Kemp et al. (1983) and Cho et al.

(2005), the proposed design achieve broadband characteristic without multisection coupled lines. Detailed design formulas are provided by the authors. The design starts by specifying the required fractional bandwidth determined from the return loss and find the corresponding odd mode impedance. The even mode impedance and the characteristic impedance of the transmission line are calculated. The physical dimensions of the coupler are then converted from the calculated parameters. A bandwidth of more than 70% is reported. All the Lange couplers and tandem couplers reviewed in this report require extra bonding wires, narrow strips width and small spacing between the coupled lines, making them inconvenient to manufacture on a printed circuit board.

The problem of narrow spacing can be alleviated by using broadside coupled structure. Chang, et al. (2008) introduced a broadside coupler using coplanar waveguide. The design uses a single layer substrate with air above and below the structure. The direct output port and the coupled ports are placed on the same side of the coupler, on the top and bottom layer, respectively. The ground planes are connected to each other using via holes to avoid undesired waveguide modes (Chiu et al., 2006). Even and odd mode analysis is performed on the coupled region. By using (1.8), (1.10) and (1.11), the even and odd mode characteristic impedances, Z_{0e} and Z_{0o} are calculated for a desired coupling value, C. The author performed analysis using HFSS to determine the relationship between Z_{0e}, Z_{0o}, and C with the spacing, s, between the coupled line and the ground plane for different width, W of the coupled line. Based on the calculated values of Z_{0o} and Z_{0e}, s and W are obtained graphically for $\varepsilon_r = 4.4$ and substrate thickness, $d = 0.35$mm. The proposed coupler offers tight coupling and good performance in terms of return loss. However, the high coupling variation limits the coupler's bandwidth to approximately 2 : 1 (with a coupling variation of ± 1dB).

Tanaka et al. (1988) presented a broadside coupler which consists of two layers of substrate. Two microstrip lines that are located on the top and bottom layers are coupled through a rectangular slots in the ground plane located at the middle layer. The lengths of the slot and the coupling strips are both equal to a quarter wavelength at center frequency. Equation (1.10) and (1.11) are used to determine the even and odd mode characteristic impedances, Z_{0e} and Z_{0o}. Design graphs are provided to determine the physical dimensions of the coupler for dielectric constant, $\varepsilon_r = 2.5$.

Abbosh and Bialkowski (2007) presented another broadside coupler constructed from two elliptically shaped microstrip lines on the top and bottom layers, coupled through an elliptical slot in the middle layer. The design concept is similar to Tanaka et al. (1988), but elliptical patch (slot) are used instead of rectangular patch (slot) to increase the operating bandwidth. The initial design stage approximates the elliptical patch and slot to their rectangular equivalent. By setting the required coupling coefficient, C, the even and odd mode characteristic impedances, Z_{0e} and Z_{0o} are calculated. The widths of the rectangular patch and slot are obtained by solving the equations given by Wong et al. (1991) and Hillberg (1969), while the length is calculated from Pozar (2005). The dimensions of the rectangular patch and slots are then converted into the dimensions of their elliptical counterparts using the approximation given by the author:

$$D_1 = \left(\sqrt{l_p^2 + w_p^2} + l_p\right)/2 \tag{2.4}$$

$$D_2 \approx 1.273\left(w_p \times l_p\right)/D_1 \tag{2.5}$$

$$D_3 \approx 1.273\left(w_s \times l_p\right)/D_1 \tag{2.6}$$

where D_1 and D_2 are the widths of the elliptical patch and the elliptical slot, respectively. D_3 is the length for both the elliptical patch and slot. The widths of the rectangular patch and slot are w_p and w_s, respectively, while l_p is the length for both the rectangular patch and slot.

The design will then be optimized using HFSS. Designs with coupling values of 3 dB, 6 dB and 10 dB are simulated and measured. The results show that the couplers exhibit wideband characteristics. However, these circuits (Tanaka et al., 1988; Abbosh and Bialkowski, 2007) require multilayer substrates which are inconvenient to manufacture. Multilayer design is also sensitive to alignment error. Misalignment of the microstrip layers forming this type of coupler may lead to high insertion loss, as demonstrated by Abbosh and Bialkowski (2007).

2.3 Design of Phase Shifters

The use of edge-coupled quarter-wave section requires extremely tight coupling in order to achieve the desired performance. This results in narrow gap-width which is very difficult to fabricate and reproduce. Some researchers

(Meschanov et al., 1994; Quirarte and Starski, 1993) have proposed the use of cascaded multiple coupled sections.

The design proposed by Meschanov et al. (1994) consists of a cascade of coupled line pairs with different lengths and coupling coefficients, and each element is connected at one end. Each of the coupling sections contributes to the phase shift performance. In the proposed design, section with maximum length has the lowest coupling coefficient while the section with minimum length has the highest coupling coefficient. In order to obtain the physical parameters of the design, the author solved the parameter optimization problem given by

$$\min_{v} \max_{\theta \in [\theta_1, \theta_2]} \left| \phi\left(v, \theta - \phi_0\right) \right| \tag{2.7}$$

where v consists of parameters such as normalized lengths and coupling coefficients of coupled sections, and the normalized length of reference line. The optimization problem was solved using one of the numerical methods of nonlinear programming (Gill et al., 1981) and Mitchel's standard maximum smoothing procedure (Demyanov and Malozemov, 1972). The proposed phase shifter was optimized for two and four coupled sections. The four-coupled sections design offers good phase ripple over a wide bandwidth, but the requirement of a large number of coupled-line pairs increases the size of the design.

Quirarte and Starski (1993) introduced a double parallel Schiffman phase shifter configuration where each section in the double Schiffman phase shifter is connected in parallel. The parallel sections have the same length. Each section can be designed to have a higher input impedance, thus achieving an equivalent phase response as the standard Schiffman phase shifter at weaker coupling coefficient. The design is easier to realize compared to the standard Schiffman phase shifter. However, high phase variations near the lower and upper frequency band indicate a narrowband performance.

Chai et al. (2003) introduced a Teflon-based asymmetric 45º Schiffman phase shifter for 2.3 GHz applications. The proposed design comprises either 1 or 2 coupling sections for both the phase shifter and the reference guide. The accuracy of the phase shift is strongly affected by the coupling lengths, especially the coupling length of the reference guide. The advantage of the proposed design is a smaller circuit size compared to the conventional Schiffman phase shifter. Higher phase stability is achieved with two coupling sections design, but the useful frequency range is limited to just few hundreds MHz.

Minnaar et al. (1997) proposed a multilayer design where a 5 mil substrate consisting the coupler is sandwiched in between two 32-mil substrates. For a certain required phase shift ϕ, the coupling coefficient, C and the coupling ripple ΔC (which relates to the phase ripple $\Delta\phi$) are given as:

$$C = 20\log\left[\sin\phi\right] \text{ dB} \tag{2.8}$$

$$\Delta C = 20\log\left[\frac{\sin\left(\phi+\Delta\phi\right)}{\sin\phi}\right] \text{ dB} \tag{2.9}$$

The design uses tapered coupled method consisting of a nine-section structure and several impedance transformers. The design parameters and line dimensions were obtained from Cristal and Young (1965), Tresselt (1966) and Shelton (1966). The proposed design operates over a bandwidth of 1 – 17 GHz. However, the insertion loss is higher than 3 dB and phase ripple is ±5º for the 45º phase shifter.

Another multisection coupled line design was introduced by Pu et al. (2015). The design consists of a reference line and three delay lines to produce differential phase shifts of 45º, 90º, and 135º. The reference line is a multisection coupled line with uniform gap width and one end open circuited. On the other hand, the delay line consists of 50 Ω transmission line and open-circuited multisection coupled line, also with a uniform gap width. The coupled sections have equal lengths of $\lambda/16$ but slightly different coupling coefficients, C_n. The designs are fabricated on Rogers RT/Duroid 5870 with dielectric thickness of 1.575mm. The phase deviation are 45º ± 2º, 90º ± 3º, and 135º ± 5º. However, the bandwidth is limited to 1.58 : 1.

Compensation technique was introduced by Gruszczynski et al. (2006) to improve the performance of the Schiffman phase shifter (Schiffman, 1958). The authors use capacitive compensation technique to improve the return loss and insertion loss caused by the parasitic reactance at the transition region between the coupled lines and the signal lines. Circuit analysis made based on the method given by Reed and Wheeler (1956) shows that the transition effects strongly deteriorate the return loss. EM analyses are later performed in order to find the optimum values and locations of the compensating capacitors. A total of six compensating capacitors have been added at various locations in the presented design and the return loss is improved by more than 10 dB. However, the technique is unable to increase the bandwidth of the phase shifter. The usable bandwidth of the compensated 90º Schiffman phase shifter is 2 to 3 GHz .

Guo et al. (2006) presented an improved version of Schiffman phase shifter with a modified ground plane under the coupled lines. The even and odd mode characteristic impedances can be increased by introducing a rectangular slot on the ground plane. The even mode impedance increases at a much faster rate compared to the odd mode impedance. At the same time, a floating rectangular conductor is placed under the coupled lines to decrease the odd mode impedance. The authors vary the width of the ground opening and the floating rectangular patch and track the even and odd mode impedance until they match the required impedance given by Quirarte and Starski (1991). The proposed method allows wider separation between coupled lines, making it more practical to be realized on a printed circuit board. The achieved bandwidth is about 2 : 1.

Abbosh (2007) introduced a three-layer broadside coupled phase shifter. It comprises two elliptical microstrip patches on the top and bottom layers, and a ground plane with elliptical slot in the middle layer. The phase shifter is modeled as a four-port device with two of the ports open circuited. A theoretical model is developed based on the analysis for the coupled microstrip lines by Riblet (1947), Oliver (1954), Jones and Bolljahn (1956), and Reed and Wheeler (1956). The return loss, S_{11} and insertion loss, S_{21} are expressed as:

$$S_{11} = \frac{1 - C^2\left(1 + \sin^2\left(\beta l\right)\right)}{\left[\sqrt{1-C^2}\cos\left(\beta l\right) + j\sin\left(\beta l\right)\right]^2} \tag{2.10}$$

$$S_{21} = \frac{j2C\sqrt{1-C^2}\sin(\beta l)}{\left[\sqrt{1-C^2}\cos(\beta l) + j\sin(\beta l)\right]^2} \tag{2.11}$$

where C is the coupling coefficient, β is the effective phase constant and l is the physical length of the coupled structure. The differential phase shift, $\Delta\Phi$ is obtained by comparing the phase shift of the structure with that of a reference transmission line:

$$\Delta\Phi = 90° - 2\tan^{-1}\left[\frac{\sin(\beta l)}{\sqrt{1-C^2}\cos(\beta l)}\right] + \beta_m l_m \tag{2.12}$$

where β_m and l_m are the phase constant and the physical length of the reference line, respectively. The phase shift is a function of coupling factor. For a certain coupling factor, the even and odd mode characteristic impedance, Z_{0e} and Z_{0o} are calculated. The physical dimensions are calculated using the equations given by the same author (Abbosh and Bialkowski, 2007). The phase shifter shows a broadband performance from 3.3 to 10.6 GHz. However, the useful phase shift range is limited to 25º - 48º with a phase deviation of ±3º.

A modified design based on the work of Abbosh (2007) and Marynowski et al. (2008) was introduced by Sorn et al. (2012) to provide 90º phase shift. The design consists of the broadside elliptical coupled section similar to Abbosh (2007). However, the transmission and coupled ports are terminated with reactive loads (rectangular patches) instead of open circuited. These elliptical and rectangular patches on the top and bottom layers are coupled through the slots cut in the ground plane located at the middle layer of the structure. The differential phase shift is given by:

$$\Delta\Phi = K\theta - 90° - 2\tan^{-1}\left(\frac{\tan\theta}{\sqrt{1-k_c^2}}\right) + 2\tan^{-1}\left(\frac{\cot\theta}{\sqrt{1-k_l^2}}\right) \qquad (2.13)$$

where k_c and k_l are the coupling coefficients of the coupled section and the reactive loads, respectively. The value of K is estimated to be 4 at the center frequency where θ_0 = 90º. The value k_c is determined based on the work of Abbosh (2007), and k_l is determined based on the allowable phase deviation from (2.13). The proposed design extends the phase shift proposed by Abbosh (2007) without cascading multiple phase shifters. However, this design offers lower bandwidth (3 to 7 GHz) with a phase deviation of ±4º for a 90º phase shifter.

Zheng et al. (2010) introduced a broadband phase shifter using a T shaped open stub loaded $\lambda/2$ transmission line. In the proposed design, an open stub with characteristic impedance of Z_s is located at the middle of a half wavelength transmission line with characteristic impedance of Z_l. The value of Z_s and Z_l is a function of the required differential phase shift which can be determined theoretically. The T shaped stub consists of an open stub terminated by triangular patches, each having a length of a quarter wavelength. Further optimization are carried out using EM simulation software. The proposed design achieves a bandwidth of 2.39 : 1, but exhibits high phase deviation of ±6.4º for a 90º phase shifter.

A broadband phase shifter constructed using a pair of three-section radial line stubs was introduced by Yeung et al. (2012). The phase shifter consists of eight microstrip line section connected in series, which includes the feed line and the impedance matching sections. A pair of radial stubs which provides the phase shift function is connected in parallel at the middle of the main line. The pair of multisection radial stubs is able to provide wider bandwidth compared to only a single radial stub. The circuit is optimized using a mutiobjective genetic algorithm (Deb et al., 2002; Yeung et al., 2012). The objectives are to minimize the insertion loss, maximize the return loss, and optimize the phase response. The phase shifter shows a wideband performance from 2.02 GHz to 6.18 GHz with a phase deviation of 90º ± 5º. The insertion loss is better than 1.2 dB. However, the circuit occupied a large area due to the pair of multisection radial stub.

Yeung et al. (2013) later proposed a modified version of wideband phase shifter consisting of a multisection radial stub and ladder networks. Two ladder networks are added to the side of the open stub and act as impedance matching network to the input and output ports (An et al., 1994). The use of only one multisection radial stub reduces the circuit size compared to the earlier design (Yeung et al. 2012). The operating frequency range is 3.1 – 10.6 GHz. Although the design offers acceptable performance in terms of return loss and insertion loss, a phase deviation as high as ±9º is observed.

Liu et al. (2014) proposed a 90º phase shifter which is designed using a two-section stepped impedance open stub and a coupled-line pair to improve the bandwidth of Zheng et al. (2010). The electrical lengths of the two-section open stub and the coupled-line are $\theta = \lambda/2$ at the center frequency. The characteristic impedances of the two sections of the open stub, Z_{s1} and Z_{s2}, and the even and odd mode impedances of the coupled line, Z_e and Z_o, can be determined from theoretical analysis. The design exhibits wideband characteristics with bandwidth ratio of 3.2 : 1 and a phase deviation of ±5º.

Another open-ended parallel coupled-line structure was introduced by Guo et al. (2016), where two L-shaped networks were added to the structure to improve the return loss performance. The differential phase shift is controlled by the coupling coefficient, which can be calculated from (Abbosh, 2007). The even and odd mode impedance for the parallel coupled-line can then be determined using (1.10) and (1.11). The characteristic impedance of the L-network is determined using the design graph provided by the author. The structure also consists of a ground slot and a patch at the ground layer to realize the required even and odd impedances in the coupled lines. The dimensions of the slot and patch are determined by the method given by Abbosh (2009). The proposed structure offers an operating bandwidth of 1 – 3 GHz with a phase deviation of ±8º. The circuit also have a larger size due to the use of the short ended stub.

2.4 The Preferred Characteristics of Directional Coupler and Phase Shifter Design

The directional coupler and phase shifter shall exhibit wideband characteristic, with high return loss and low insertion loss across the operating frequency range. Small coupling variation and low phase ripple are desired for the coupler and phase shifter, respectively.

The design should be simple, compact and easy to fabricate. In order to achieve these objectives, a single coupled section structure which does not require more than one layer of substrate is preferred. The design shall be able to achieve tight coupling without the need of narrow gap width and thin strip width, making it practical to realize on a printed circuit board.

In addition, a simple design procedure is preferred so that the circuit can be designed easily. These include the characterization of the electrical parameters and the computation of the physical dimensions of the device.

In order to meet these preferred characteristics, an edge-coupled structure which uses only two conducting layers is introduced in this thesis. The structure consists of two semi-elliptical lines on the top layer and an elliptical defected ground plane on the bottom layer to increase the coupling coefficient and operating bandwidth. Design graphs which relate the even and odd mode characteristic impedances to the physical dimensions are also formulated to facilitate the design of the proposed directional coupler and phase shifter.

CHAPTER 3

DESIGN AND ANALYSIS OF WIDEBAND DIRECTIONAL COUPLER

3.1 Introduction

In this chapter, a semi-elliptical edge-coupled structure with a defected ground is proposed. Defected ground structure has been used in various microwave circuits to increase the coupling coefficient and to reduce the size of microwave circuits (Weng et al., 2008; Velazquez-Ahumada et al., 2004; Wang and Song, 2016). As a result, larger spacing between the coupled lines can be used compared to the conventional microstrip coupler, making it practical to realize on a PCB. In order to facilitate the coupler design, analysis of even and odd mode characteristic impedances are performed and sets of design graphs are formulated. These design graphs can be used to determine the physical dimensions of the proposed coupler and will also be useful for the design of other microstrip devices such as a phase shifter (Lo and Chung, 2012), which requires tight coupling and wide bandwidth. The validity of the proposed design is verified experimentally.

3.2 Configuration and Analysis

The proposed directional coupler is a two-layer device. One layer consists of an edge-coupled semi-elliptical structure and the other layer consists of an elliptical defected ground plane, as shown in Figure 3.1. The use of elliptical structure provides an almost constant coupling coefficient over a wide bandwidth.

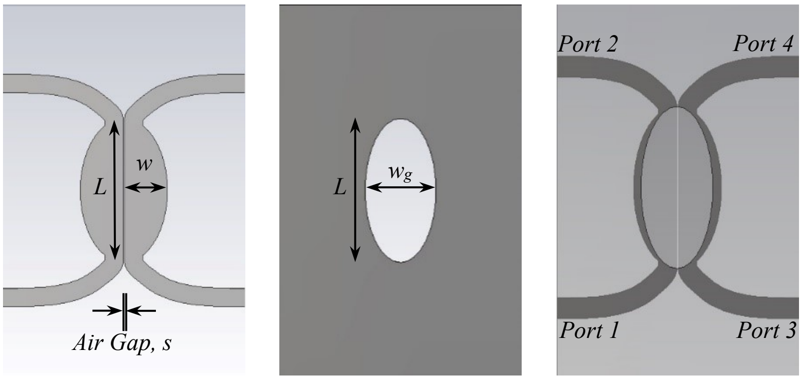

(a) (b) (c)

Figure 3.1: Configuration of the proposed directional coupler. (a) Top layer, (b) Bottom layer, and (c) Overlay of the two layers.

The directional coupler is a four-port device, having a symmetry with respect to the vertical plane. Curved microstrip lines are used to make connections to the subminiature A (SMA) connectors.

The length and width of the top semi-elliptical patch are denoted as L and w, respectively. The defected ground plane has the same length, L as the top patch, and a width denoted by w_g. The axial ratio of the top elliptical patch is defined as $2w/L$ (denoted as *"ratio"*), whereas the axial ratio of the bottom defected ground is defined as w_g/L (also denoted as *"gratio"*).

Even and odd mode analysis has been performed to characterize the circuit. In this case, port 1 and port 3 are excited with even and odd mode signals. The analysis is carried out using the CST Microwave Studio. The simulation setup is shown in Figure 3.2 and Figure 3.3. Discrete face ports are used in order to reduce the ports' inductance. In order to improve the accuracy of simulation results, local mesh settings are used on the semi-elliptical patches and the air gap. The edge refinement factor is increased to 10 and the air gap is set to contain 4 mesh cells. Mix mode converter is used in order to excite port 1 and port 3 with even and odd mode signals, as shown in Figure 3.3 (a) and Figure 3.3 (b). A voltage probe is placed at port 1 and a current probe is placed at port 2 to monitor the voltage and current, respectively. A multi-sequence parameter sweep is set up with varying *s/d* (11 samples) and *w/d* (8 samples) for each *ratio* and *gratio* configuration. A total of 88 points are obtained in order generate a design graph. The analysis follows the procedures given in Appendix A (Edwards and Steer, 2000).

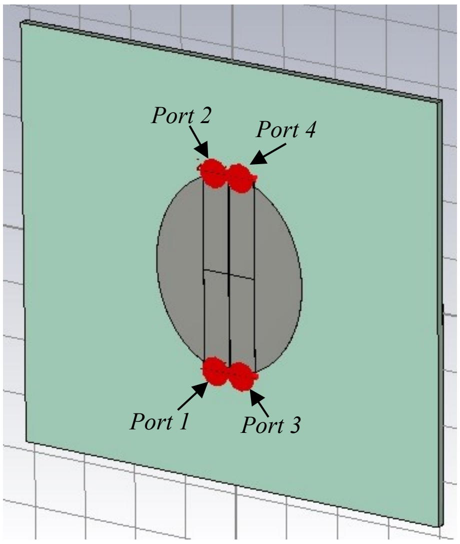

Figure 3.2: Simulation setup in the CST Microwave Studio.

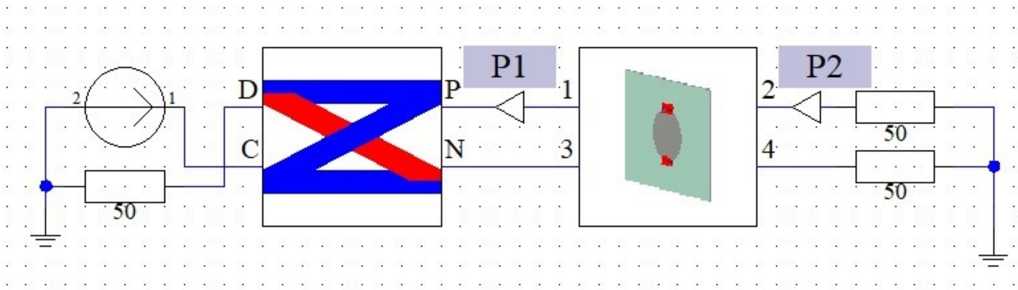

(a)

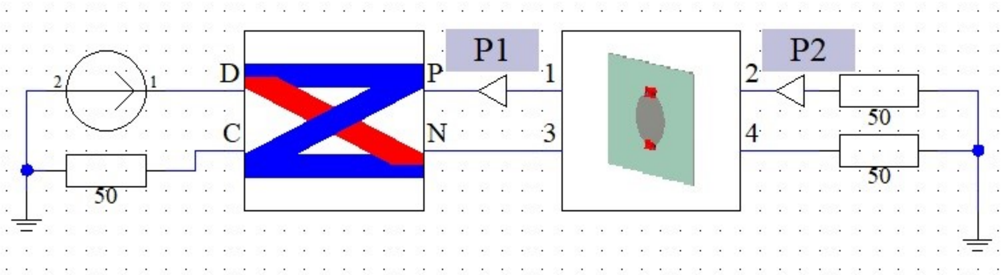

(b)

Figure 3.3: Even and odd mode analysis. (a) Even mode, and (b) Odd mode.

As shown in Figure 3.4, the electric field distributes itself in both the dielectric and in the air for even and odd mode excitations. For a certain desired coupling factor, the even (Z_{0e}) and odd (Z_{0o}) mode characteristic impedances can be calculated as follows:

$$Z_{0e} = Z_0 \sqrt{\frac{1+10^{-C/20}}{1-10^{-C/20}}} \tag{3.1}$$

$$Z_{0o} = Z_0 \sqrt{\frac{1-10^{-C/20}}{1+10^{-C/20}}} \tag{3.2}$$

where Z_0 is the characteristic impedance of the coupler and C is the coupling factor in dB.

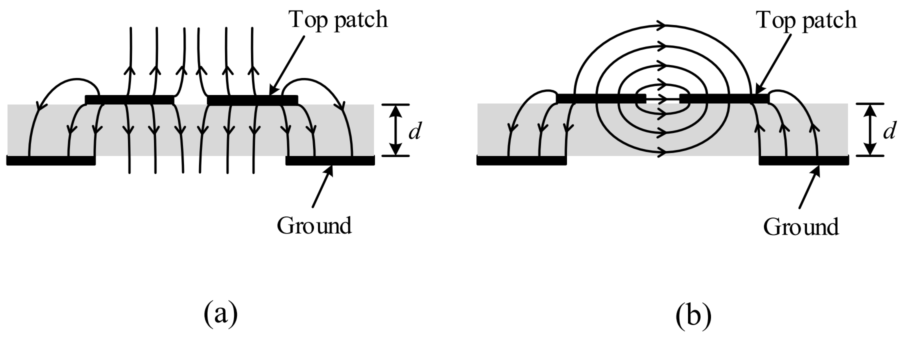

Figure 3.4: Electric field for (a) Even mode excitation, (b) Odd mode excitation.

Assuming that Z_0 = 50 Ω and the desired coupling factor C is 10 dB ± 1 dB, the values of Z_{0e} and Z_{0o} can be calculated using (3.1) and (3.2) as 72.45 Ω and 34.5 Ω, respectively.

3.3 Design of Wideband Directional Coupler

Even and odd mode analysis is performed using CST Microwave Studio. Sets of design graphs are generated by varying the ratio *s/d* and *w/d* for various defected ground axial ratios (gratio) and top patch axial ratios (ratio) to facilitate the design of the directional coupler, as shown in Figure 3.5 and Figure 3.6 for dielectric constant, ε_r = 2.2 and 3.38, respectively. The design graphs enable one to design the coupler directly without the need of EM simulation software. Using these design graphs, the physical dimensions of the coupler can be determined and the circuit can be fabricated.

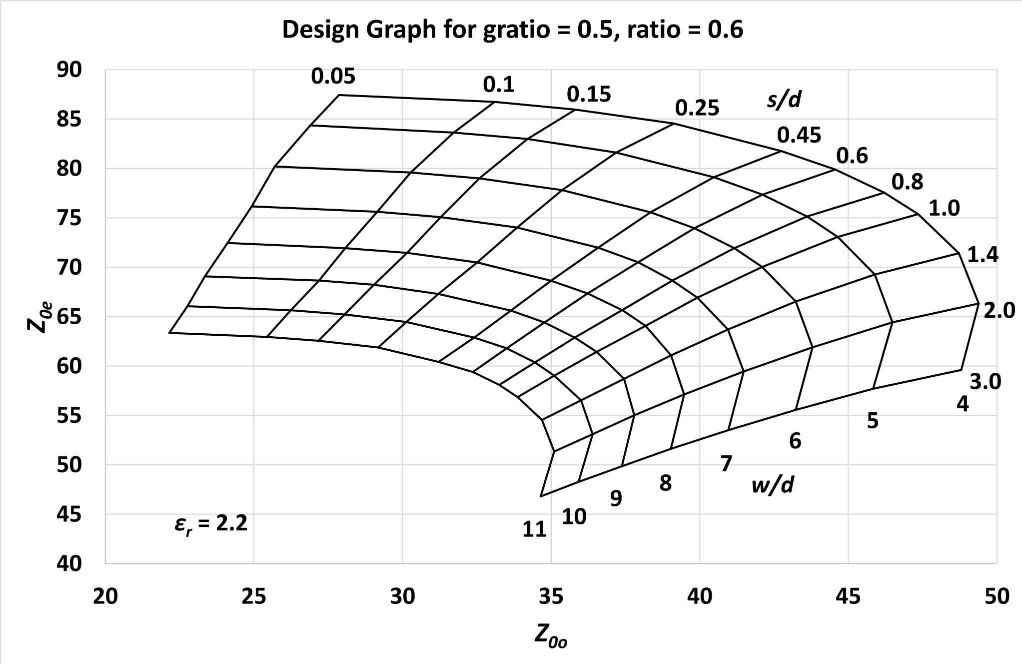
Design Graph for gratio = 0.5, ratio = 0.6
s/d
0.05
0.1
0.15
0.25
0.45
0.6
0.8
1.0
1.4
2.0
3.0
4
5
6
7
8
9
10
11
w/d
ε_r = 2.2
Z_{0e}
Z_{0o}
90
85
80
75
70
65
60
55
50
45
40
20
25
30
35
40
45
50

(a)

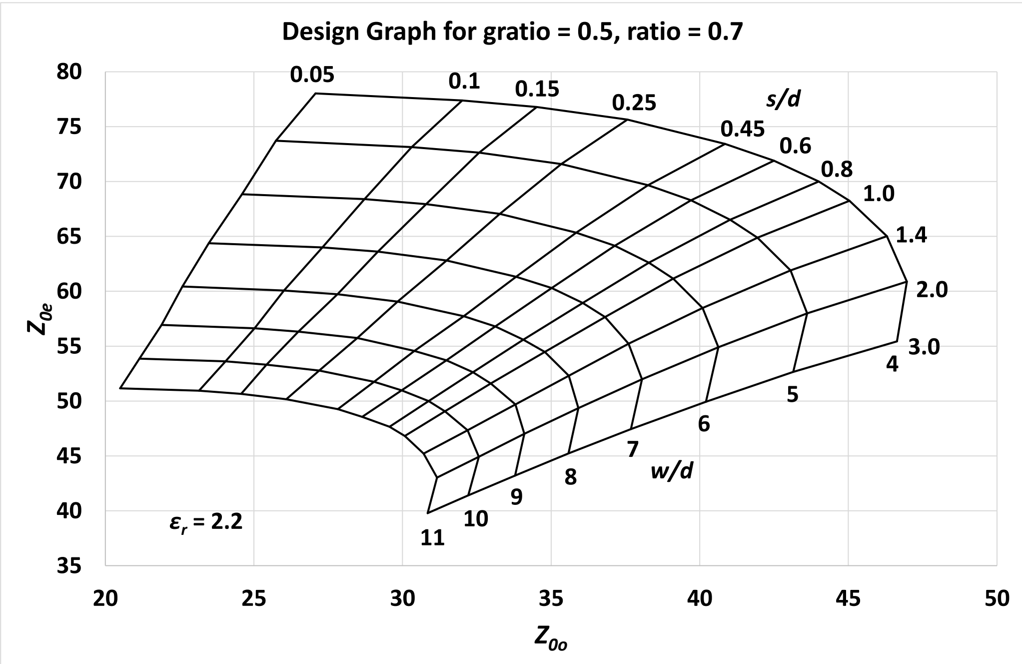
Design Graph for gratio = 0.5, ratio = 0.7
s/d
0.05
0.1
0.15
0.25
0.45
0.6
0.8
1.0
1.4
2.0
3.0
4
5
6
7
8
9
10
11
w/d
ε_r = 2.2
Z_{0e}
Z_{0o}
80
75
70
65
60
55
50
45
40
35
20
25
30
35
40
45
50

(b)

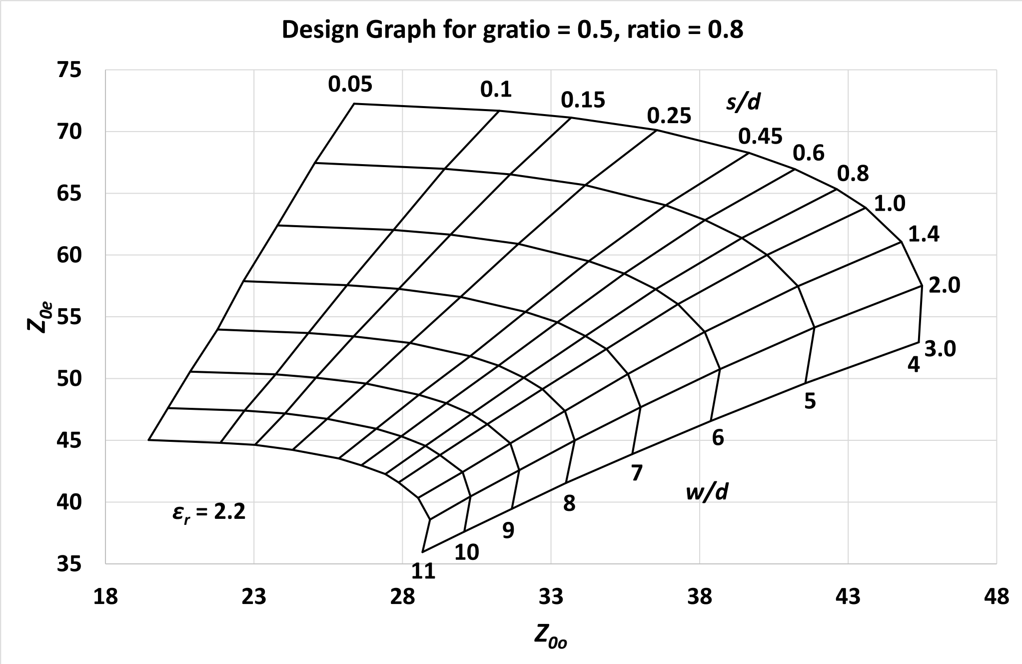

Design Graph for gratio = 0.5, ratio = 0.8
0.05
0.1
0.15
0.25
s/d
0.45
0.6
0.8
1.0
1.4
2.0
3.0
4
5
6
7
w/d
8
9
10
11
εr = 2.2
Z0e
Z0o
75
70
65
60
55
50
45
40
35
18
23
28
33
38
43
48

(c)

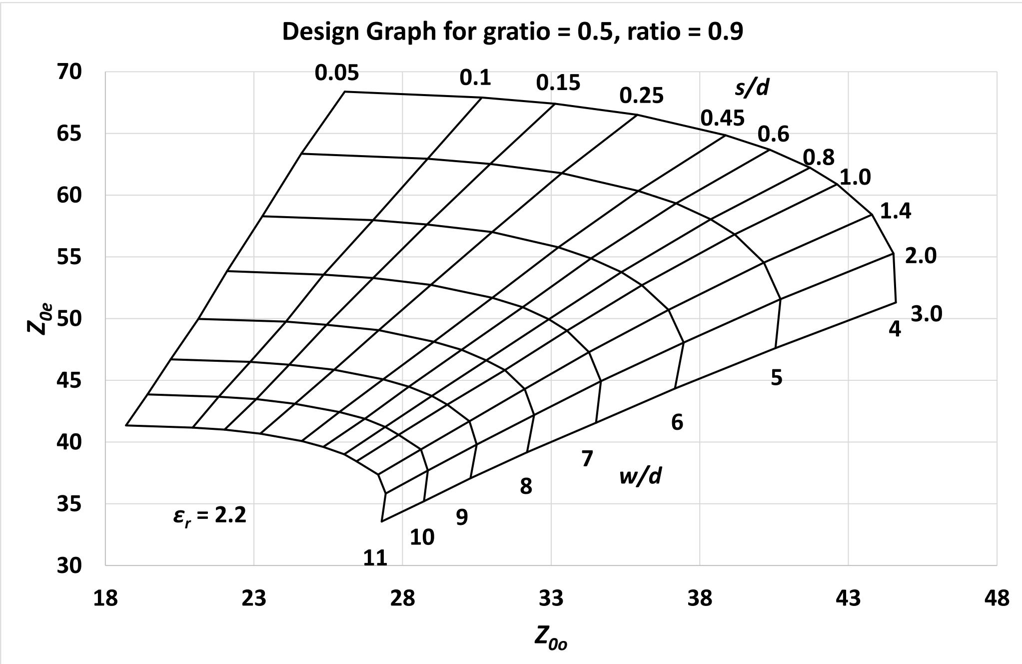

Design Graph for gratio = 0.5, ratio = 0.9
0.05
0.1
0.15
0.25
s/d
0.45
0.6
0.8
1.0
1.4
2.0
3.0
4
5
6
7
w/d
8
9
10
11
εr = 2.2
Z0e
Z0o
70
65
60
55
50
45
40
35
30
18
23
28
33
38
43
48

(d)

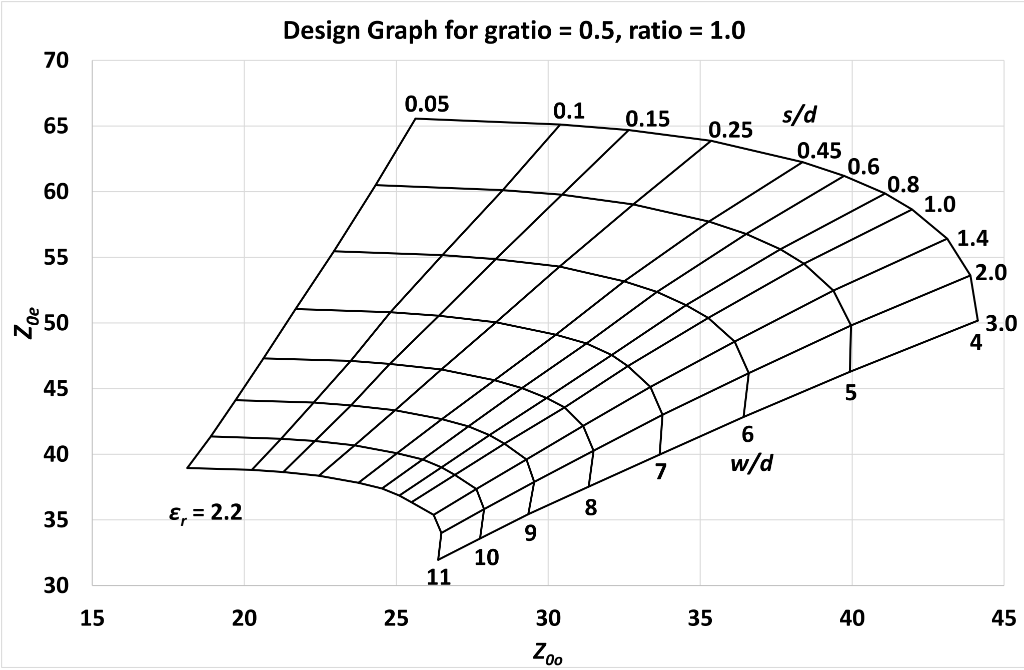

Design Graph for gratio = 0.5, ratio = 1.0
70
65
60
55
50
45
40
35
30
15
20
25
30
35
40
45
Z_{0e}
Z_{0o}
0.05
0.1
0.15
0.25
s/d
0.45
0.6
0.8
1.0
1.4
2.0
3.0
4
5
6
w/d
7
8
9
10
11
ε_r = 2.2

(e)

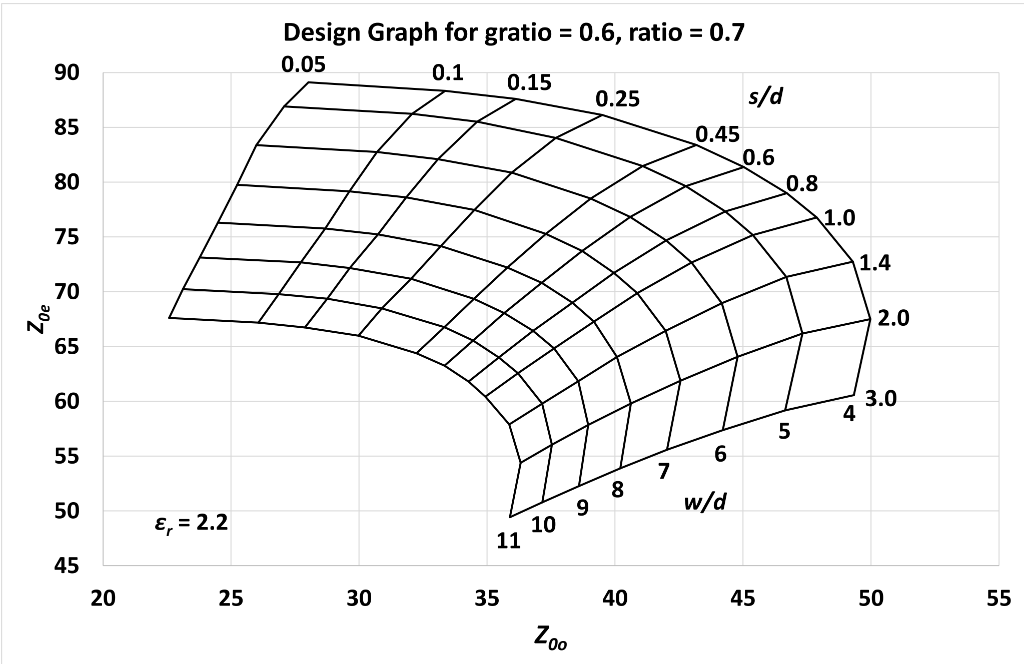

Design Graph for gratio = 0.6, ratio = 0.7
90
85
80
75
70
65
60
55
50
45
20
25
30
35
40
45
50
55
Z_{0e}
Z_{0o}
0.05
0.1
0.15
0.25
s/d
0.45
0.6
0.8
1.0
1.4
2.0
3.0
4
5
6
7
8
9
w/d
10
11
ε_r = 2.2

(f)

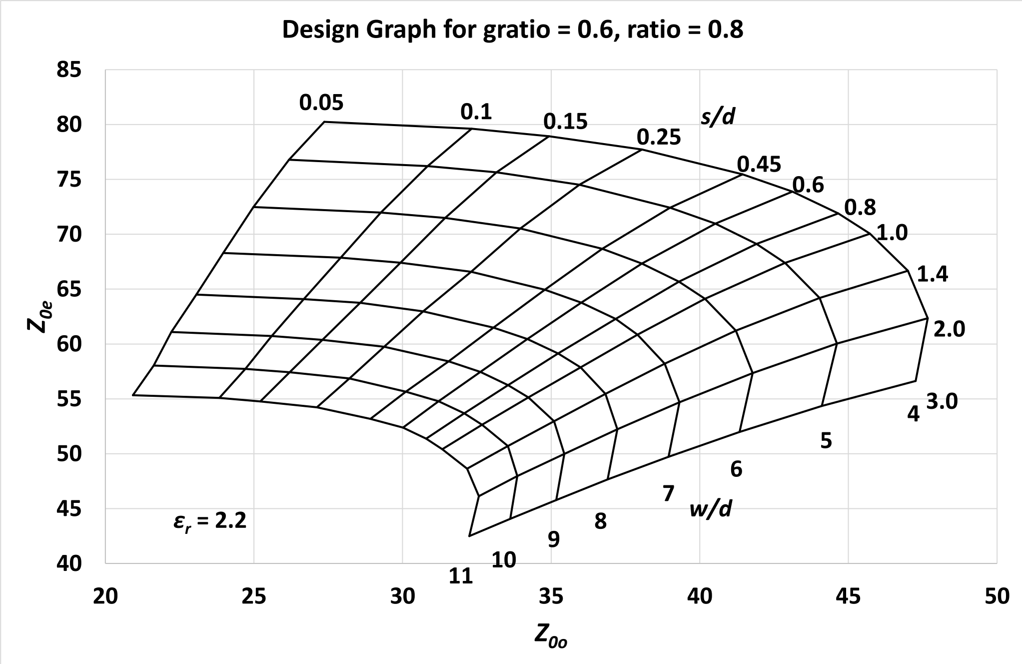
Design Graph for gratio = 0.6, ratio = 0.8
85
80
75
70
65
60
55
50
45
40
20
25
30
35
40
45
50
Z_{0e}
Z_{0o}
s/d
0.05
0.1
0.15
0.25
0.45
0.6
0.8
1.0
1.4
2.0
3.0
w/d
4
5
6
7
8
9
10
11
ε_r = 2.2

(g)

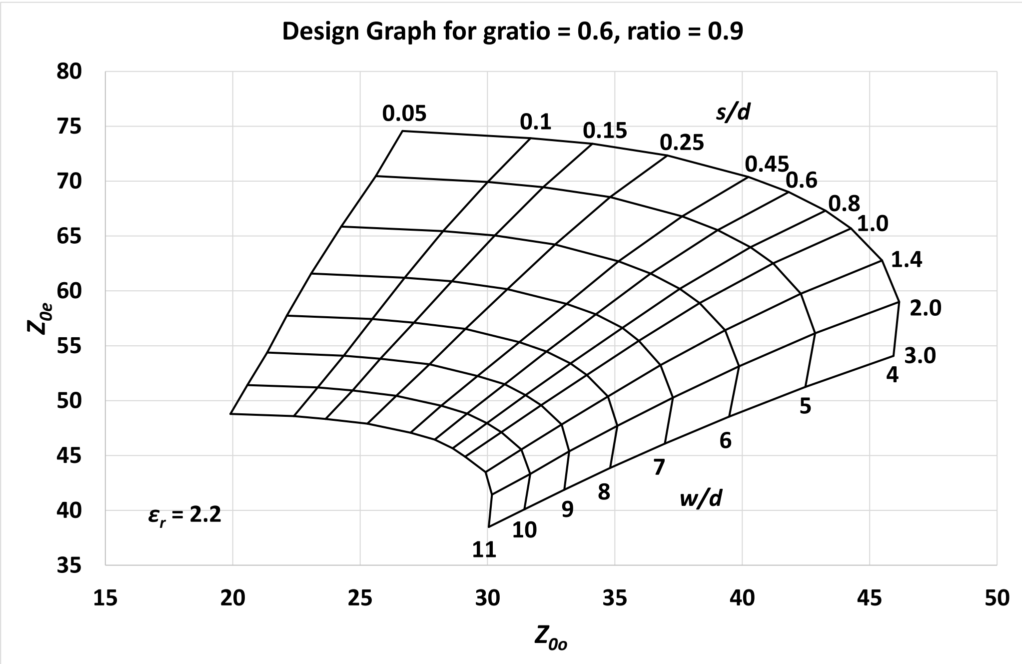
Design Graph for gratio = 0.6, ratio = 0.9
80
75
70
65
60
55
50
45
40
35
15
20
25
30
35
40
45
50
Z_{0e}
Z_{0o}
s/d
0.05
0.1
0.15
0.25
0.45
0.6
0.8
1.0
1.4
2.0
3.0
w/d
4
5
6
7
8
9
10
11
ε_r = 2.2

(h)

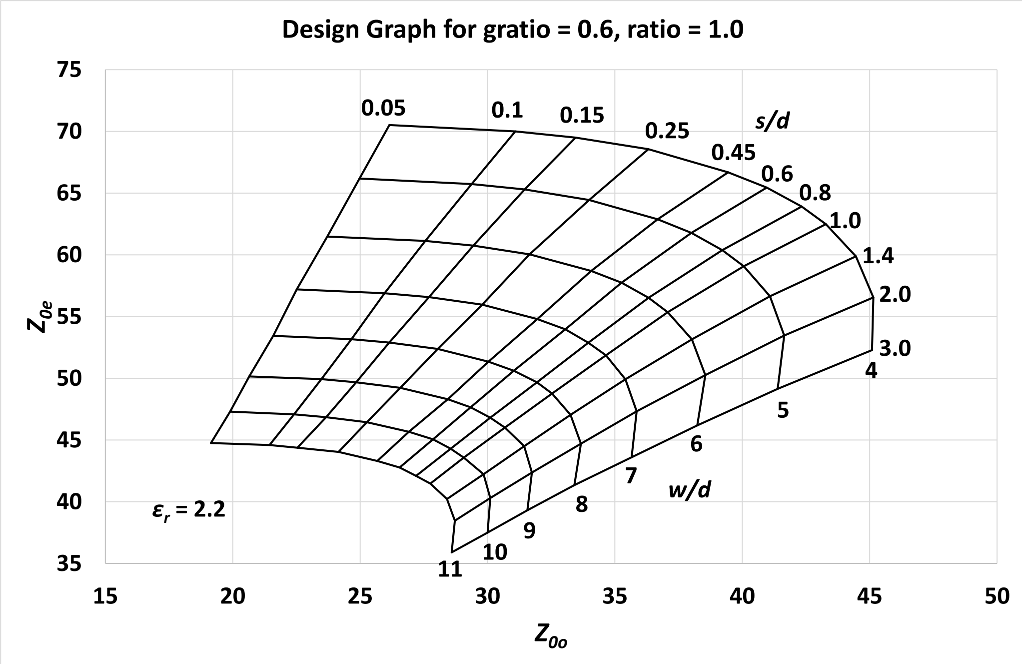
Design Graph for gratio = 0.6, ratio = 1.0
0.05
0.1
0.15
0.25
s/d
0.45
0.6
0.8
1.0
1.4
2.0
3.0
4
5
6
7
w/d
8
9
10
11
ε_r = 2.2
Z_{0e}
Z_{0o}
75
70
65
60
55
50
45
40
35
15
20
25
30
35
40
45
50

(i)

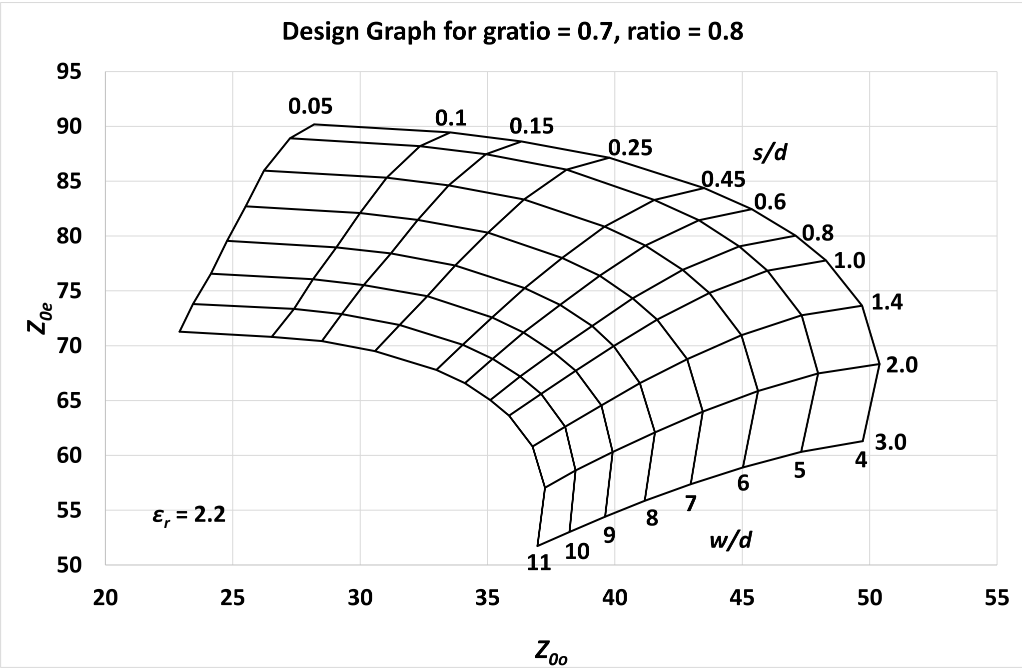
Design Graph for gratio = 0.7, ratio = 0.8
0.05
0.1
0.15
0.25
s/d
0.45
0.6
0.8
1.0
1.4
2.0
3.0
4
5
6
7
8
9
10
11
w/d
ε_r = 2.2
Z_{0e}
Z_{0o}
95
90
85
80
75
70
65
60
55
50
20
25
30
35
40
45
50
55

(j)

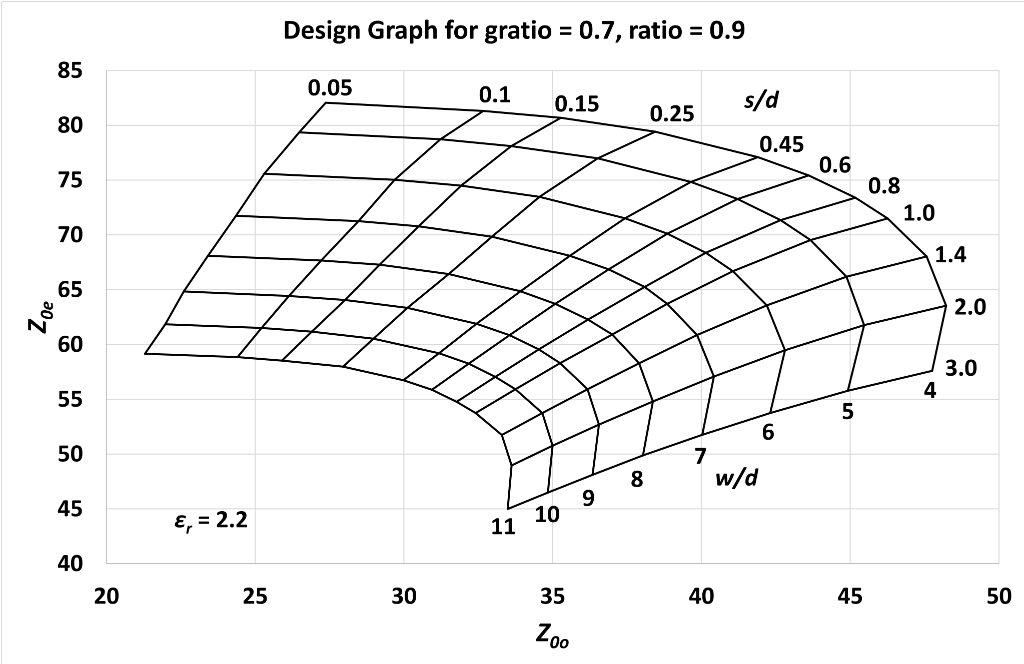
Design Graph for gratio = 0.7, ratio = 0.9
s/d
0.05
0.1
0.15
0.25
0.45
0.6
0.8
1.0
1.4
2.0
3.0
4
5
6
7
8
9
10
11
w/d
εr = 2.2
Z0e
Z0o
85
80
75
70
65
60
55
50
45
40
20
25
30
35
40
45
50

(k)

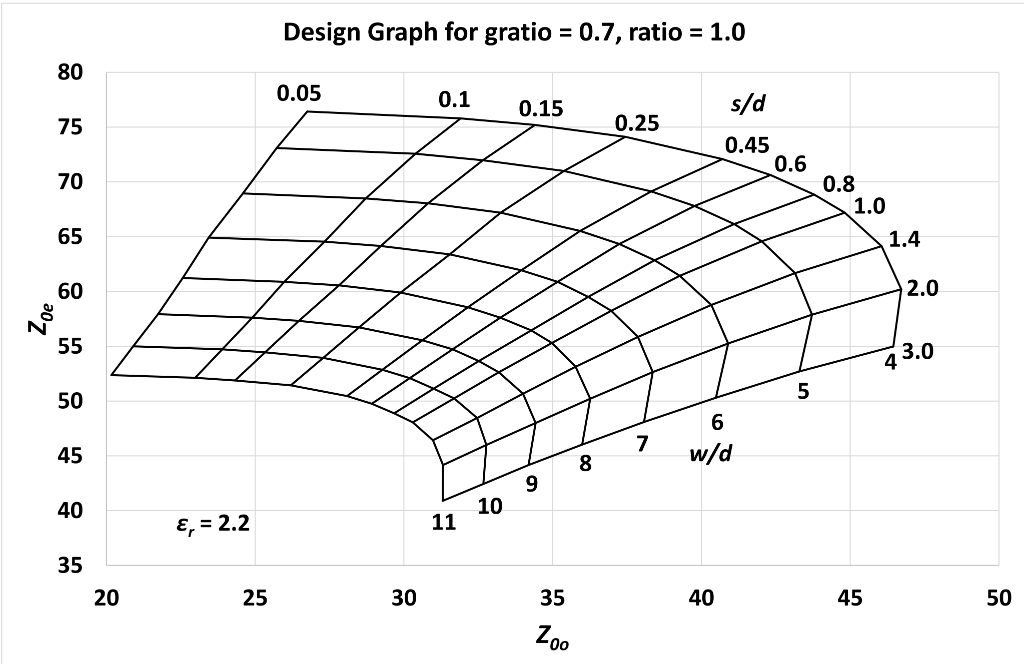
Design Graph for gratio = 0.7, ratio = 1.0
s/d
0.05
0.1
0.15
0.25
0.45
0.6
0.8
1.0
1.4
2.0
3.0
4
5
6
7
8
9
10
11
w/d
εr = 2.2
Z0e
Z0o
80
75
70
65
60
55
50
45
40
35
20
25
30
35
40
45
50

(l)

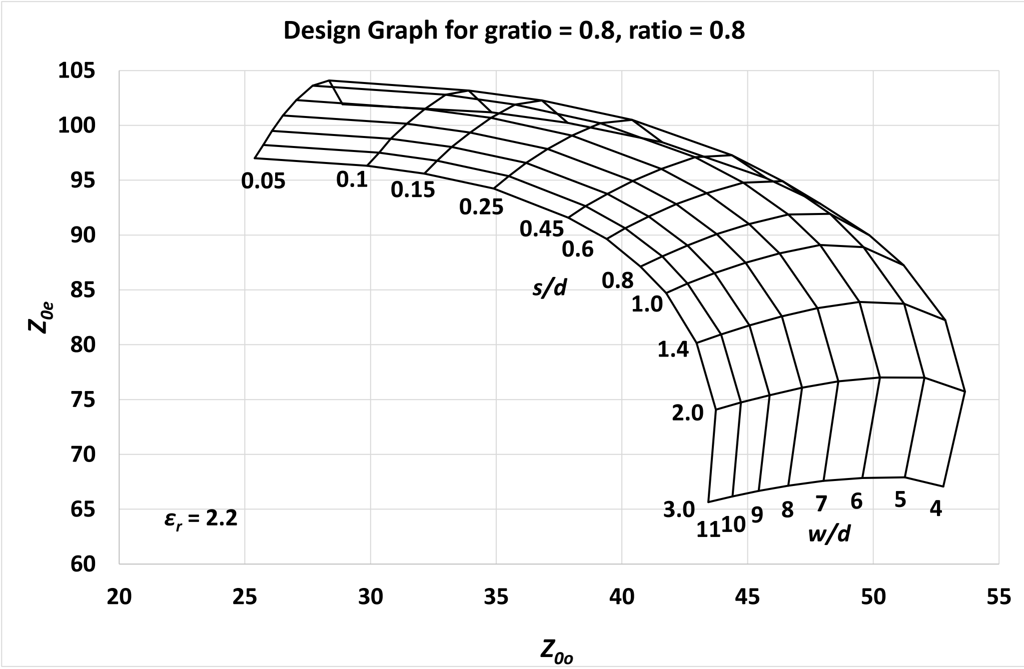
Design Graph for gratio = 0.8, ratio = 0.8
Z_{0e}
Z_{0o}
s/d
w/d
ε_r = 2.2
0.05
0.1
0.15
0.25
0.45
0.6
0.8
1.0
1.4
2.0
3.0
11 10 9 8 7 6 5 4

(m)

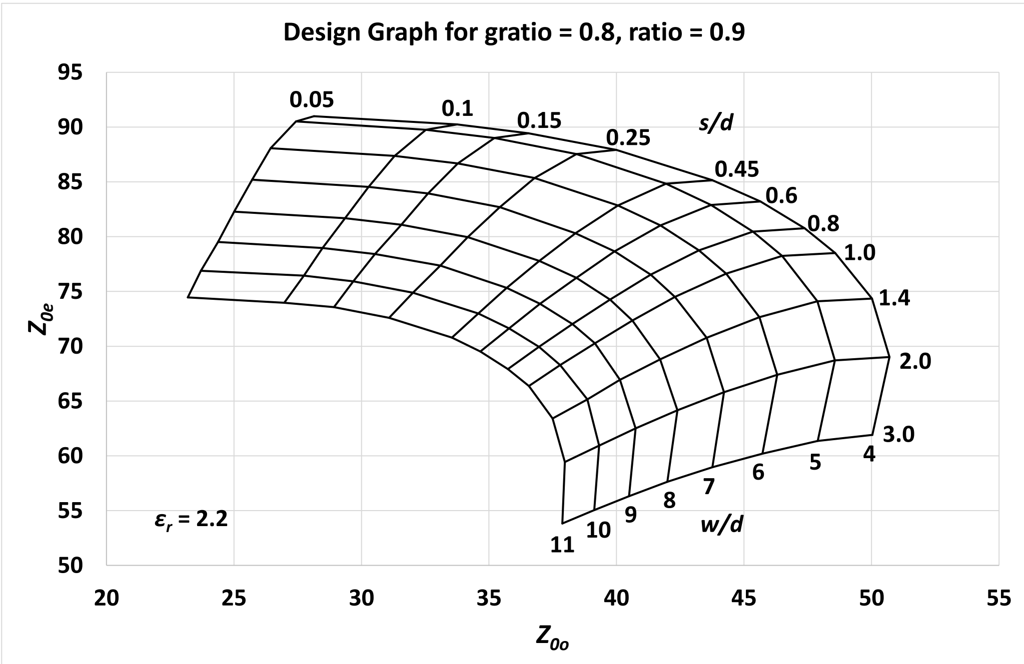
Design Graph for gratio = 0.8, ratio = 0.9
Z_{0e}
Z_{0o}
s/d
w/d
ε_r = 2.2
0.05
0.1
0.15
0.25
0.45
0.6
0.8
1.0
1.4
2.0
3.0
11 10 9 8 7 6 5 4

(n)

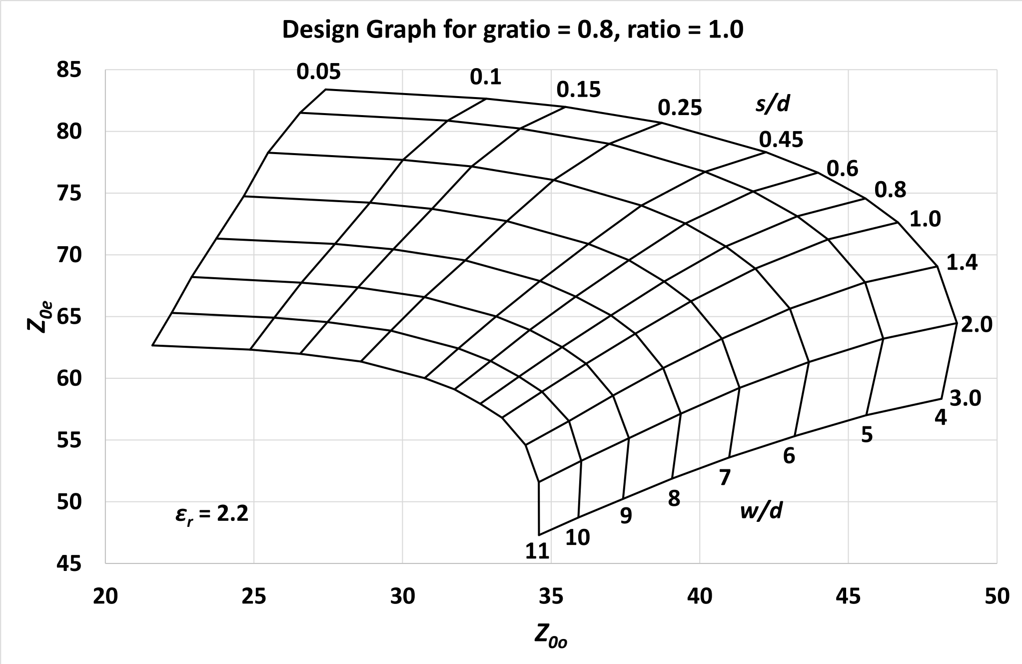
Design Graph for gratio = 0.8, ratio = 1.0
0.05
0.1
0.15
0.25
s/d
0.45
0.6
0.8
1.0
1.4
2.0
3.0
4
5
6
7
8
9
10
11
w/d
ε_r = 2.2
Z_0e
Z_0o

(o)

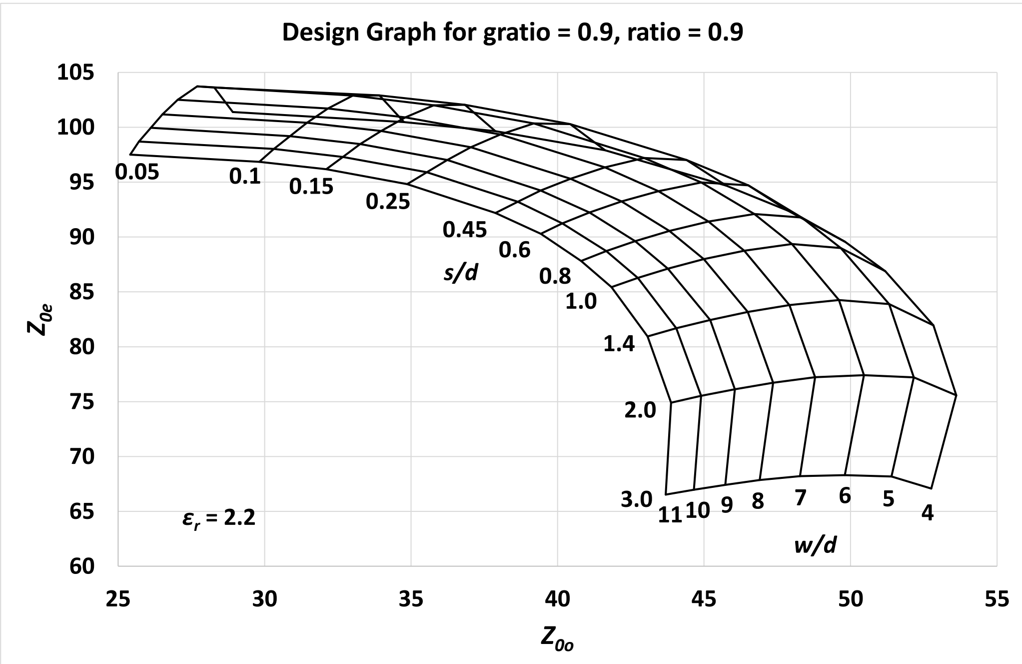
Design Graph for gratio = 0.9, ratio = 0.9
0.05
0.1
0.15
0.25
0.45
0.6
s/d
0.8
1.0
1.4
2.0
3.0
11 10 9 8 7 6 5 4
w/d
ε_r = 2.2
Z_0e
Z_0o

(p)

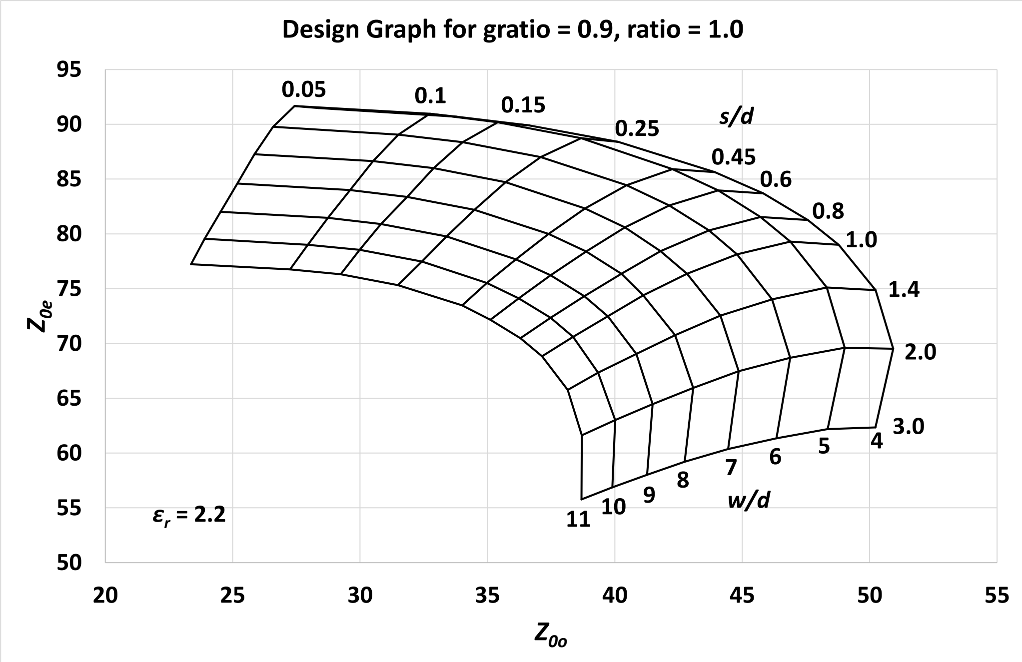

(q)

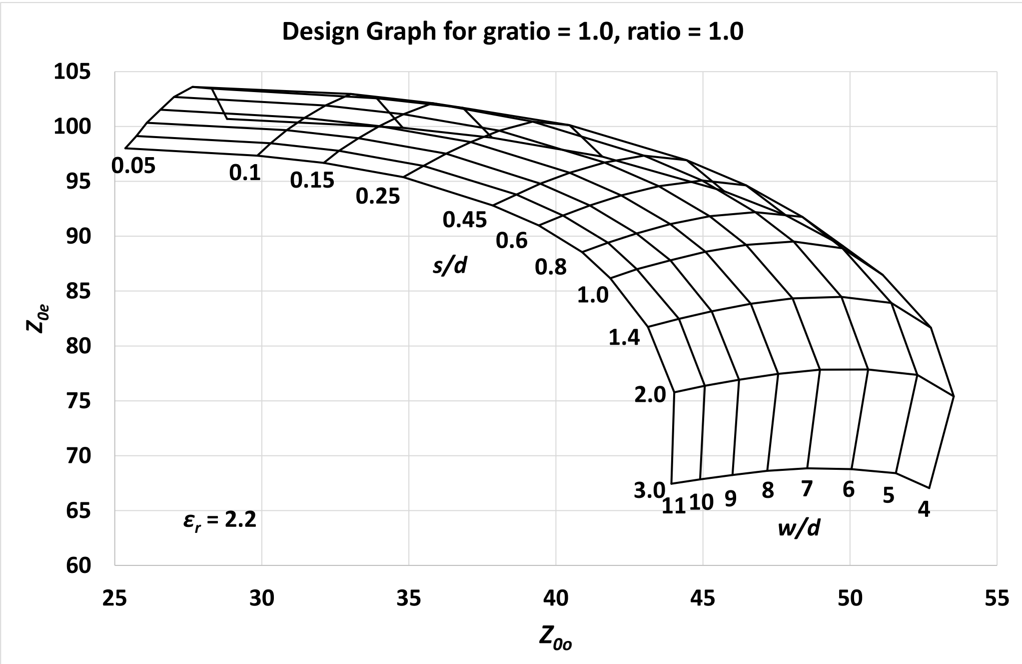

(r)

Figure 3.5: Design graphs for $\varepsilon_r = 2.2$ (a) gratio = 0.5, ratio = 0.6, (b) gratio = 0.5, ratio = 0.7, (c) gratio = 0.5, ratio = 0.8, (d) gratio = 0.5, ratio = 0.9, (e) gratio = 0.5, ratio = 1.0, (f) gratio = 0.6, ratio = 0.7, (g) gratio = 0.6, ratio = 0.8, (h) gratio = 0.6, ratio = 0.9, (i) gratio = 0.6, ratio = 1.0, (j) gratio = 0.7, ratio = 0.8, (k) gratio = 0.7, ratio = 0.9, (l) gratio = 0.7, ratio = 1.0, (m) gratio = 0.8, ratio = 0.8, (n) gratio = 0.8, ratio = 0.9, (o) gratio = 0.8, ratio = 1.0, (p) gratio = 0.9, ratio = 0.9, (q) gratio = 0.9, ratio = 1.0, and (r) gratio = 1.0, ratio = 1.0.

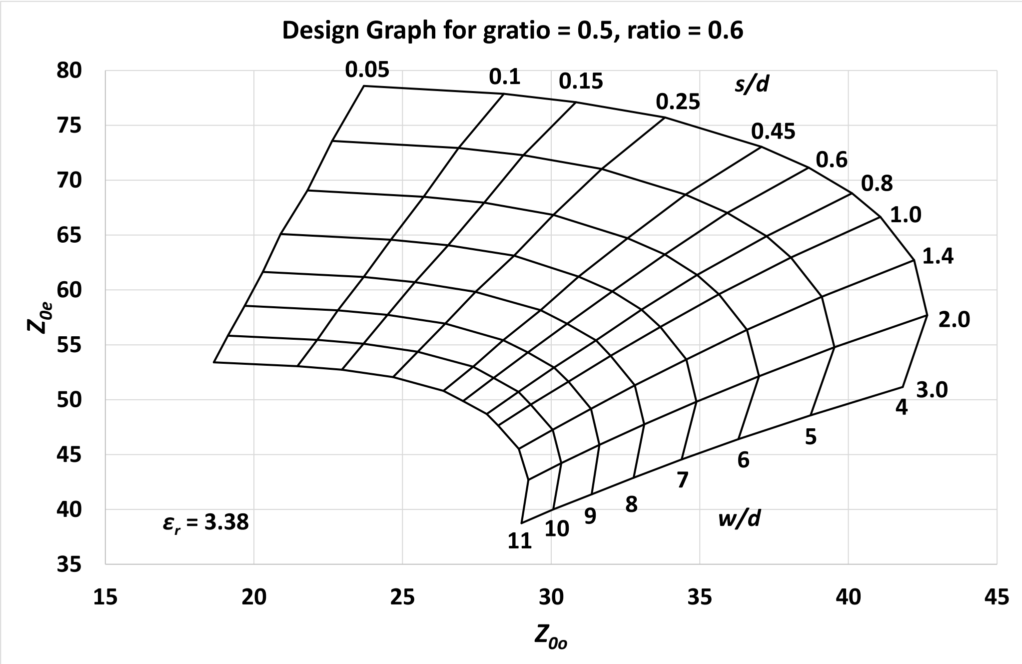

Design Graph for gratio = 0.5, ratio = 0.6
s/d
0.05
0.1
0.15
0.25
0.45
0.6
0.8
1.0
1.4
2.0
3.0
4
5
6
7
8
9
10
11
w/d
ε_r = 3.38
Z_{0e}
Z_{0o}
80
75
70
65
60
55
50
45
40
35
15
20
25
30
35
40
45

(a)

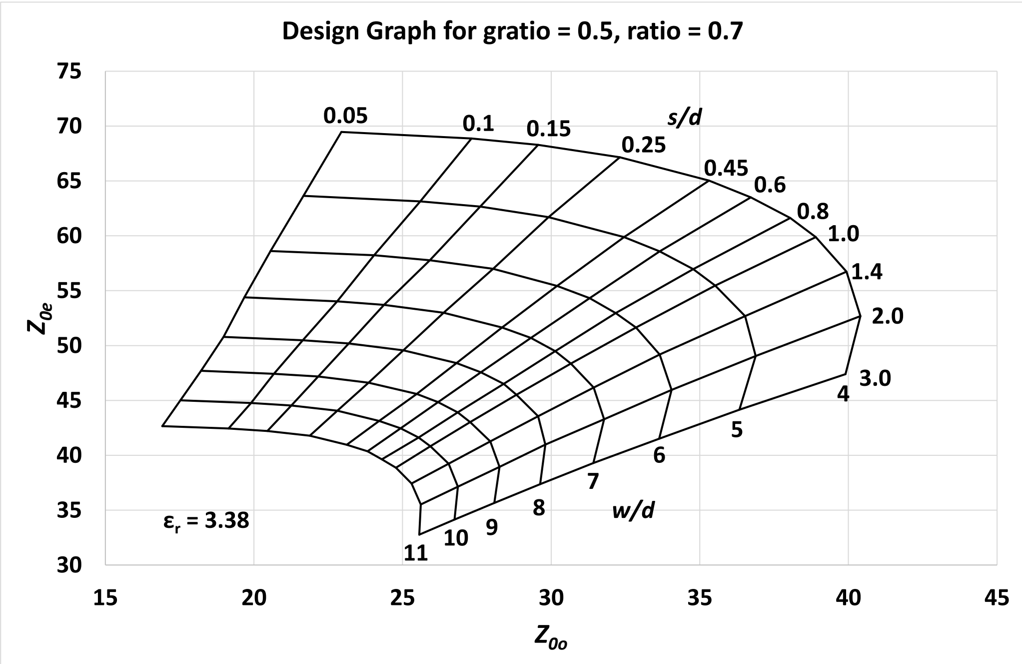

Design Graph for gratio = 0.5, ratio = 0.7
s/d
0.05
0.1
0.15
0.25
0.45
0.6
0.8
1.0
1.4
2.0
3.0
4
5
6
7
8
9
10
11
w/d
ε_r = 3.38
Z_{0e}
Z_{0o}
75
70
65
60
55
50
45
40
35
30
15
20
25
30
35
40
45

(b)

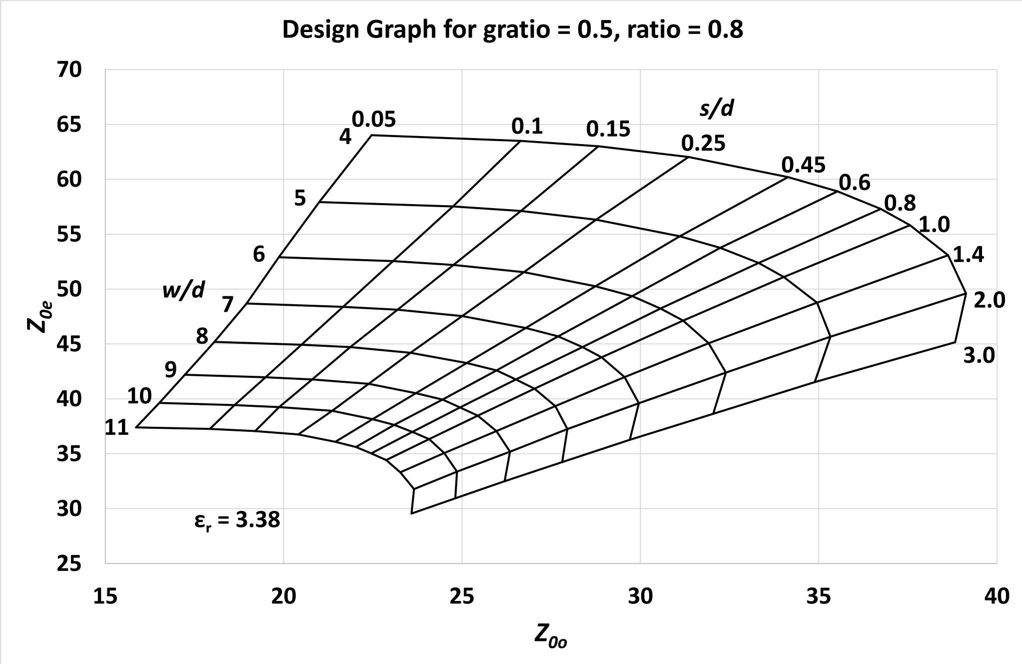
Design Graph for gratio = 0.5, ratio = 0.8
70
65
60
55
50
45
40
35
30
25
15
20
25
30
35
40
Z0e
Z0o
s/d
0.05
0.1
0.15
0.25
0.45
0.6
0.8
1.0
1.4
2.0
3.0
w/d
4
5
6
7
8
9
10
11
εr = 3.38

(c)

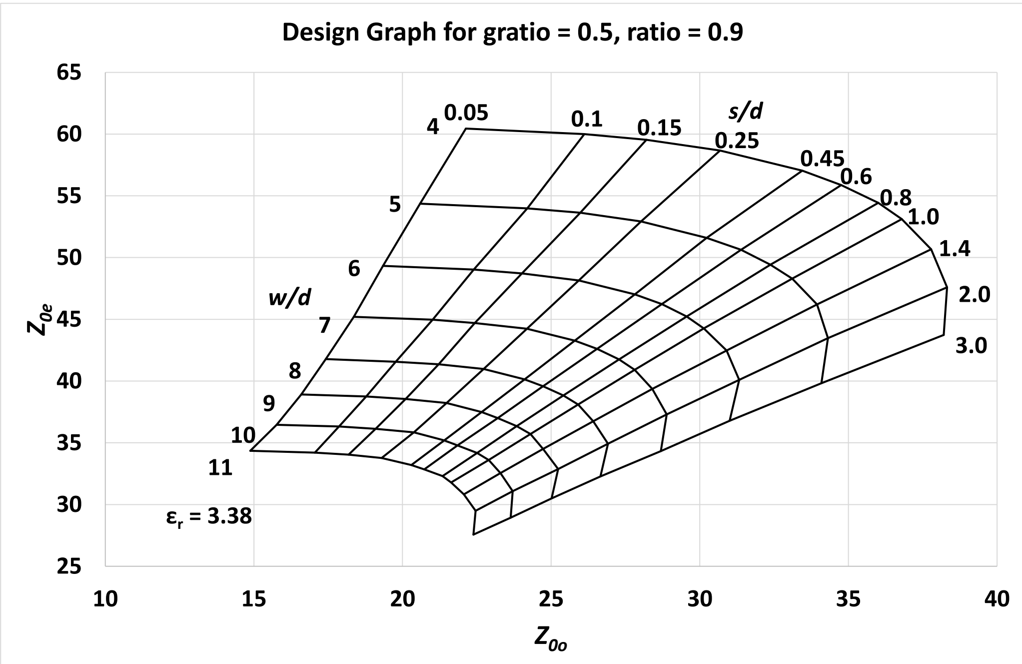
Design Graph for gratio = 0.5, ratio = 0.9
65
60
55
50
45
40
35
30
25
10
15
20
25
30
35
40
Z0e
Z0o
s/d
0.05
0.1
0.15
0.25
0.45
0.6
0.8
1.0
1.4
2.0
3.0
w/d
4
5
6
7
8
9
10
11
εr = 3.38

(d)

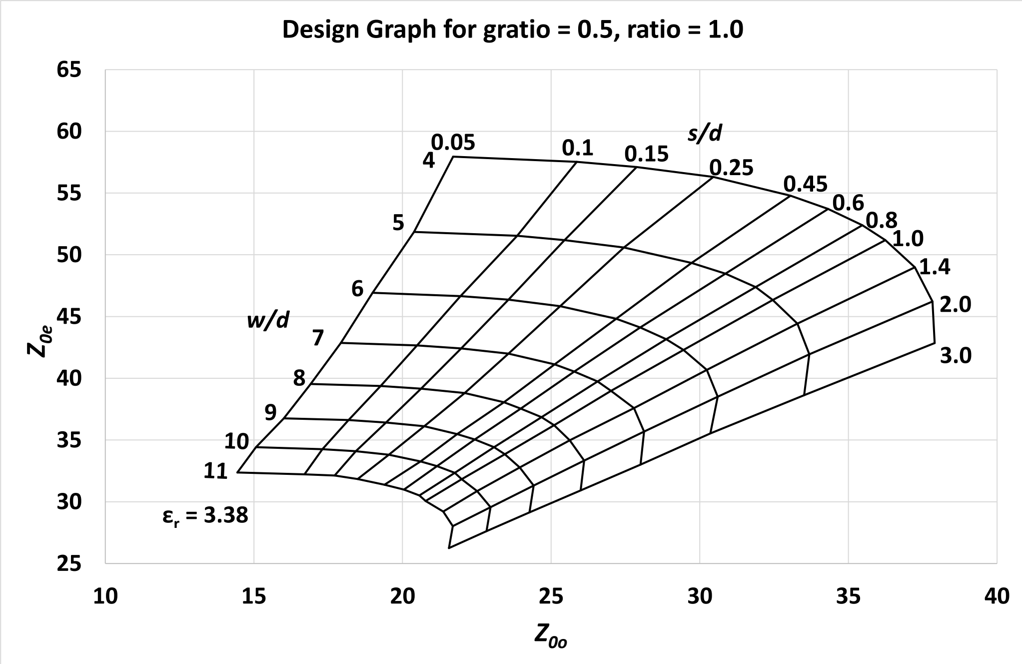
Design Graph for gratio = 0.5, ratio = 1.0
s/d
0.05
0.1
0.15
0.25
0.45
0.6
0.8
1.0
1.4
2.0
3.0
w/d
4
5
6
7
8
9
10
11
εr = 3.38
Z0e
Z0o

(e)

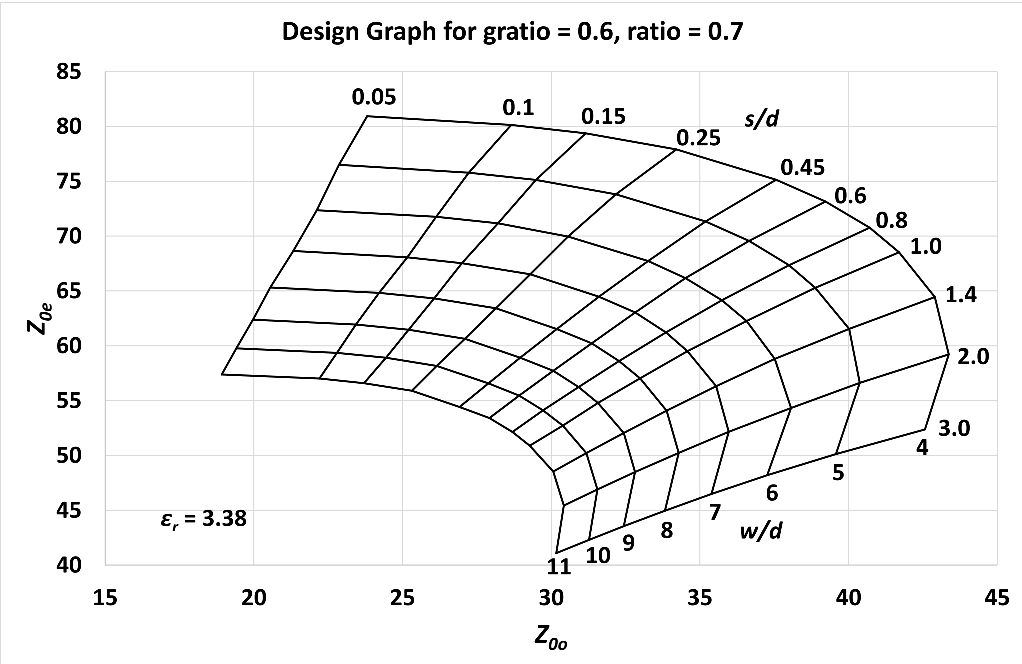
Design Graph for gratio = 0.6, ratio = 0.7
s/d
0.05
0.1
0.15
0.25
0.45
0.6
0.8
1.0
1.4
2.0
3.0
w/d
4
5
6
7
8
9
10
11
εr = 3.38
Z0e
Z0o

(f)

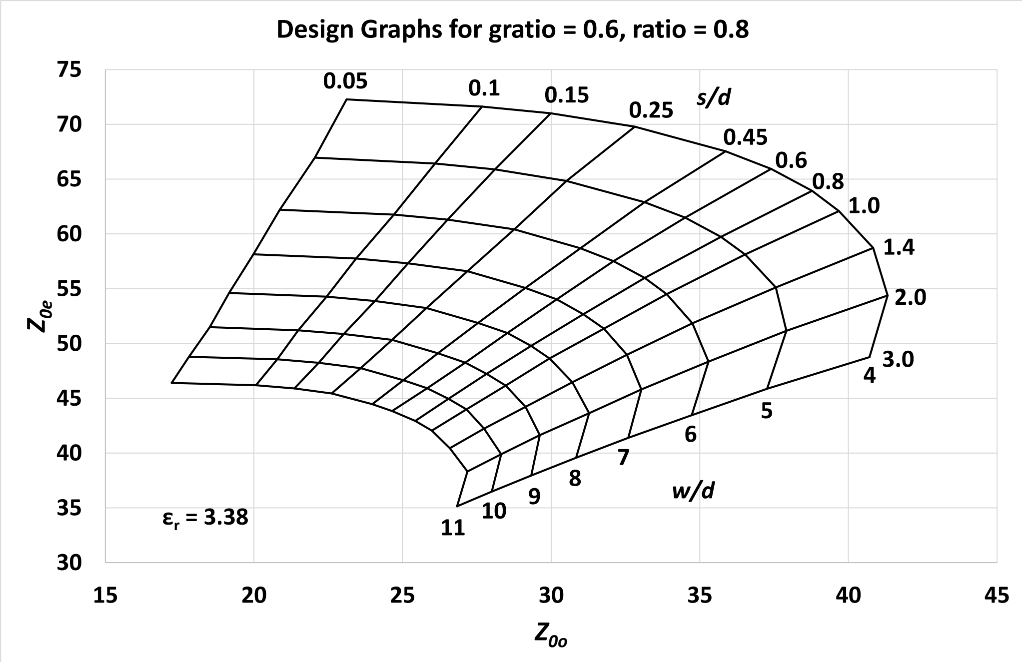

Design Graphs for gratio = 0.6, ratio = 0.8
75
70
65
60
55
50
45
40
35
30
15
20
25
30
35
40
45
Z_{0e}
Z_{0o}
0.05
0.1
0.15
0.25
s/d
0.45
0.6
0.8
1.0
1.4
2.0
3.0
4
5
6
7
8
9
10
11
w/d
ε_r = 3.38

(g)

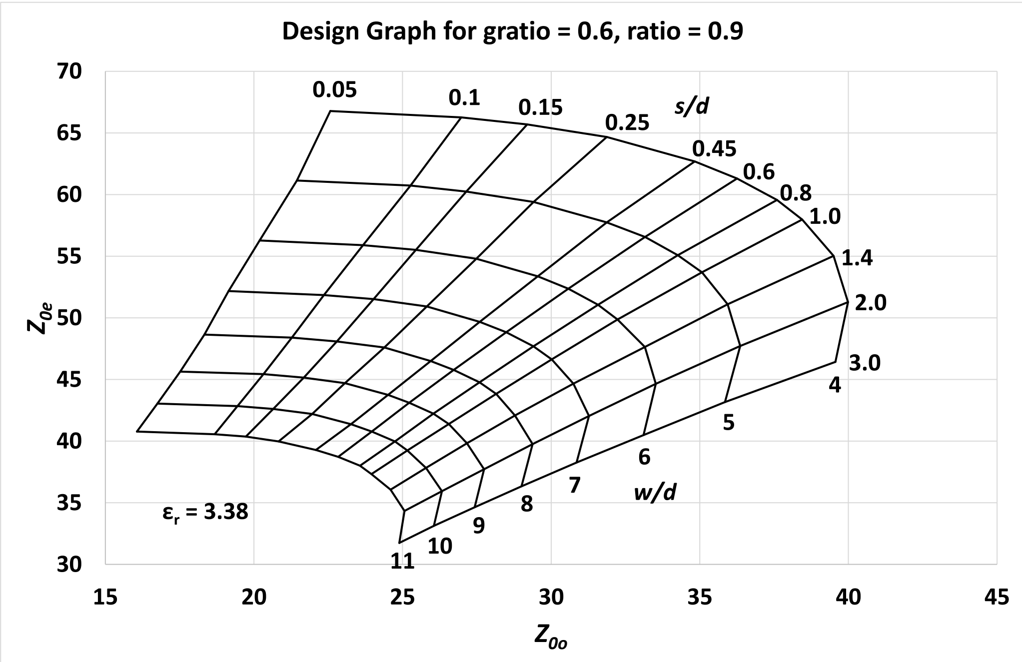

Design Graph for gratio = 0.6, ratio = 0.9
70
65
60
55
50
45
40
35
30
15
20
25
30
35
40
45
Z_{0e}
Z_{0o}
0.05
0.1
0.15
0.25
s/d
0.45
0.6
0.8
1.0
1.4
2.0
3.0
4
5
6
7
8
9
10
11
w/d
ε_r = 3.38

(h)

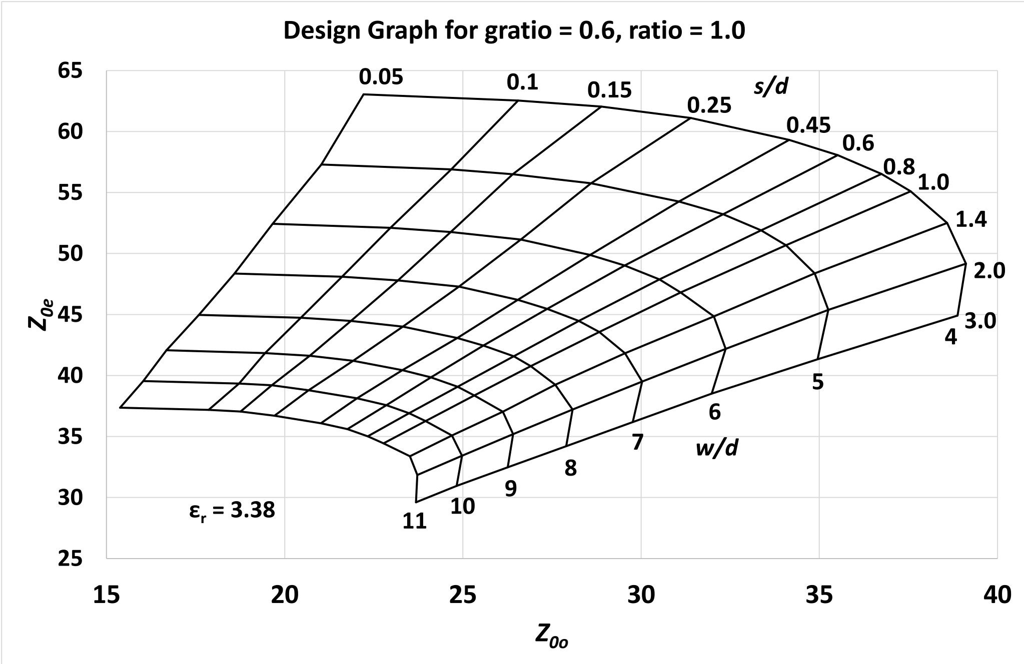
Design Graph for gratio = 0.6, ratio = 1.0
s/d
0.05
0.1
0.15
0.25
0.45
0.6
0.8
1.0
1.4
2.0
3.0
w/d
4
5
6
7
8
9
10
11
ε_r = 3.38
Z_0e
Z_0o
65
60
55
50
45
40
35
30
25
15
20
25
30
35
40
(i)

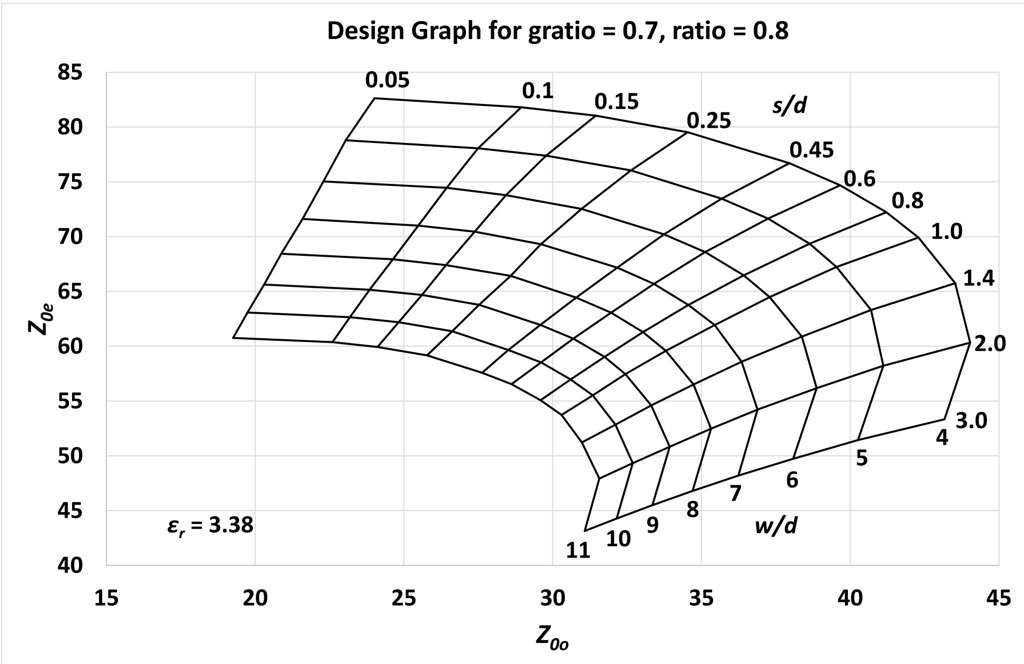
Design Graph for gratio = 0.7, ratio = 0.8
s/d
0.05
0.1
0.15
0.25
0.45
0.6
0.8
1.0
1.4
2.0
3.0
w/d
4
5
6
7
8
9
10
11
ε_r = 3.38
Z_0e
Z_0o
85
80
75
70
65
60
55
50
45
40
15
20
25
30
35
40
45
(j)

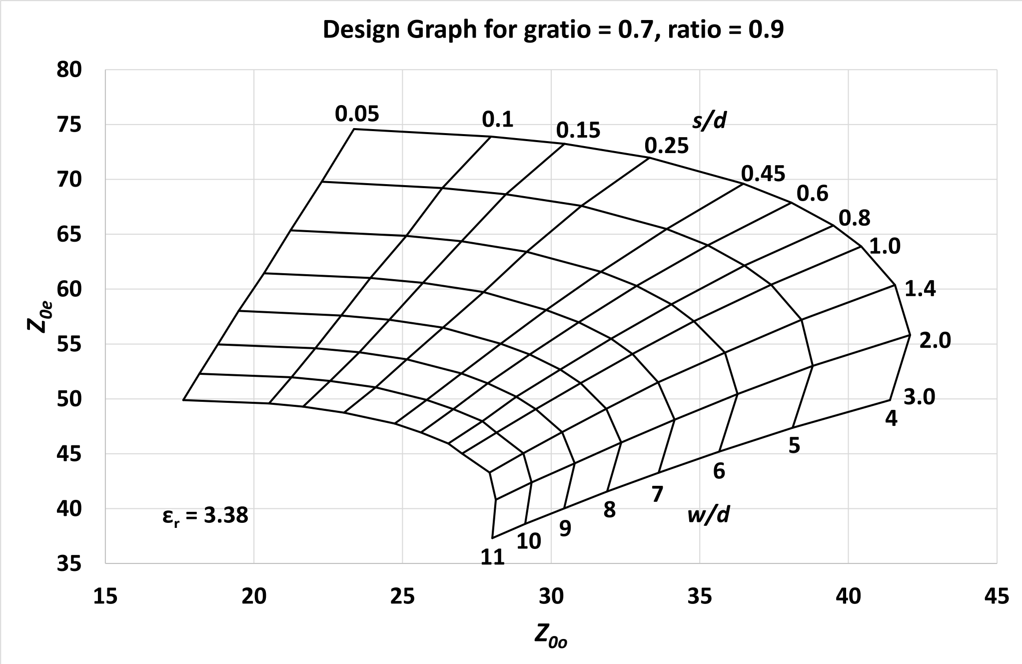
Design Graph for gratio = 0.7, ratio = 0.9
s/d
0.05
0.1
0.15
0.25
0.45
0.6
0.8
1.0
1.4
2.0
3.0
w/d
4
5
6
7
8
9
10
11
εr = 3.38
Z0e
Z0o
80
75
70
65
60
55
50
45
40
35
15
20
25
30
35
40
45

(k)

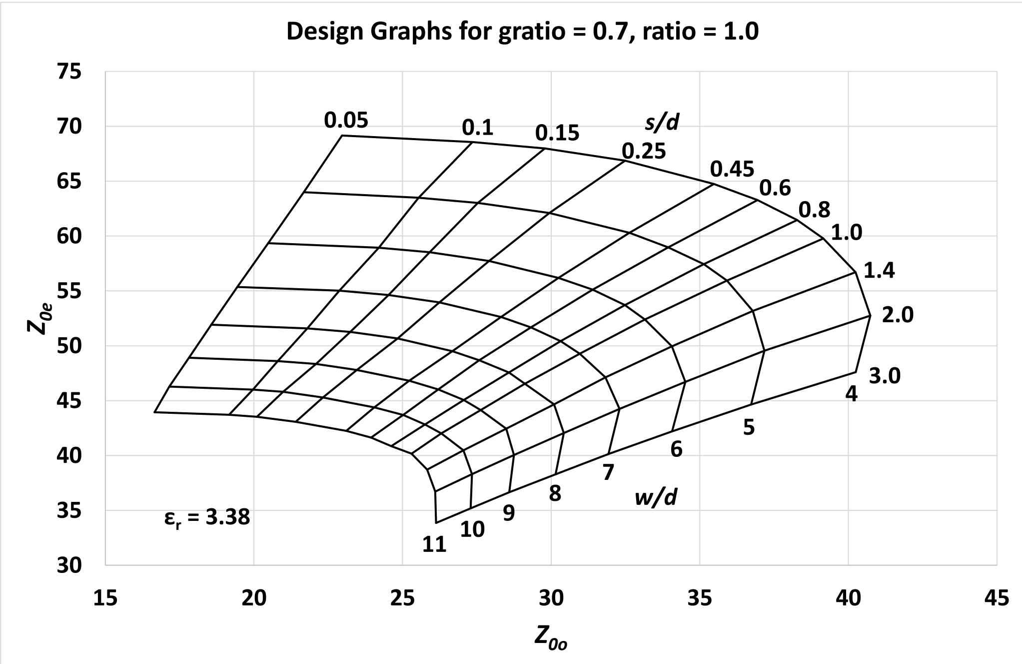
Design Graphs for gratio = 0.7, ratio = 1.0
s/d
0.05
0.1
0.15
0.25
0.45
0.6
0.8
1.0
1.4
2.0
3.0
w/d
4
5
6
7
8
9
10
11
εr = 3.38
Z0e
Z0o
75
70
65
60
55
50
45
40
35
30
15
20
25
30
35
40
45

(l)

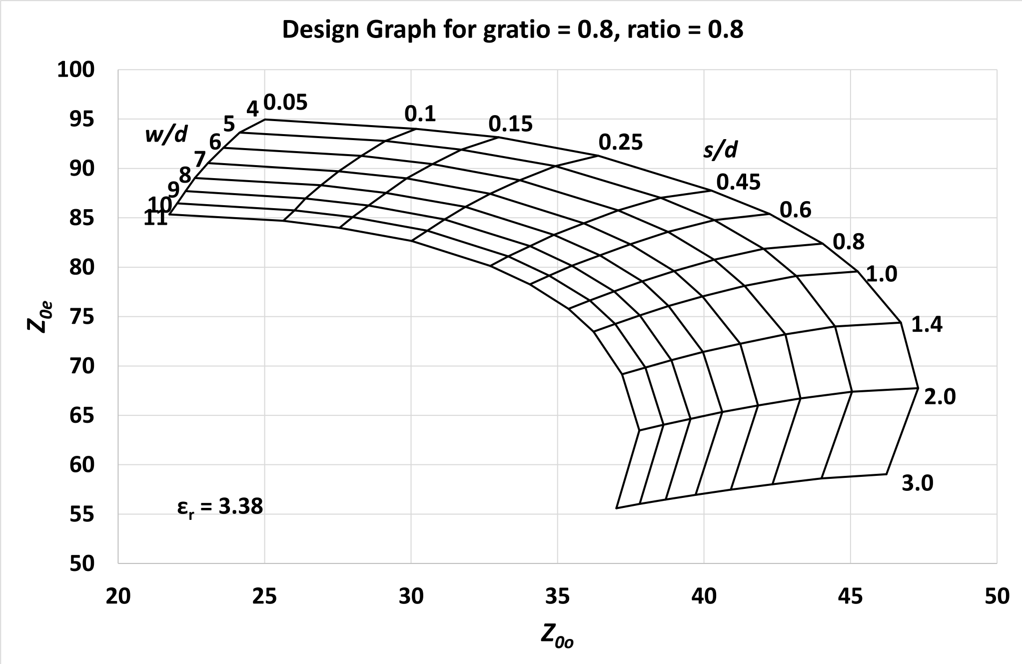

Design Graph for gratio = 0.8, ratio = 0.8
100
95
90
85
80
75
70
65
60
55
50
20
25
30
35
40
45
50
Z_{0e}
Z_{0o}
w/d
4
5
6
7
8
9
10
11
0.05
0.1
0.15
0.25
s/d
0.45
0.6
0.8
1.0
1.4
2.0
3.0
ε_r = 3.38

(m)

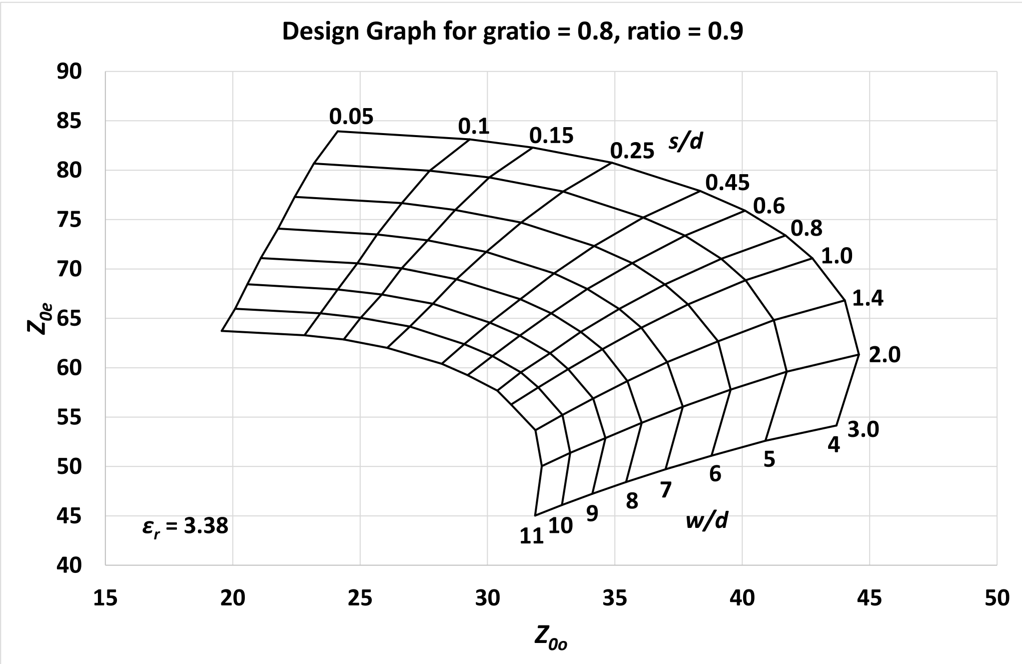

Design Graph for gratio = 0.8, ratio = 0.9
90
85
80
75
70
65
60
55
50
45
40
15
20
25
30
35
40
45
50
Z_{0e}
Z_{0o}
0.05
0.1
0.15
0.25
s/d
0.45
0.6
0.8
1.0
1.4
2.0
3.0
4
5
6
7
8
9
10
11
w/d
ε_r = 3.38

(n)

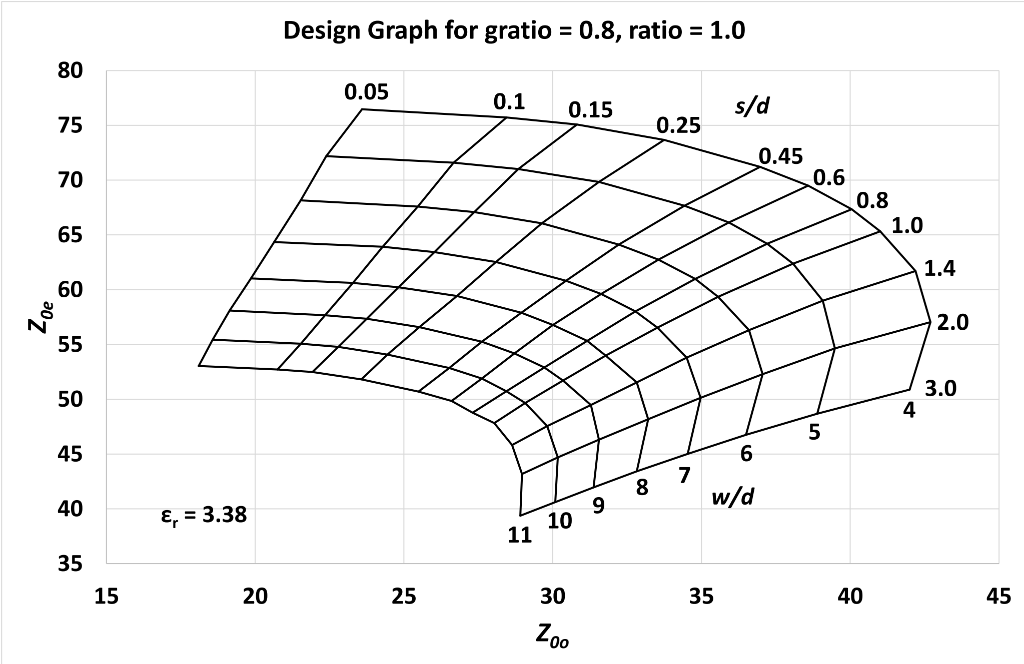
Design Graph for gratio = 0.8, ratio = 1.0
80
75
70
65
60
55
50
45
40
35
15
20
25
30
35
40
45
Z0e
Z0o
0.05
0.1
0.15
0.25
s/d
0.45
0.6
0.8
1.0
1.4
2.0
3.0
4
5
6
7
8
9
10
11
w/d
εr = 3.38

(o)

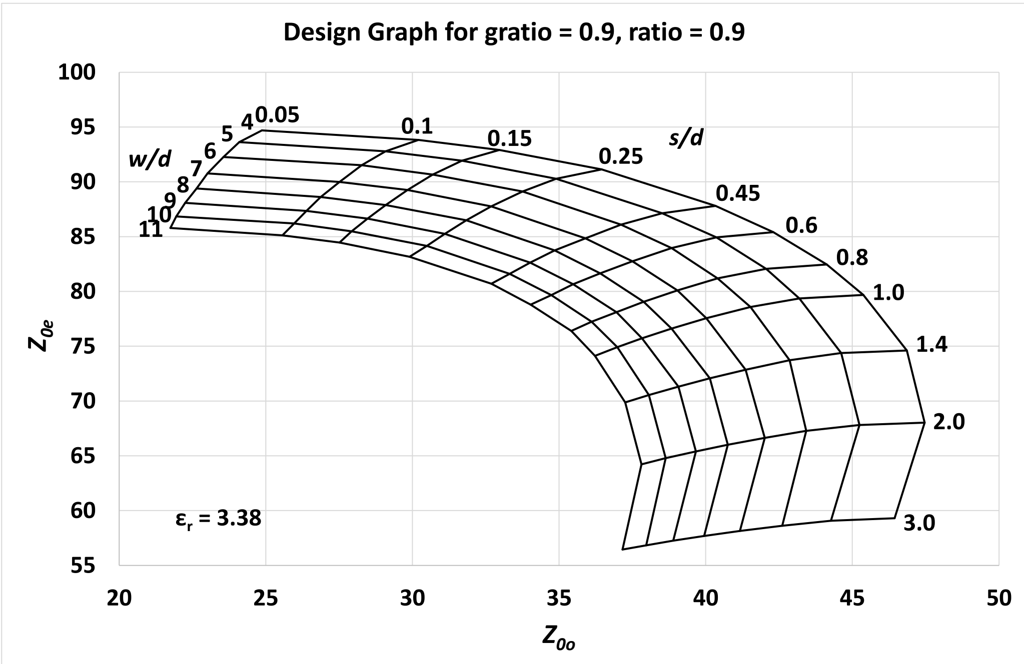
Design Graph for gratio = 0.9, ratio = 0.9
100
95
90
85
80
75
70
65
60
55
20
25
30
35
40
45
50
Z0e
Z0o
0.05
0.1
0.15
0.25
s/d
0.45
0.6
0.8
1.0
1.4
2.0
3.0
4
5
6
7
8
9
10
11
w/d
εr = 3.38

(p)

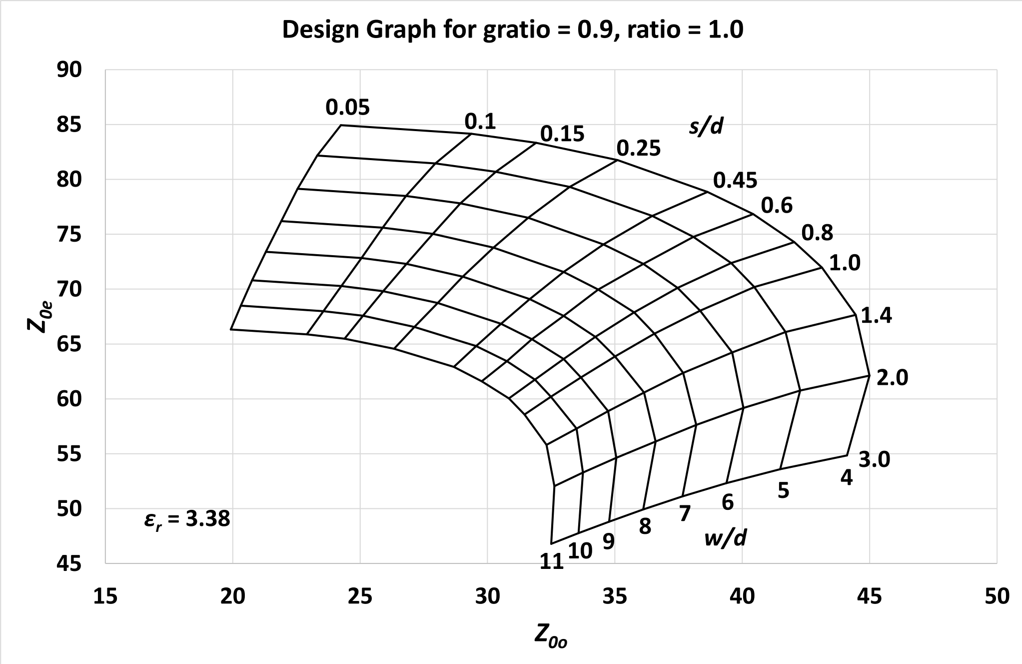

(q)

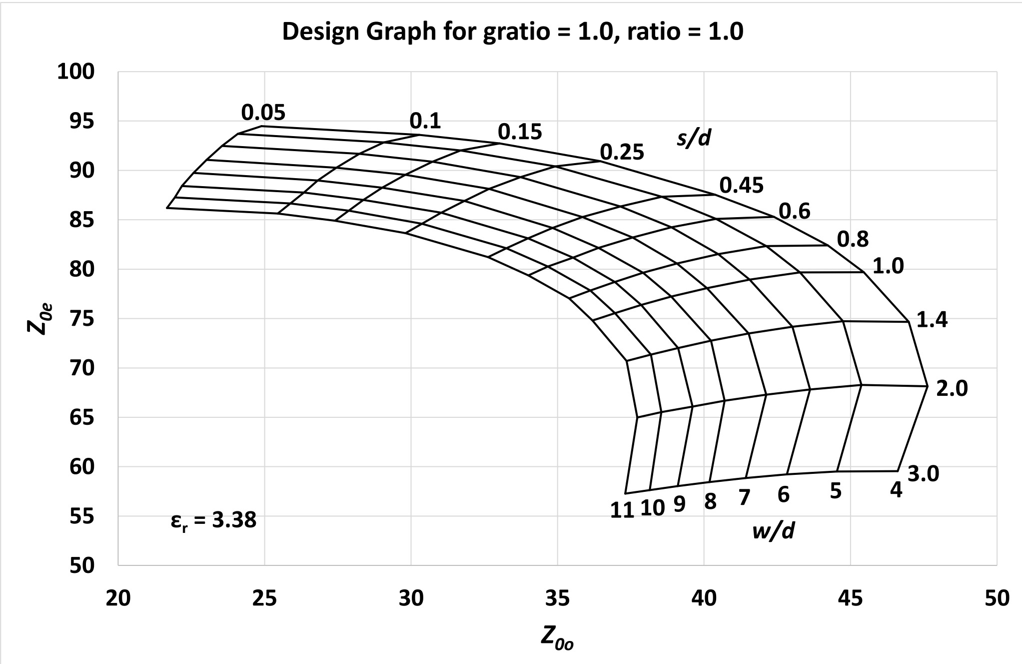

(r)

Figure 3.6: Design graphs for ε_r = 3.38 (a) gratio = 0.5, ratio = 0.6, (b) gratio = 0.5, ratio = 0.7, (c) gratio = 0.5, ratio = 0.8, (d) gratio = 0.5, ratio = 0.9, (e) gratio = 0.5, ratio = 1.0, (f) gratio = 0.6, ratio = 0.7, (g) gratio = 0.6, ratio = 0.8, (h) gratio = 0.6, ratio = 0.9, (i) gratio = 0.6, ratio = 1.0, (j) gratio = 0.7, ratio = 0.8, (k) gratio = 0.7, ratio = 0.9, (l) gratio = 0.7, ratio = 1.0, (m) gratio = 0.8, ratio = 0.8, (n) gratio = 0.8, ratio = 0.9, (o) gratio = 0.8, ratio = 1.0, (p) gratio = 0.9, ratio = 0.9, (q) gratio = 0.9, ratio = 1.0, and (r) gratio = 1.0, ratio = 1.0.

.

From Figure 3.5 and Figure 3.6, one can see that Z_{0o} increases with s, as the larger separation between the top patches reduces its capacitance. However, the rate of increment reduces as the top patches are separated further apart. The larger separation distance reduces the capacitance between the top patches, but increases the capacitance between the top patches and the ground conductor. On the other hand, Z_{0e} decreases with s because of the larger overlapping area between the top patch and the ground plane, which in effect increases the capacitance. Increase in w causes the capacitance per unit length to increase. This results in the decrease of both even and odd mode impedances.

From the design graphs, it can be shown that there are many possible combinations of s/d and w/d to achieve the same coupling factor. Different parameter combinations, together with the thickness of the substrate, result in different physical dimensions of the coupler. The effective wavelength at center frequency, $\lambda_{0(eff)}$ can be estimated using the following equation:

$$\lambda_{0(eff)} = \frac{\lambda_0}{\sqrt{\varepsilon_{eff}}} \tag{3.3}$$

where $\varepsilon_{eff} \approx \dfrac{1+\varepsilon_r}{2}$

This approximation is made based on the assumption that the electric field is distributed equally in the dielectric and in the air for this coupler structure, as illustrated in Figure 3.4.

Using the approximate equation of an ellipse, the physical dimension of the structure can be related to the effective wavelength, $\lambda_{0(eff)}$ (and hence the center frequency) using the following approximation:

$$\lambda_{0(eff)} \approx \pi(L+w)\left(1+\frac{3k}{10+\sqrt{4-3k}}\right) \tag{3.4}$$

where $k=\frac{(L-w)^2}{(L+w)^2}$, L is the coupler length and w is the coupler width.

3.4 Summary of the Design Procedure for Directional Coupler

The proposed directional coupler can be designed with the following procedure:

1. For a desired coupling factor, C, determine the even and odd mode characteristic impedances, Z_{0e} and Z_{0o} using Equation (3.1) and Equation (3.2).
2. Using the design graphs in Figure 3.5 and Figure 3.6, find the corresponding *s/d* and *w/d*.
3. The gap width, s and the width of the semi-elliptical patches, w can be calculated from the values of *s/d* and *w/d*, where d is the thickness of the substrate.
4. The length, L of the coupler can be calculated from the axial ratio ("*ratio*") indicated on the design graph. Finally, the width of the defected ground, w_g, is calculated from the defected ground axial ratio ("*gratio*").

3.5 Results and Discussion

Using the design graphs in Figure 3.5 and Figure 3.6, the parameters for coupling factor, $C = 10$ dB ± 1 dB are determined and shown in Table 3.1:

Table 3.1: Design parameters of directional couplers.

ε_r	*s/d*	*w/d*	*d (mm)*	*L (mm)*	*w (mm)*	*s (mm)*	w_g *(mm)*
2.2	0.325	7.240	1.575	38.010	11.403	0.512	19.005
2.2	0.325	7.240	0.787	18.993	5.698	0.256	9.496
3.38	0.353	4.400	1.524	22.352	6.706	0.538	11.176
3.38	0.353	4.400	0.813	11.924	3.577	0.287	5.962

Using (3.4), the estimated center frequencies for $\varepsilon_r = 2.2$ and substrate thickness of 1.575 mm and 0.787 mm are found to be 1.423 GHz and 2.847 GHz, respectively. For $\varepsilon_r = 3.38$ and substrate thickness of 1.524 mm and 0.813 mm, the estimated center frequencies are 2.029 GHz and 3.804 GHz, respectively.

The reflection coefficient, insertion loss, coupling, and isolation of the proposed couplers are first verified using CST Microwave Studio. The designs are fabricated on Rogers RT/Duroid 5880 and RO4003C with different substrate thicknesses. The photographs of the fabricated couplers are shown in Figure 3.7.

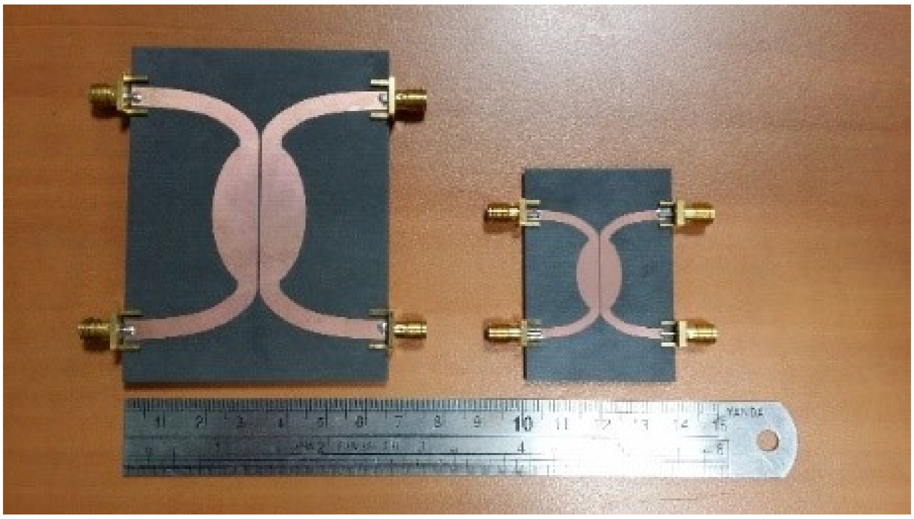

(a)

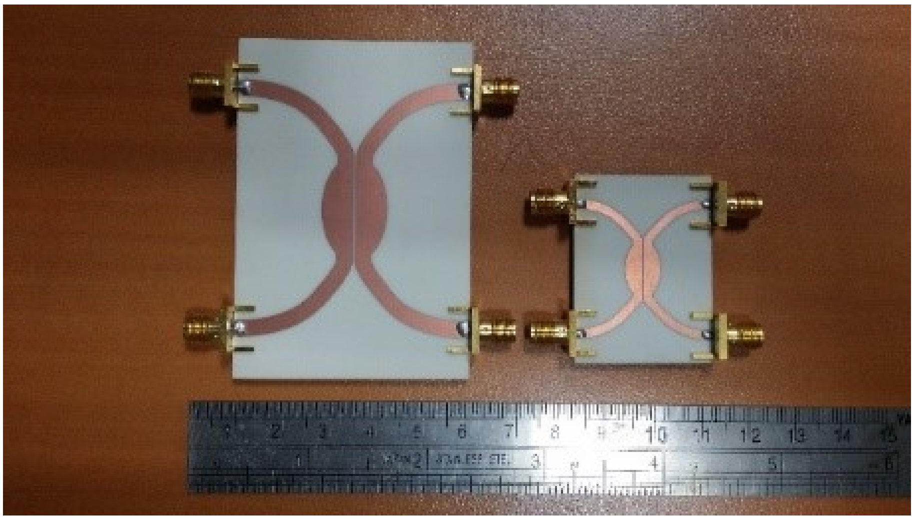

(b)

Figure 3.7: Fabricated couplers. (a) RT/Duroid 5880, (b) RO4003C.

The fabricated couplers are tested using a two-port vector network analyzer as shown in Figure 3.8. A full two port SOLT calibration is performed before the measurements are made. For each measurement, two of the unused ports are terminated with match loads.

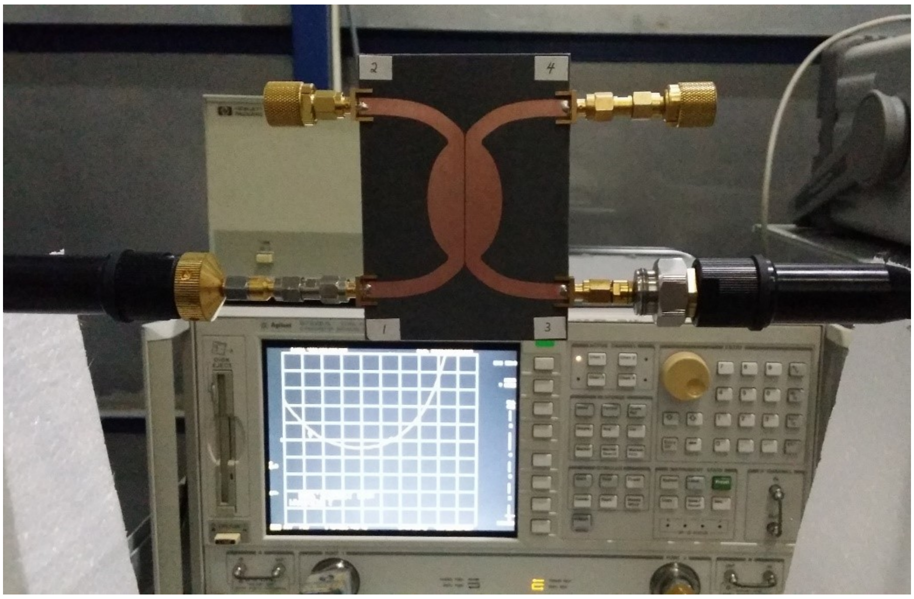

Figure 3.8: Measurement setup for the directional coupler.

The simulation and measurement results are shown in Figure 3.9 to Figure 3.12.

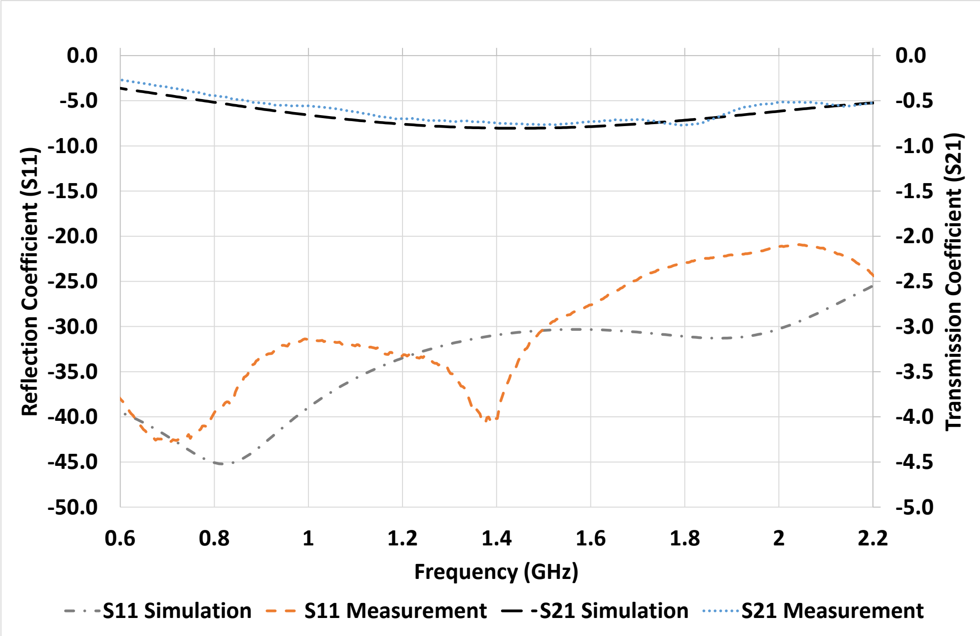

(a)

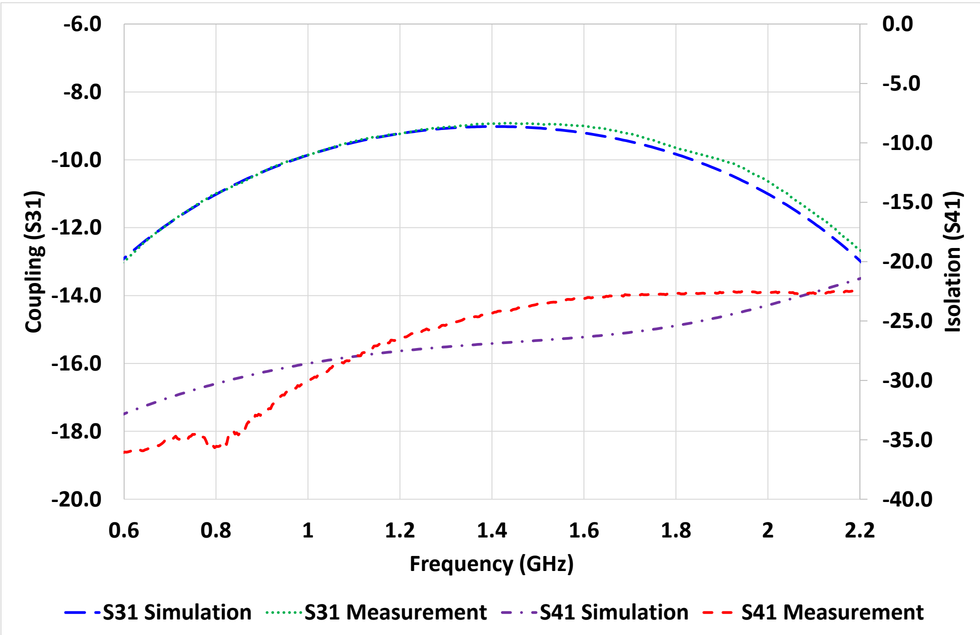

(b)

Figure 3.9: Simulation and measurement results for RT/Duroid 5880, d = 1.575mm. (a) Reflection coefficient and transmission coefficient, and (b) Coupling and isolation.

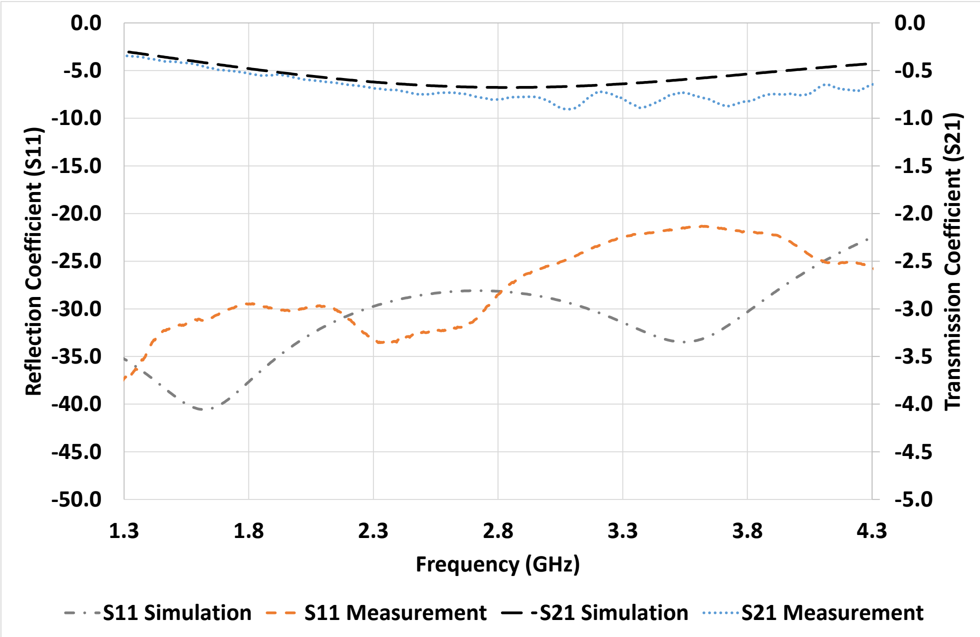

(a)

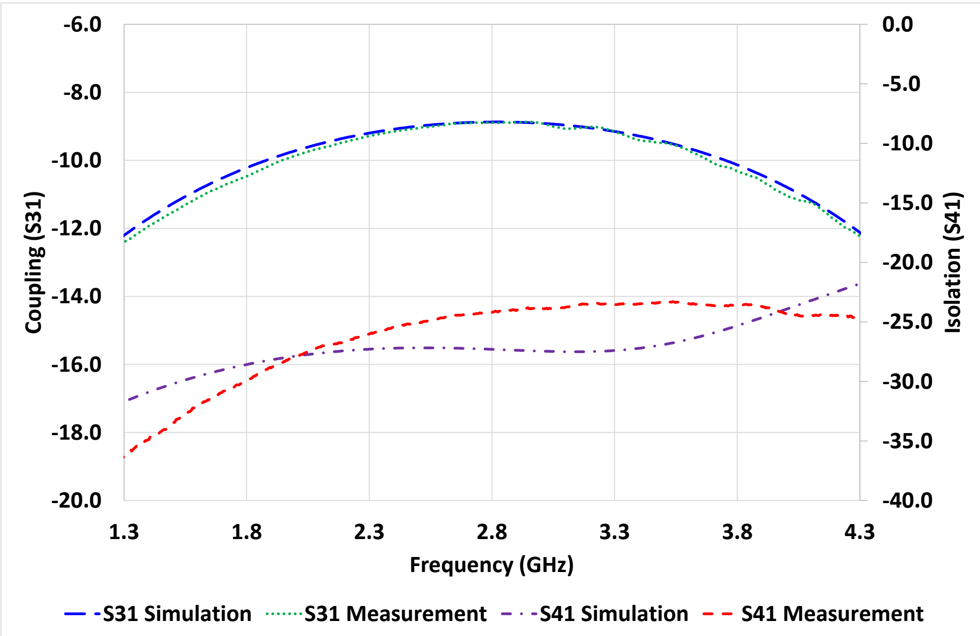

(b)

Figure 3.10: Simulation and measurement results for RT/Duroid 5880, d = 0.787mm. (a) Reflection coefficient and transmission coefficient, and (b) Coupling and isolation.

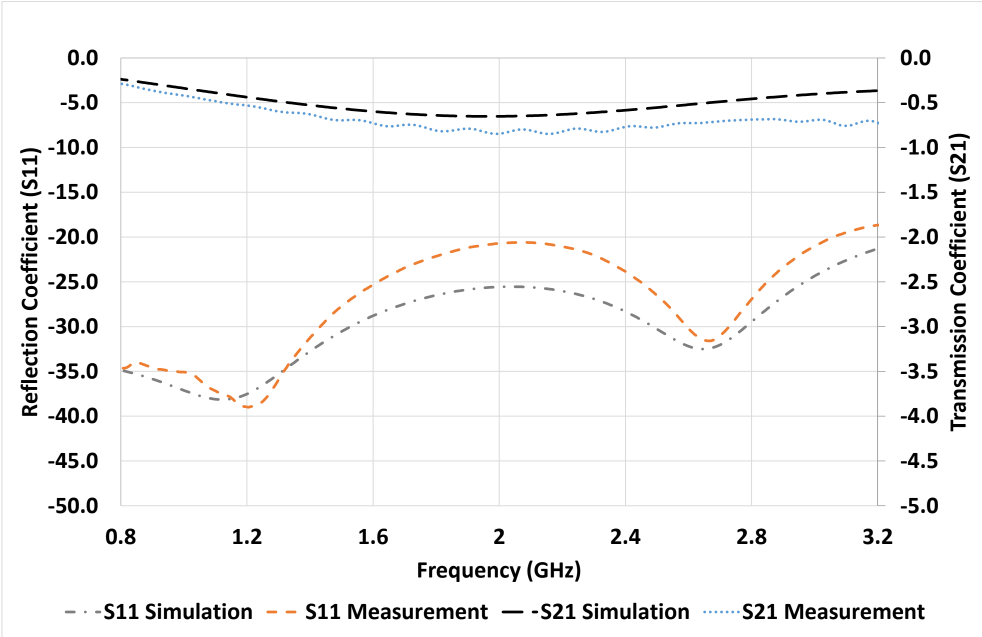

(a)

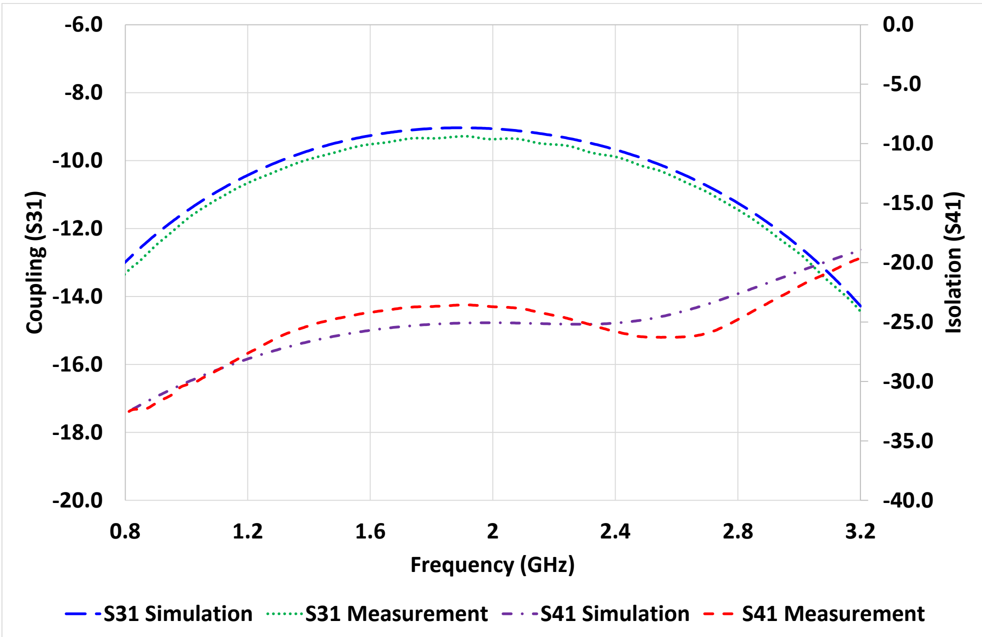

(b)

Figure 3.11: Simulation and measurement results for RO4003C, $d = 1.524$mm. (a) Reflection coefficient and transmission coefficient, and (b) Coupling and isolation.

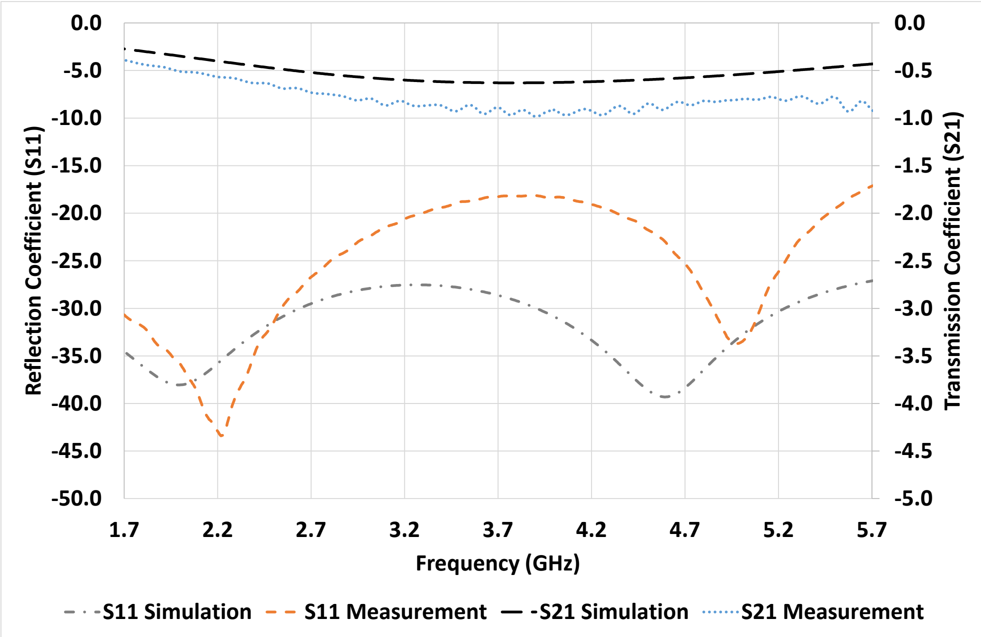

(a)

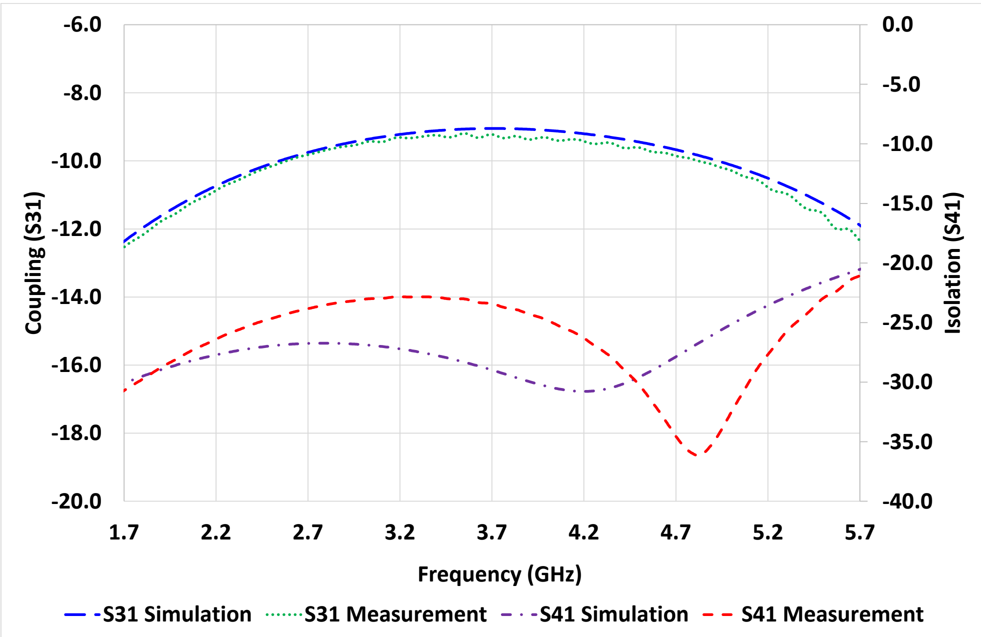

(b)

Figure 3.12: Simulation and measurement results for RO4003C, $d = 0.813$mm. (a) Reflection coefficient and transmission coefficient, and (b) Coupling and isolation.

The center frequencies and the couplers' bandwidths are summarized in Table 3.2 and Table 3.3:

Table 3.2: Simulated and measured center frequencies and bandwidths for RT/Duroid 5880.

	Simulation Results		Measurement Results	
Substrate thickness (mm)	1.575	0.787	1.575	0.787
Center frequency, f_c (GHz)	1.401	2.811	1.420	2.808
Bandwidth (GHz)	1.194	2.490	1.246	2.364
Bandwidth ratio	2.485	2.590	2.564	2.453
Fractional Bandwidth (%)	85.22	88.58	87.77	84.16

Table 3.3: Simulated and measured center frequencies and bandwidths for RO4003C.

	Simulation Results		Measurement Results	
Substrate thickness (mm)	1.524	0.813	1.524	0.813
Center frequency, f_c (GHz)	1.917	3.753	1.922	3.727
Bandwidth (GHz)	1.674	3.306	1.699	3.279
Bandwidth ratio	2.550	2.574	2.583	2.576
Fractional Bandwidth (%)	87.32	88.09	88.37	88.15

The measured insertion loss is generally higher than the simulated results, especially at higher frequencies due to the slight mismatch between the SMA connectors and the microstrip line. Apart from that, the simulation and measurement results for all four couplers agree very well.

Both the simulated and measured center frequencies agree very well with the estimated center frequencies that are calculated using (3.4). The simulation and measurement results show that the proposed coupler design exhibits wideband characteristics.

Figure 3.9 and Figure 3.10 show the simulation and measurement results for the coupler fabricated on RT/Duroid 5880 with a coupling of 10 dB ± 1 dB. The operating frequency range is 0.8 – 2 GHz and 1.6 GHz – 4 GHz for substrate thicknesses of 1.575 mm and 0.787 mm, respectively. Both couplers have a reflection coefficient of better than -20 dB, isolation of better than 22 dB, and insertion loss of less than 1 dB.

For the coupler fabricated on RO4003C with the same coupling factor, the results in Figure 3.11 and Figure 3.12 show that the operating frequency ranges are 1.1 – 2.7 GHz and 2.1 GHz – 5.4 GHz for substrate thicknesses of 1.524 mm and 0.813 mm, respectively. Both couplers have a reflection coefficient of better than -18 dB, isolation of better than 22 dB, and insertion loss of less than 1 dB.

A comparison between the required air gap width between the proposed coupler and parallel microstrip coupler is made and illustrated in Table 3.4. The required air gaps for the proposed 10 dB coupler are 0.512 mm and 0.256 mm for the RT/Duroid 5880 substrate with thicknesses of 1.575 mm and 0.787 mm, respectively. For the RO4003C substrate with thicknesses of 1.524 mm and 0.813 mm, the required air gaps are 0.538 mm and 0.287 mm, respectively. In the case of parallel microstrip couplers, the required air gaps for 10 dB couplers are 0.142 mm and 0.0787 mm for the RT/Duroid 5880 substrate with thicknesses of 1.575 mm and 0.787 mm, respectively. For the RO4003C substrate with thicknesses of 1.524mm and 0.813mm, the required air gaps for 10 dB coupling coefficient become 0.18 mm and 0.106 mm, respectively, in the case of parallel microstrip couplers. The required spacing and tolerance can be difficult for practical implementation, especially when tight coupling is required for substrate with low dielectric constant.

Table 3.4: Comparison of air gap width requirement.

	Required Air Gap width (mm)	
RT/Duroid 5880	Thickness = 1.575 mm	Thickness = 0.787 mm
Microstrip coupler	0.142	0.0787
Proposed design	0.512	0.256
RO4003C	Thickness = 1.524 mm	Thickness = 0.813 mm
Microstrip coupler	0.18	0.106
Proposed design	0.538	0.287

The bandwidth ratio for 10 dB ± 1.5 dB coupling coefficient of the three-layer broadside coupler by Abbosh (2007) is approximately 3.4. Applying the same criteria, the bandwidth ratio for the proposed coupler is approximately 3.2. This shows that the proposed coupler has a bandwidth comparable to the design by Abbosh (2007) despite being a two-layer device. At the same time, the proposed coupler offers similar performance in terms of insertion loss, reflection coefficient and isolation.

3.6 Conclusion

A new wideband directional coupler that is designed using the semi-elliptical edge-coupled structure is presented. This structure consists of two semi-elliptical patches on the top layer and an elliptical defected ground plane on the bottom layer. Sets of design graphs are formulated to facilitate the design of the coupler. The operating frequency and coupling can be controlled by changing the dimensions of the elliptical patch and the width of the air gap. The structure is compact, simple, easy to fabricate and low cost. Both the simulation and measurement results show that the proposed design exhibits wideband characteristic with a bandwidth ratio of more than 2.4 for coupling deviation of ±1 dB. Both of the return loss and the isolation are better than 20 dB, while the insertion loss is less than 1 dB.

CHAPTER 4

DESIGN AND ANALYSIS OF WIDEBAND PHASE SHIFTER

4.1 Introduction

In this chapter, a phase shifter design which requires only two conductive layers is proposed. It uses semi elliptical structures similar to the directional coupler introduced in Chapter 3. One layer consists of an edge-coupled semi-elliptical structure and the other layer consists of an elliptical defected ground plane, as shown in Figure 4.1. Tight coupling to provide different values of phase shift with broadband performance can be achieved without the need for narrow gap width at the coupled region.

4.2 Configuration and Analysis

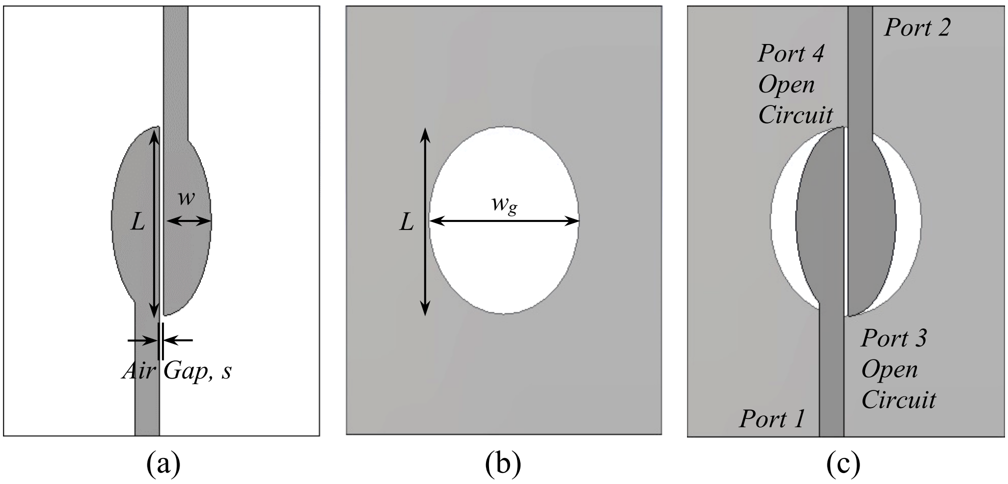

Figure 4.1: Configuration of the proposed phase shifter. (a) Top layer, (b) Bottom layer and (c) overlay of the two layers.

The phase shifter is modeled as a four port device where two of its ports are open circuited. Port 1 and port 2 are the input and output ports, respectively, as shown in Figure 4.1. The performance is defined by its insertion loss, return loss, and the deviation of the differential phase shift. Microstrip lines are included to make connections to the subminiature A (SMA) connectors.

The length and width of the top semi-elliptical line is denoted as *L* and *w*, respectively. The defected ground plane has the same length, *L*, and a width denoted by w_g. The axial ratio of the top elliptical structure is defined as $2w/L$ (denoted as *"ratio")*, whereas the axial ratio of the bottom defected ground is defined as w_g/L (denoted as *"gratio")*.

The input impedance and the two-port Z-parameter of the open-circuited coupled line is given by D. M. Pozar (2011):

$$Z_i = \frac{\sqrt{\left(Z_{0e} - Z_{0o}\right)^2 - \left(Z_{0e} + Z_{0o}\right)^2 \cos^2\theta}}{2\sin\theta} \tag{4.1}$$

$$\begin{bmatrix} Z_{11} & Z_{21} \\ Z_{21} & Z_{22} \end{bmatrix} = \frac{-j}{2}\begin{bmatrix} (Z_{0e} + Z_{0o})\cot\beta l & (Z_{0e} - Z_{0o})\csc\beta l \\ (Z_{0e} - Z_{0o})\csc\beta l & (Z_{0e} + Z_{0o})\cot\beta l \end{bmatrix} \tag{4.2}$$

The reflection coefficient, S_{11} and the transmission coefficient, S_{21} can be obtained from the Z-parameter and expressed as (4.3) and (4.4). The derivation is shown in Appendix B.

$$S_{11} = \frac{\left(1 - C^2\right)\cos^2\theta}{\cos^2\theta - \left(1 + \sin^2\theta\right)C^2 + j2C\cos\theta\sin\theta} \tag{4.3}$$

$$S_{12} = \frac{j2C^2\sin\theta}{\cos^2\theta - \left(1 + \sin^2\theta\right)C^2 + j2C\cos\theta\sin\theta} \tag{4.4}$$

where $C = \left(Z_{0e} - Z_{0o}\right) / \left(Z_{0e} + Z_{0o}\right)$ is the coupling factor and $\theta = \beta l$ is the coupling length.

The phase shift between the input and output signal can be found from (4.4) as:

$$\Phi = 90^o - \tan^{-1}\left(\frac{2C\cos\theta\sin\theta}{\cos^2\theta - \left(1+\sin^2\theta\right)C^2}\right) \tag{4.5}$$

In order to obtain the differential phase shift, a comparison is made with a reference transmission line of length l_m. The differential phase shift, $\Delta\Phi$ can be expressed as:

$$\Delta\Phi = \Phi - \beta_m l_m = 90^o - \tan^{-1}\left(\frac{2C\cos\theta\sin\theta}{\cos^2\theta - \left(1+\sin^2\theta\right)C^2}\right) - \beta_m l_m \tag{4.6}$$

where β_m is the phase constant.

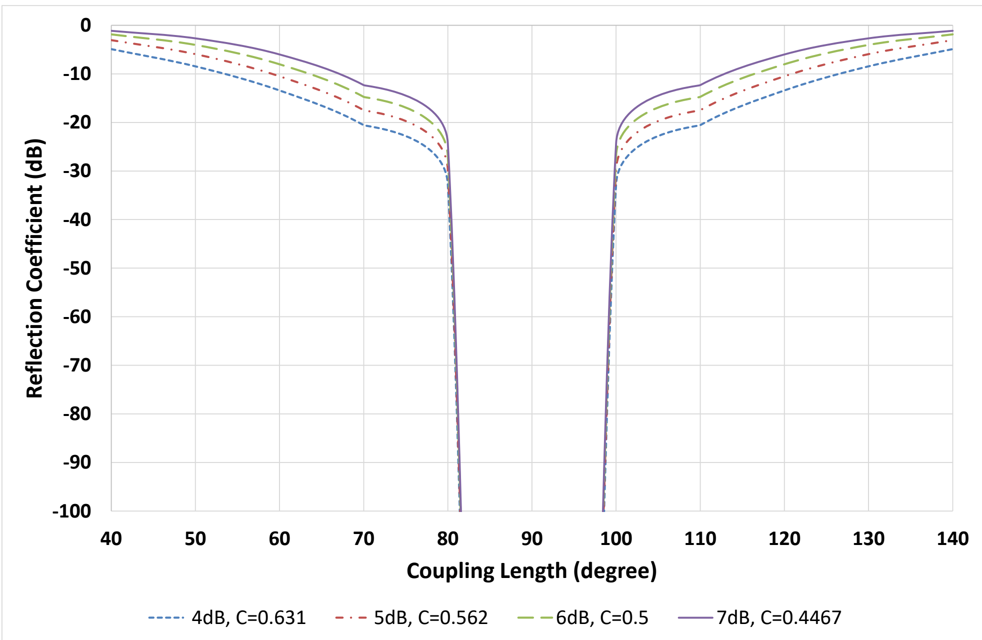

(a)

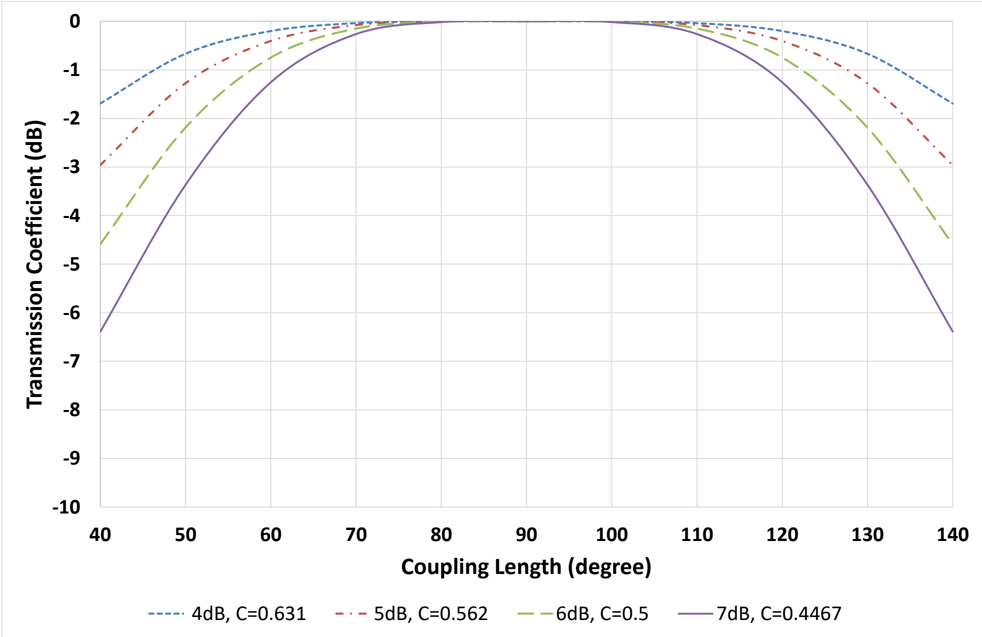

(b)

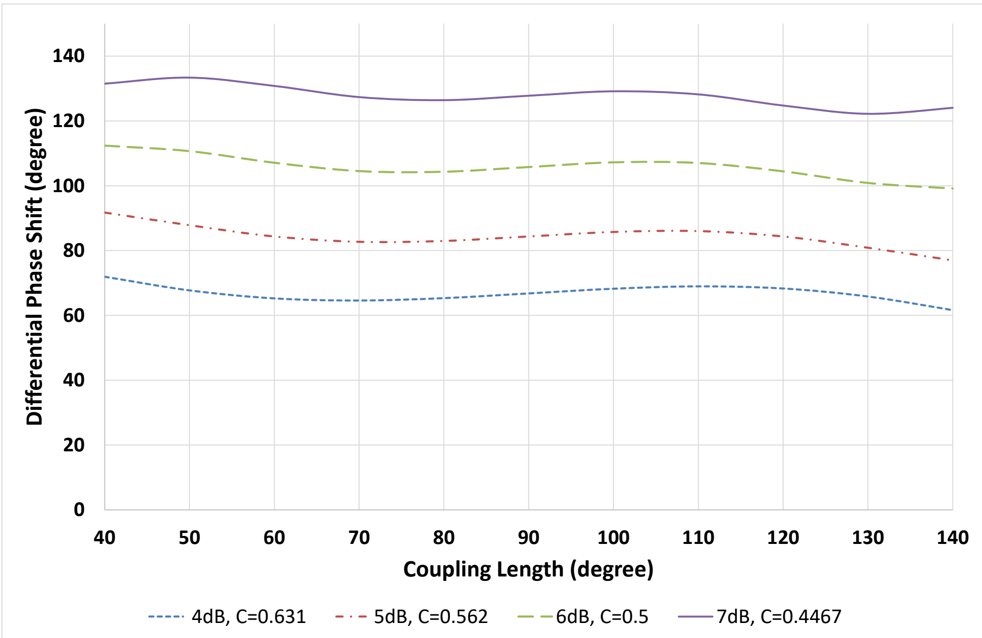

(c)

Figure 4.2: Theoretical estimation of (a) Reflection coefficient, (b) Transmission coefficient, and (c) Differential phase shift.

From Figure 4.2(a) and (b), it can be seen that the operating bandwidth is affected by the coupling factor. Higher coupling factor results in wider bandwidth. Figure 4.2(c) shows the differential phase shift, $\Delta\Phi$ for different coupling factors *C*. Analysis shows that the amount of differential phase shift is inversely proportional to the coupling factor where higher coupling factor results in lower differential phase shift. Hence, it is possible to design a phase shifter with different phase shifts by varying the coupling factor of the proposed structure.

4.3 Design of Wideband Phase Shifter

The design of the proposed phase shifter requires different range of even and odd mode characteristic impedances compared to the design of directional coupler in Chapter 3. This range of impedances can only be obtained through different top patch axial ratios and defected ground axial ratios combinations. Therefore, extended sets of design graphs are generated by varying the ratio *s/d* and *w/d* for various top patch axial ratios and defected ground axial ratios to facilitate the design of the phase shifter, as shown in Figure 4.3 and Figure 4.4 for dielectric constants, ε_r = 2.2 and 3.38, respectively. The design graphs enable one to design the phase shifter directly without the need of EM simulation software. Using these design graphs, the physical dimensions of the phase shifter can be determined and the circuit can be fabricated.

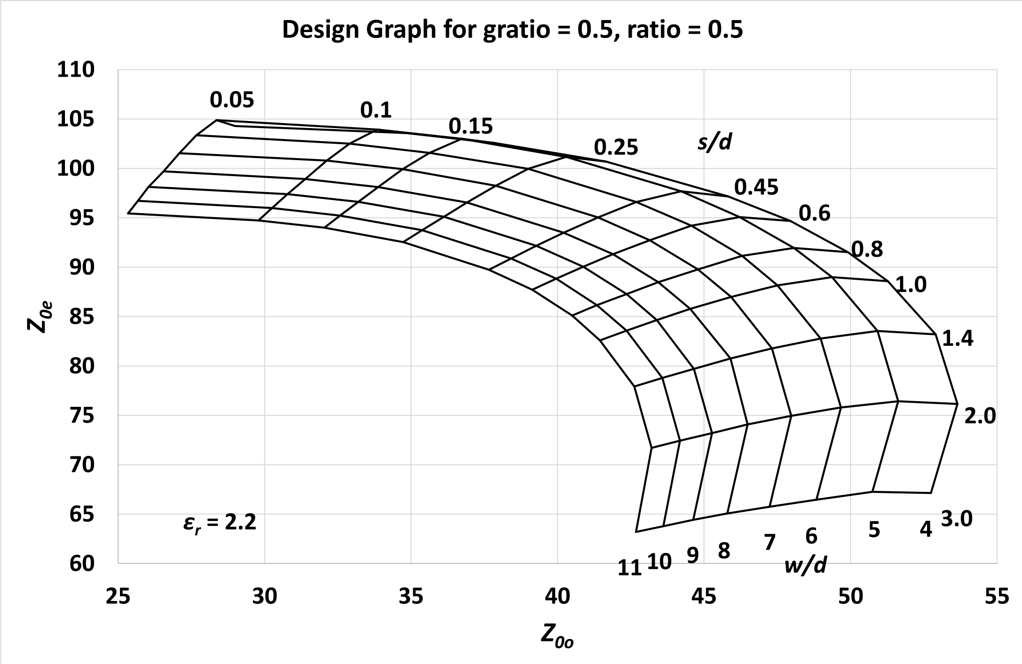
Design Graph for gratio = 0.5, ratio = 0.5
Z_{0e}
Z_{0o}
s/d
w/d
ε_r = 2.2

(a)

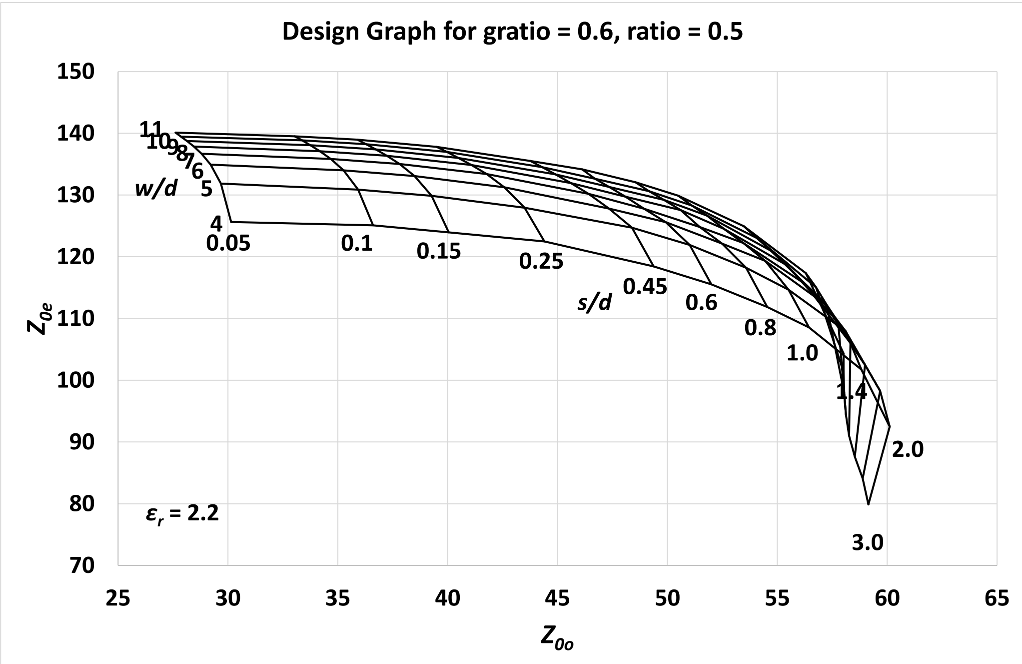
Design Graph for gratio = 0.6, ratio = 0.5
Z_{0e}
Z_{0o}
s/d
w/d
ε_r = 2.2

(b)

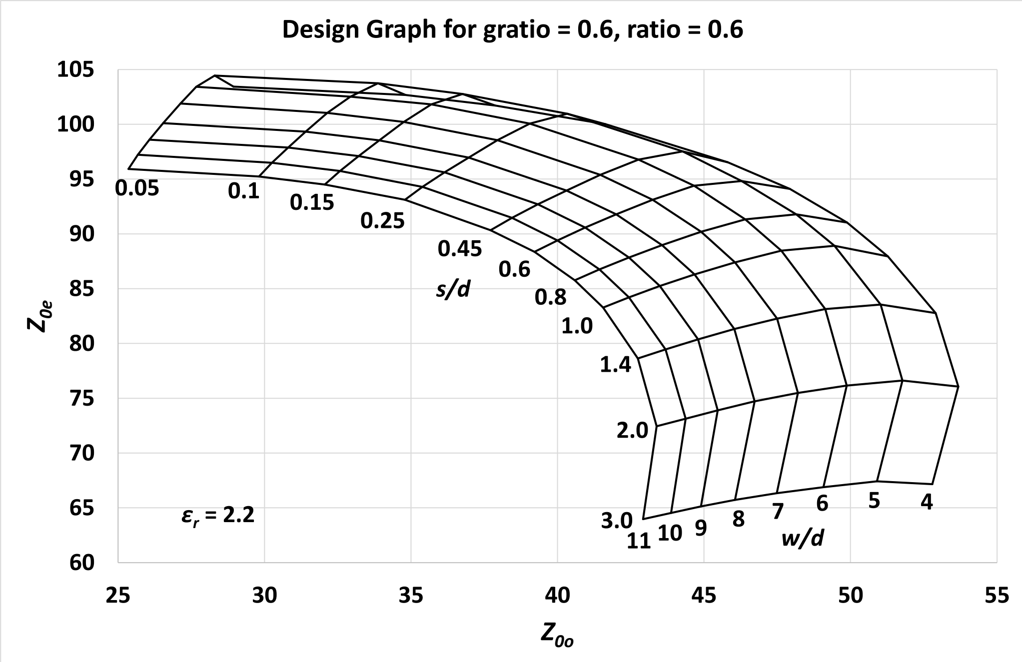
Design Graph for gratio = 0.6, ratio = 0.6
105
100
95
90
85
80
75
70
65
60
25
30
35
40
45
50
55
Z_{0e}
Z_{0o}
0.05
0.1
0.15
0.25
0.45
0.6
0.8
1.0
1.4
2.0
3.0
s/d
11 10 9 8 7 6 5 4
w/d
ε_r = 2.2

(c)

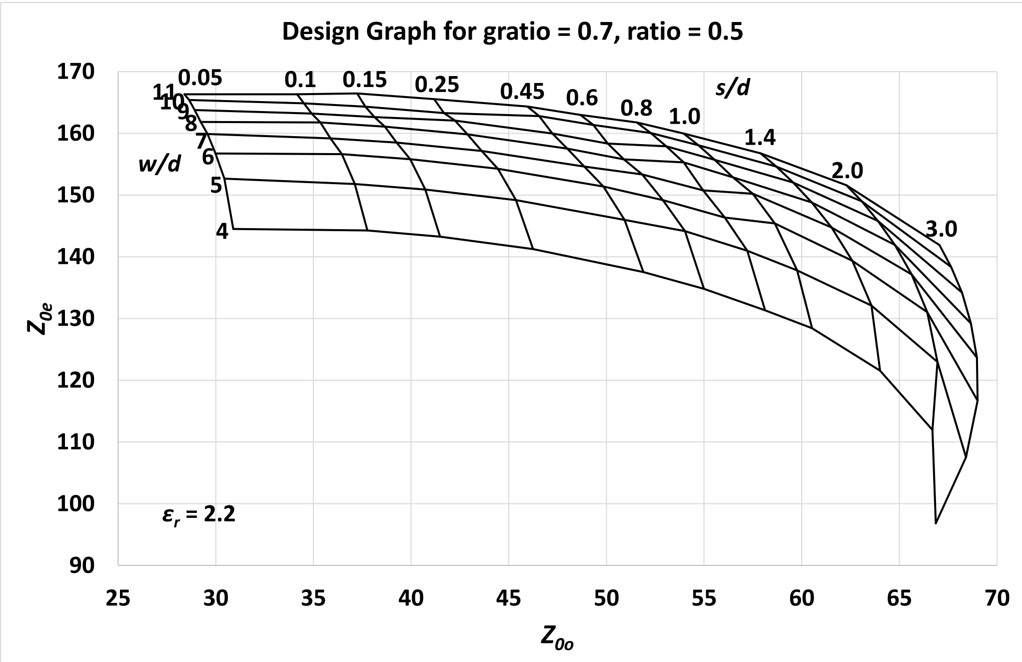
Design Graph for gratio = 0.7, ratio = 0.5
170
160
150
140
130
120
110
100
90
25
30
35
40
45
50
55
60
65
70
Z_{0e}
Z_{0o}
0.05 0.1 0.15 0.25 0.45 0.6 0.8 1.0 1.4 2.0 3.0
s/d
11 10 9 8 7 6 5 4
w/d
ε_r = 2.2

(d)

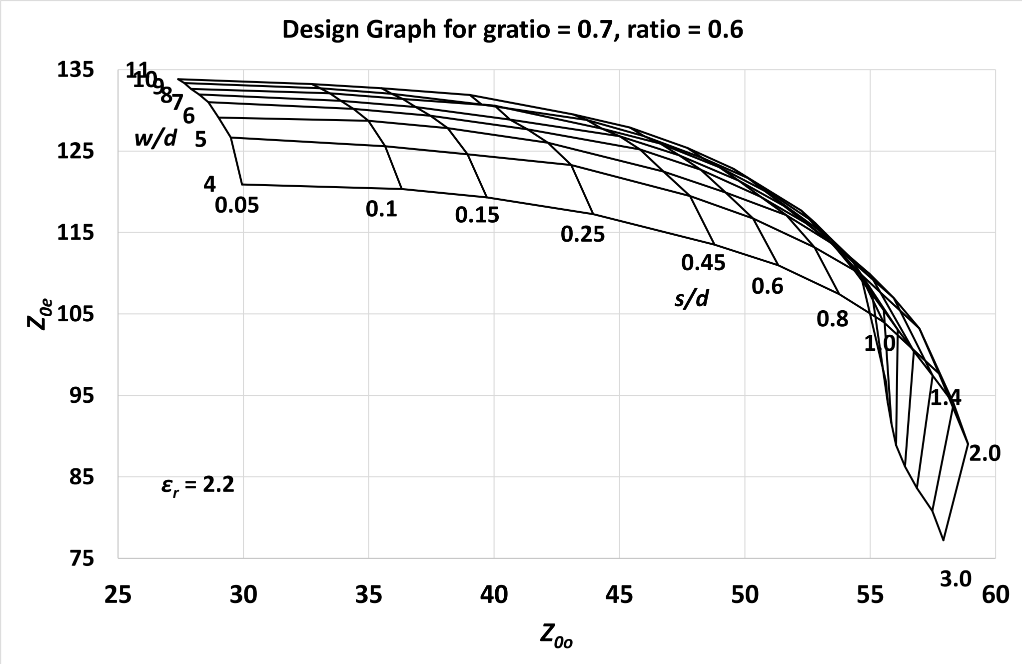
Design Graph for gratio = 0.7, ratio = 0.6
135
125
115
105
95
85
75
25
30
35
40
45
50
55
60
Z_{0e}
Z_{0o}
11
10
9
8
7
6
w/d
5
4
0.05
0.1
0.15
0.25
0.45
0.6
s/d
0.8
1.0
1.4
2.0
3.0
ε_r = 2.2

(e)

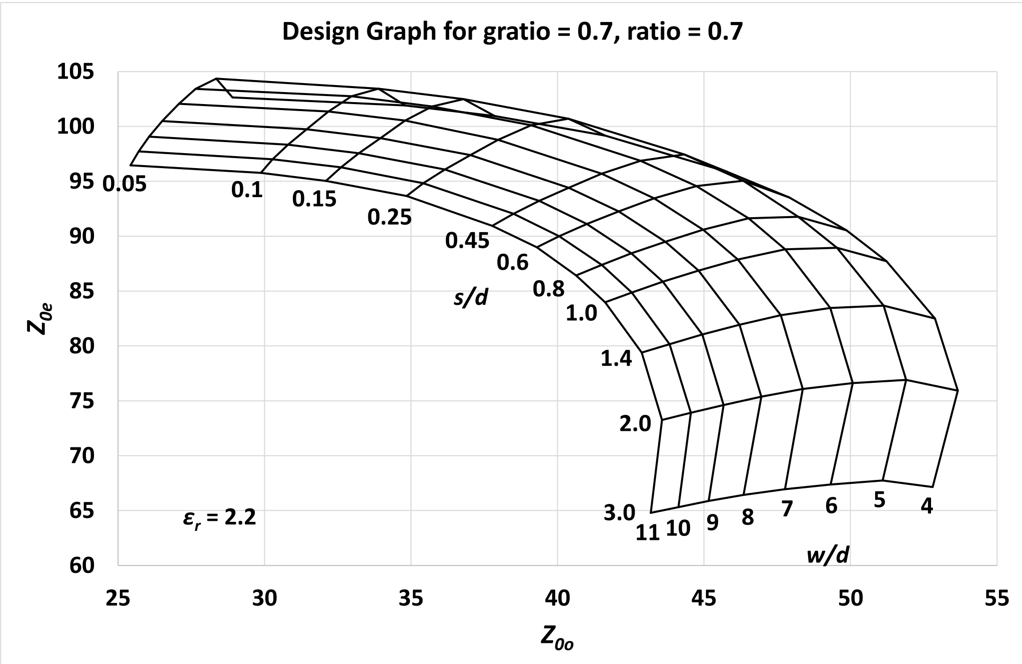
Design Graph for gratio = 0.7, ratio = 0.7
105
100
95
90
85
80
75
70
65
60
25
30
35
40
45
50
55
Z_{0e}
Z_{0o}
0.05
0.1
0.15
0.25
0.45
0.6
0.8
s/d
1.0
1.4
2.0
3.0
11
10
9
8
7
6
5
4
w/d
ε_r = 2.2

(f)

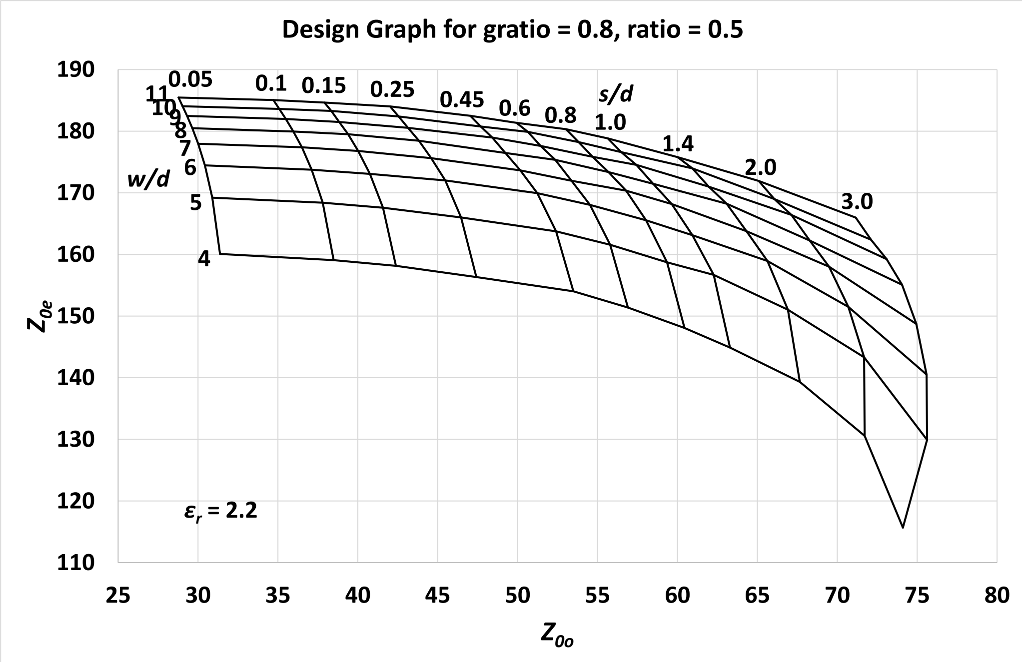
Design Graph for gratio = 0.8, ratio = 0.5
0.05
0.1
0.15
0.25
0.45
0.6
0.8
s/d
1.0
1.4
2.0
3.0
11
10
9
8
7
6
w/d
5
4
ε_r = 2.2
Z_0e
Z_0o
190
180
170
160
150
140
130
120
110
25
30
35
40
45
50
55
60
65
70
75
80

(g)

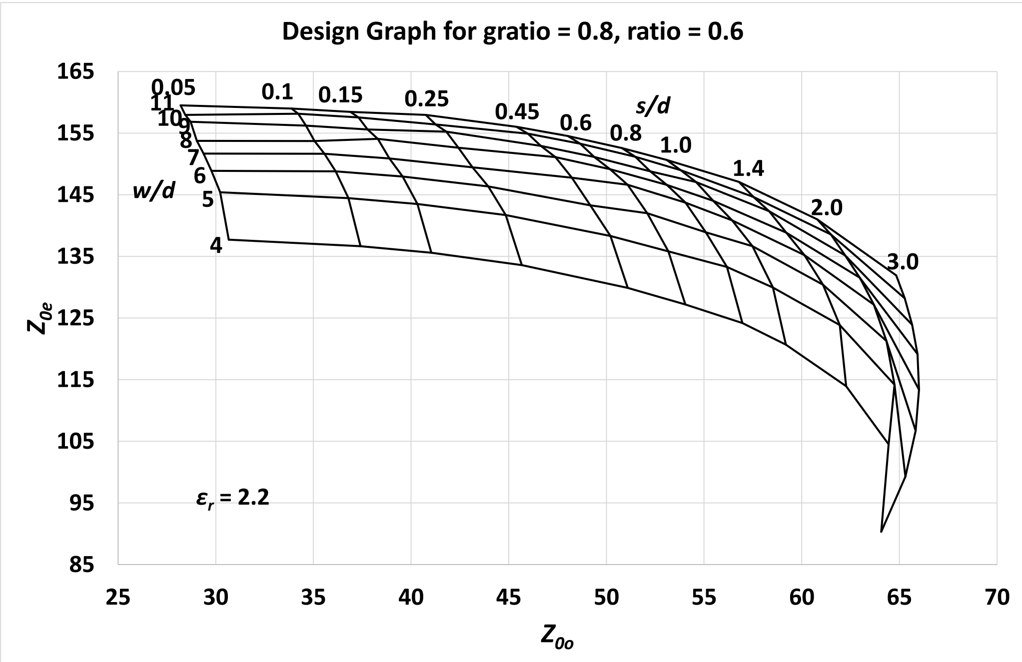
Design Graph for gratio = 0.8, ratio = 0.6
0.05
0.1
0.15
0.25
0.45
0.6
0.8
s/d
1.0
1.4
2.0
3.0
11
10
9
8
7
6
w/d
5
4
ε_r = 2.2
Z_0e
Z_0o
165
155
145
135
125
115
105
95
85
25
30
35
40
45
50
55
60
65
70

(h)

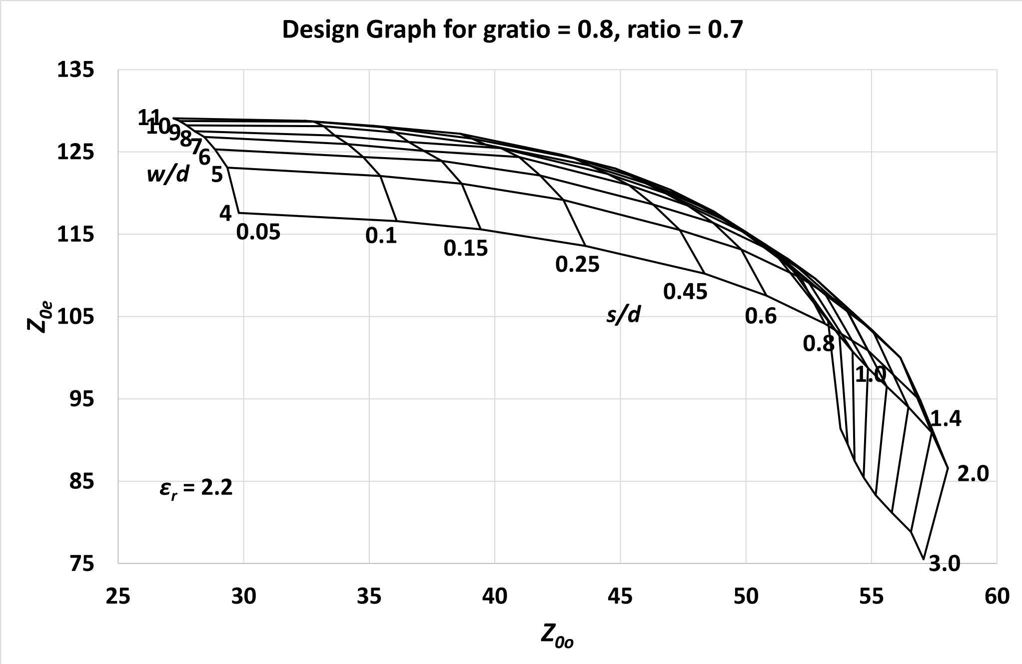
Design Graph for gratio = 0.8, ratio = 0.7
w/d
11
10
9
8
7
6
5
4
s/d
0.05
0.1
0.15
0.25
0.45
0.6
0.8
1.0
1.4
2.0
3.0
εr = 2.2
Z0e
Z0o
135
125
115
105
95
85
75
25
30
35
40
45
50
55
60

(i)

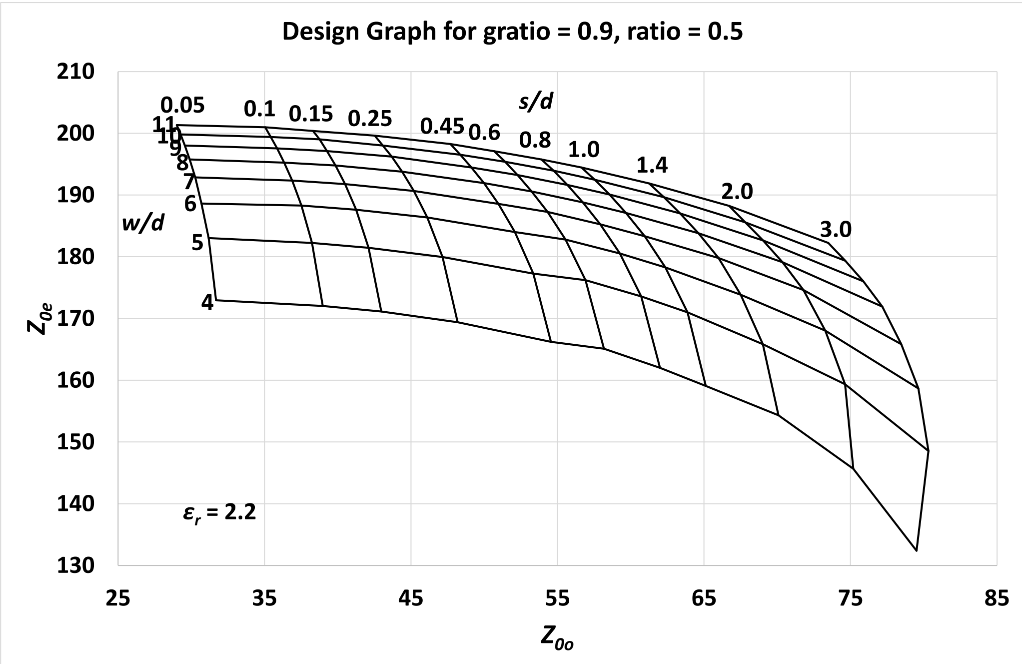
Design Graph for gratio = 0.9, ratio = 0.5
s/d
0.05
0.1
0.15
0.25
0.45
0.6
0.8
1.0
1.4
2.0
3.0
w/d
11
10
9
8
7
6
5
4
εr = 2.2
Z0e
Z0o
210
200
190
180
170
160
150
140
130
25
35
45
55
65
75
85

(j)

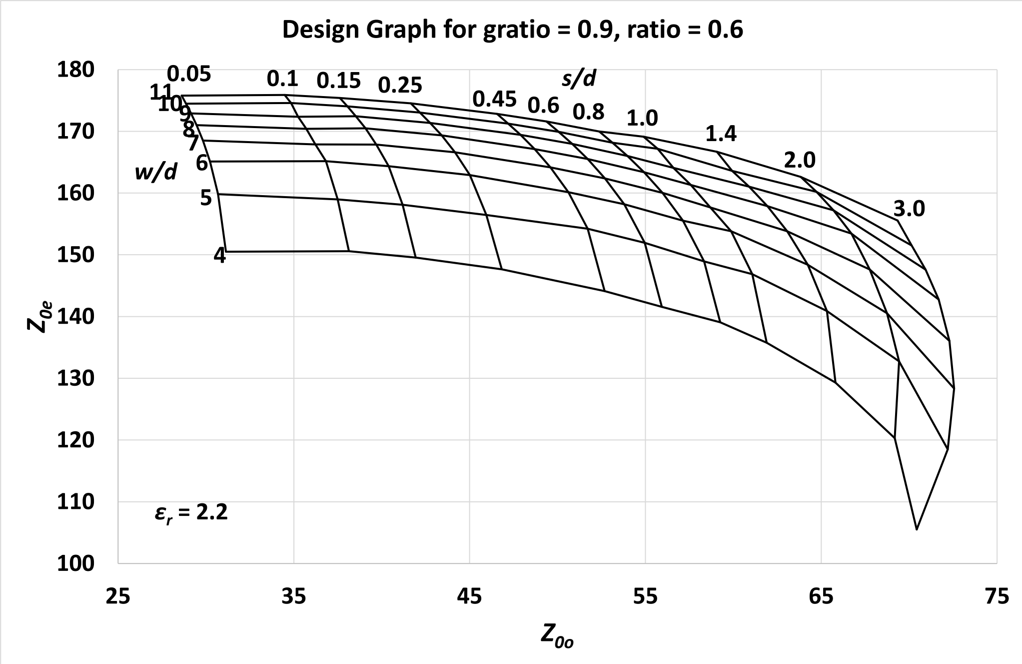

Design Graph for gratio = 0.9, ratio = 0.6
s/d
0.05
0.1
0.15
0.25
0.45
0.6
0.8
1.0
1.4
2.0
3.0
w/d
11
10
9
8
7
6
5
4
ε_r = 2.2
Z_{0e}
180
170
160
150
140
130
120
110
100
Z_{0o}
25
35
45
55
65
75

(k)

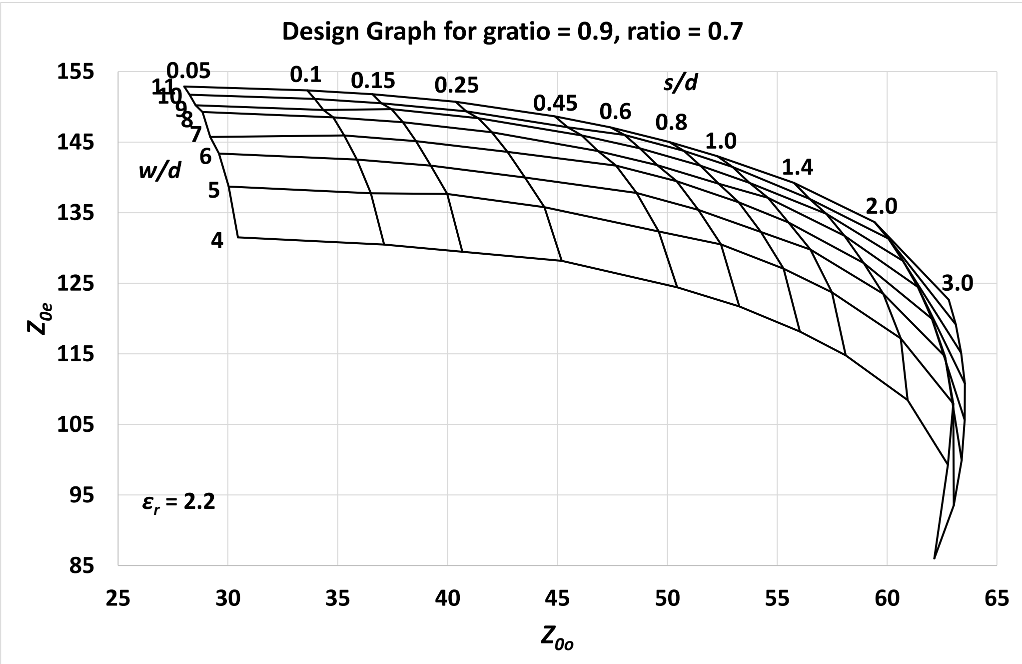

Design Graph for gratio = 0.9, ratio = 0.7
s/d
0.05
0.1
0.15
0.25
0.45
0.6
0.8
1.0
1.4
2.0
3.0
w/d
11
10
9
8
7
6
5
4
ε_r = 2.2
Z_{0e}
155
145
135
125
115
105
95
85
Z_{0o}
25
30
35
40
45
50
55
60
65

(l)

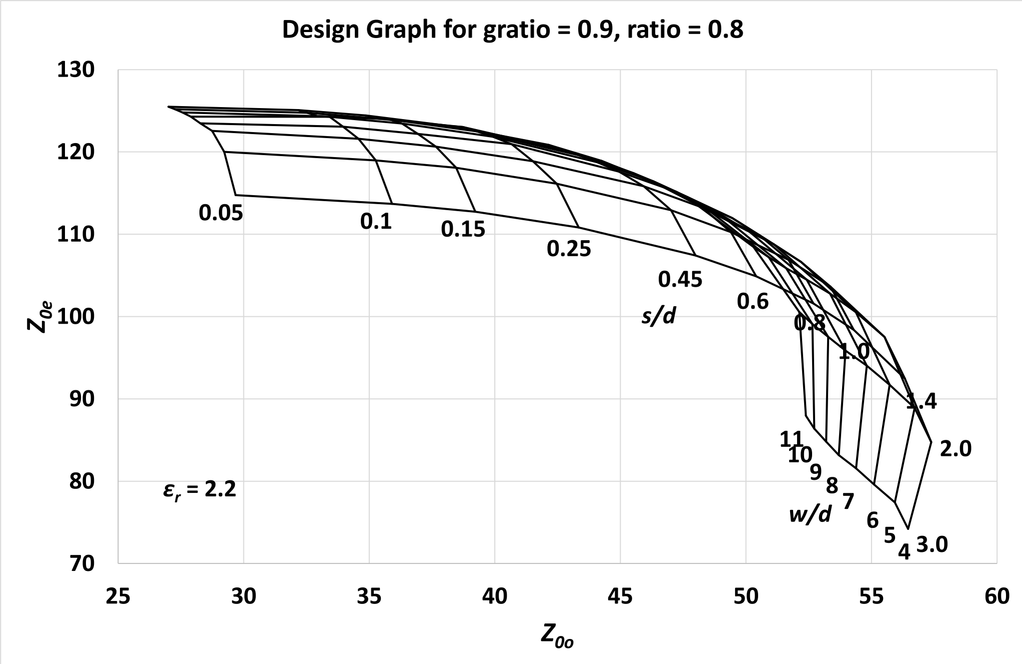

Design Graph for gratio = 0.9, ratio = 0.8
130
120
110
100
90
80
70
25
30
35
40
45
50
55
60
Z_{0e}
Z_{0o}
0.05
0.1
0.15
0.25
0.45
0.6
0.8
1.0
1.4
2.0
3.0
s/d
11
10
9
8
7
6
5
4
w/d
ε_r = 2.2

(m)

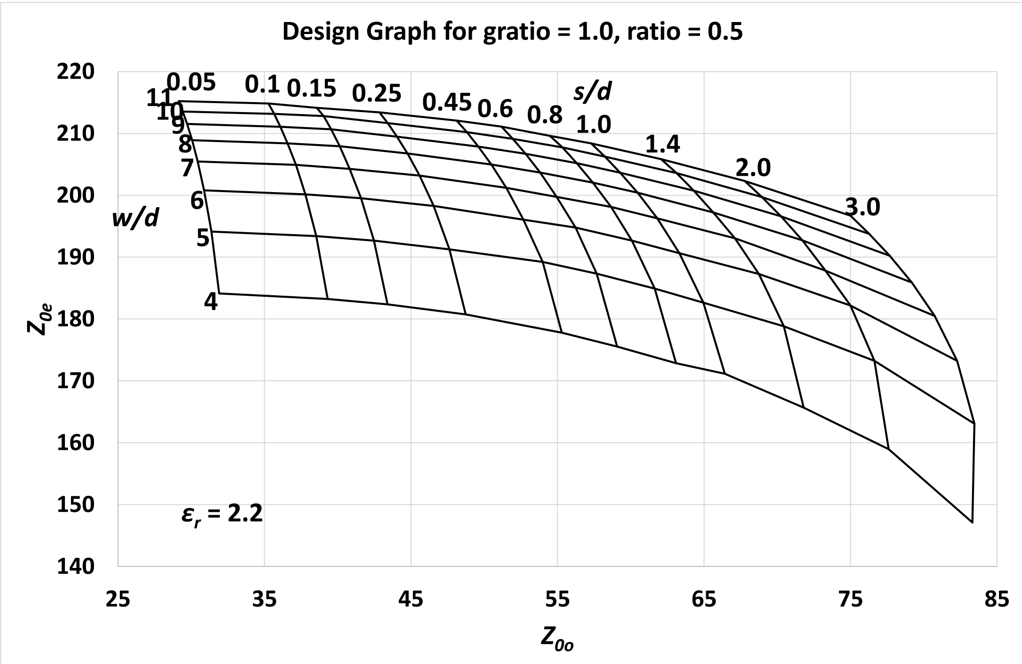

Design Graph for gratio = 1.0, ratio = 0.5
220
210
200
190
180
170
160
150
140
25
35
45
55
65
75
85
Z_{0e}
Z_{0o}
0.05
0.1
0.15
0.25
0.45
0.6
0.8
1.0
1.4
2.0
3.0
s/d
11
10
9
8
7
6
5
4
w/d
ε_r = 2.2

(n)

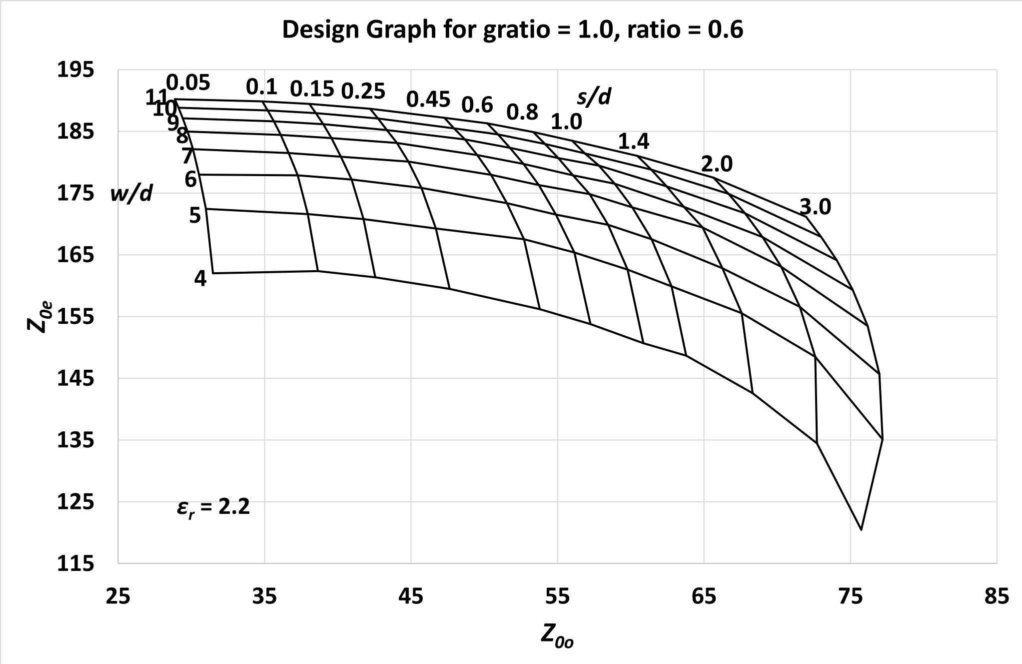
Design Graph for gratio = 1.0, ratio = 0.6
s/d
0.05
0.1
0.15
0.25
0.45
0.6
0.8
1.0
1.4
2.0
3.0
w/d
11
10
9
8
7
6
5
4
ε_r = 2.2
Z_{0e}
Z_{0o}
195
185
175
165
155
145
135
125
115
25
35
45
55
65
75
85

(o)

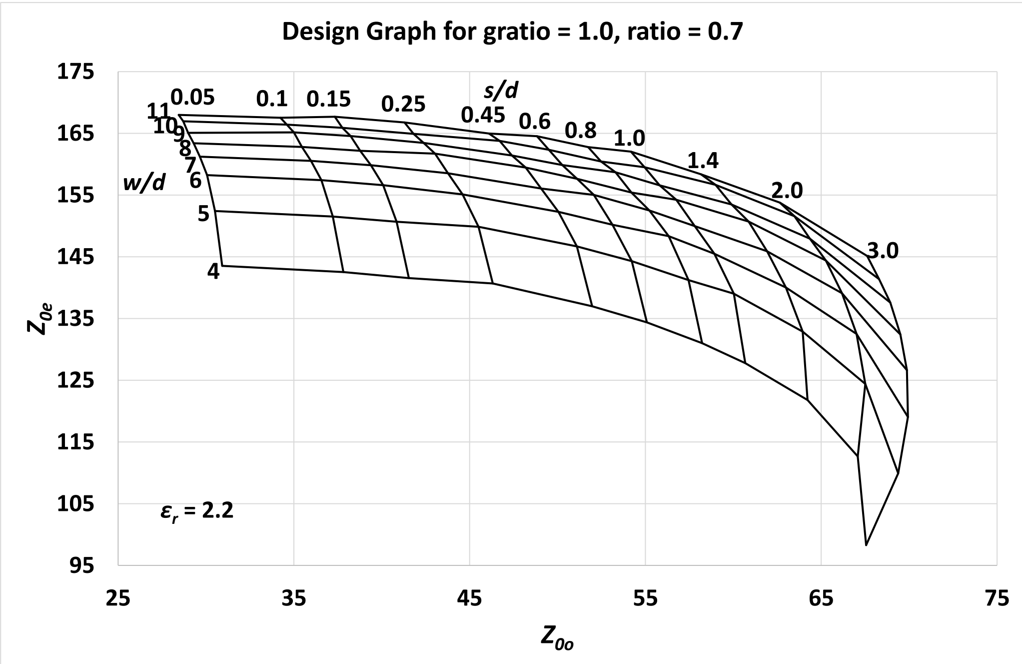
Design Graph for gratio = 1.0, ratio = 0.7
s/d
0.05
0.1
0.15
0.25
0.45
0.6
0.8
1.0
1.4
2.0
3.0
w/d
11
10
9
8
7
6
5
4
ε_r = 2.2
Z_{0e}
Z_{0o}
175
165
155
145
135
125
115
105
95
25
35
45
55
65
75

(p)

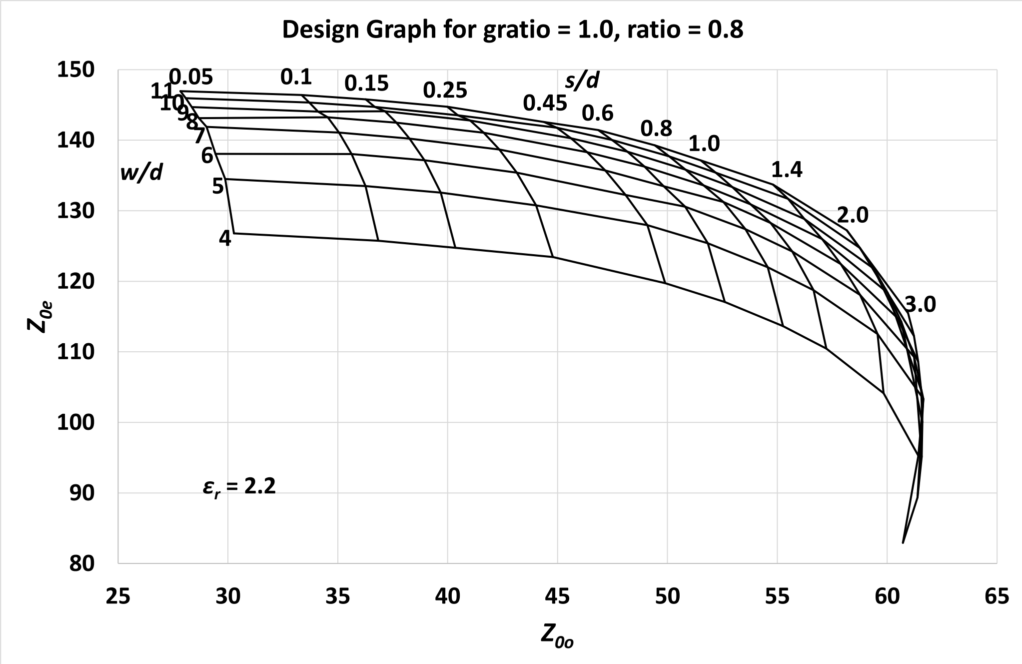

(q)

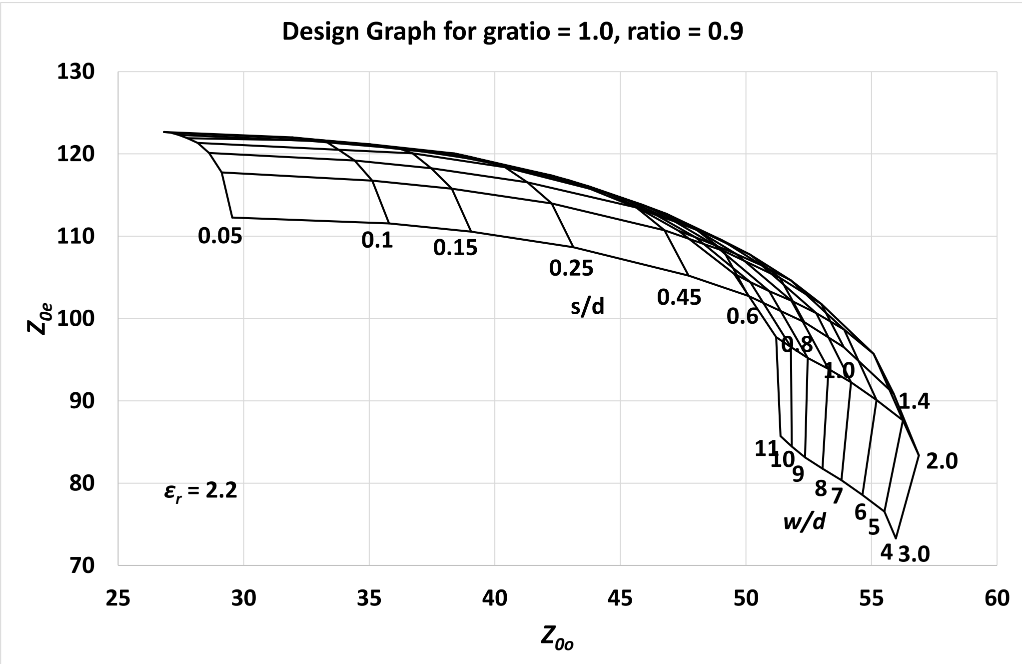

(r)

Figure 4.3: Design graphs for $\varepsilon_r = 2.2$ (a) gratio = 0.5, ratio = 0.5, (b) gratio = 0.6, ratio = 0.5, (c) gratio = 0.6, ratio = 0.6, (d) gratio = 0.7, ratio = 0.5, (e) gratio = 0.7, ratio = 0.6, (f) gratio = 0.7, ratio = 0.7, (g) gratio = 0.8, ratio = 0.5, (h) gratio = 0.8, ratio = 0.6, (i) gratio = 0.8, ratio = 0.7, (j) gratio = 0.9, ratio = 0.5, (k) gratio = 0.9, ratio = 0.6, (l) gratio = 0.9, ratio = 0.7, (m) gratio = 0.9, ratio = 0.8, (n) gratio = 1.0, ratio = 0.5, (o) gratio = 1.0, ratio = 0.6, (p) gratio = 1.0, ratio = 0.7, (q) gratio = 1.0, ratio = 0.8, and (r) gratio = 1.0, ratio = 0.9.

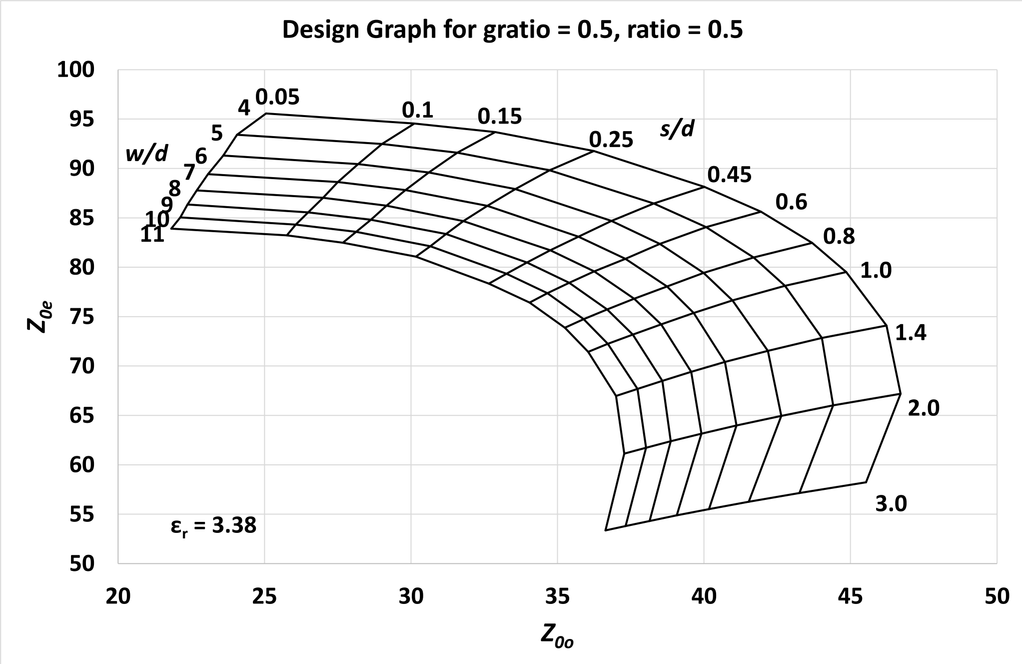

Design Graph for gratio = 0.5, ratio = 0.5
w/d
s/d
0.05
0.1
0.15
0.25
0.45
0.6
0.8
1.0
1.4
2.0
3.0
4
5
6
7
8
9
10
11
ε_r = 3.38
Z_0e
Z_0o

(a)

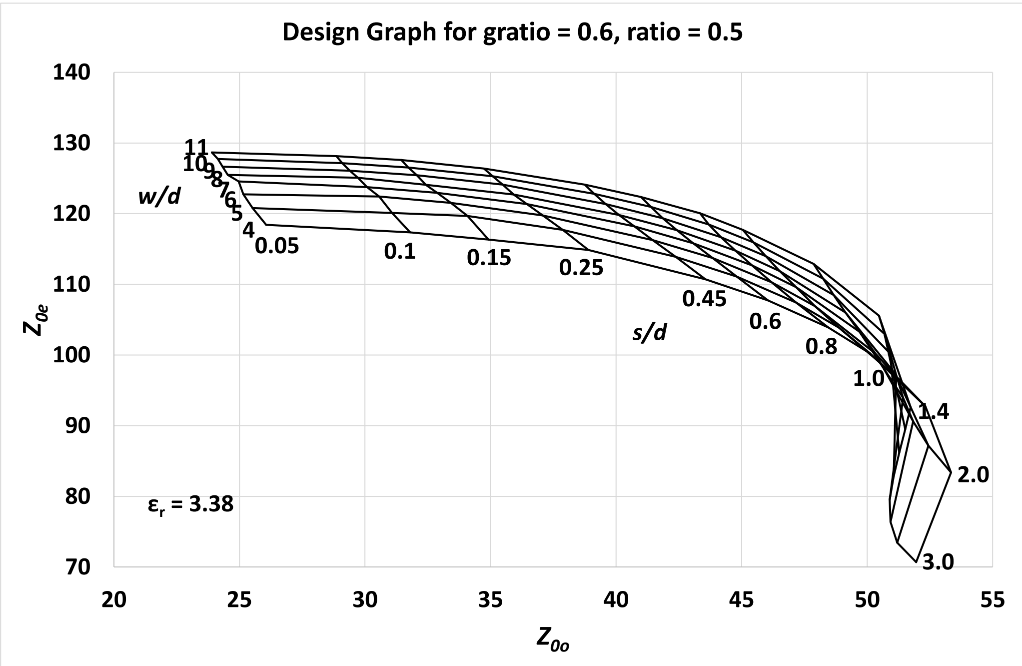

Design Graph for gratio = 0.6, ratio = 0.5
w/d
s/d
11
10
9
8
7
6
5
4
0.05
0.1
0.15
0.25
0.45
0.6
0.8
1.0
1.4
2.0
3.0
ε_r = 3.38
Z_0e
Z_0o

(b)

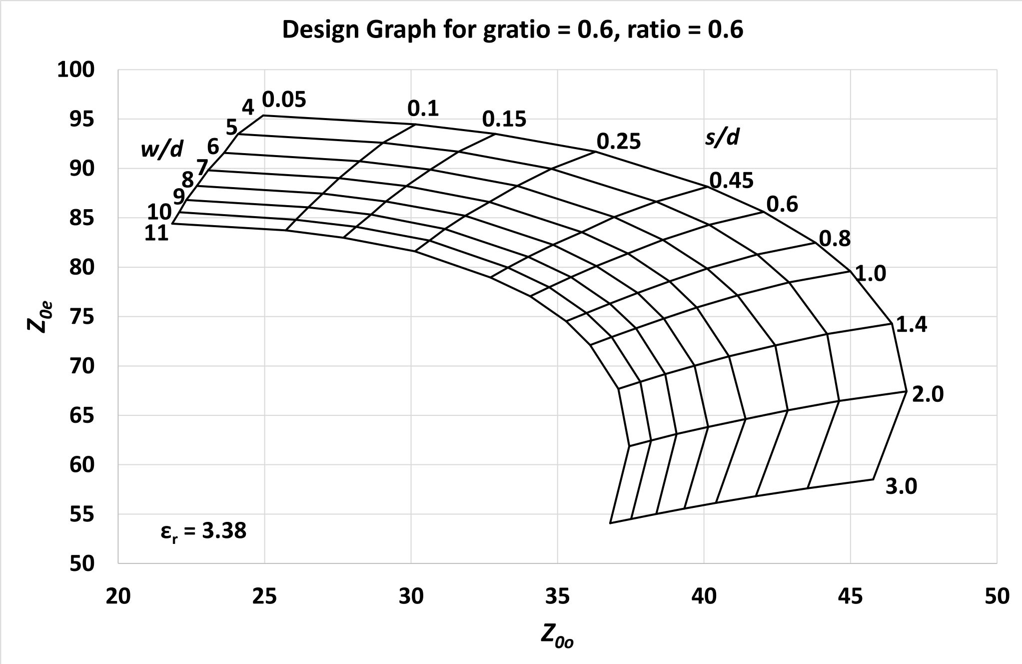
Design Graph for gratio = 0.6, ratio = 0.6
Z0e
Z0o
w/d
s/d
4
5
6
7
8
9
10
11
0.05
0.1
0.15
0.25
0.45
0.6
0.8
1.0
1.4
2.0
3.0
εr = 3.38

(c)

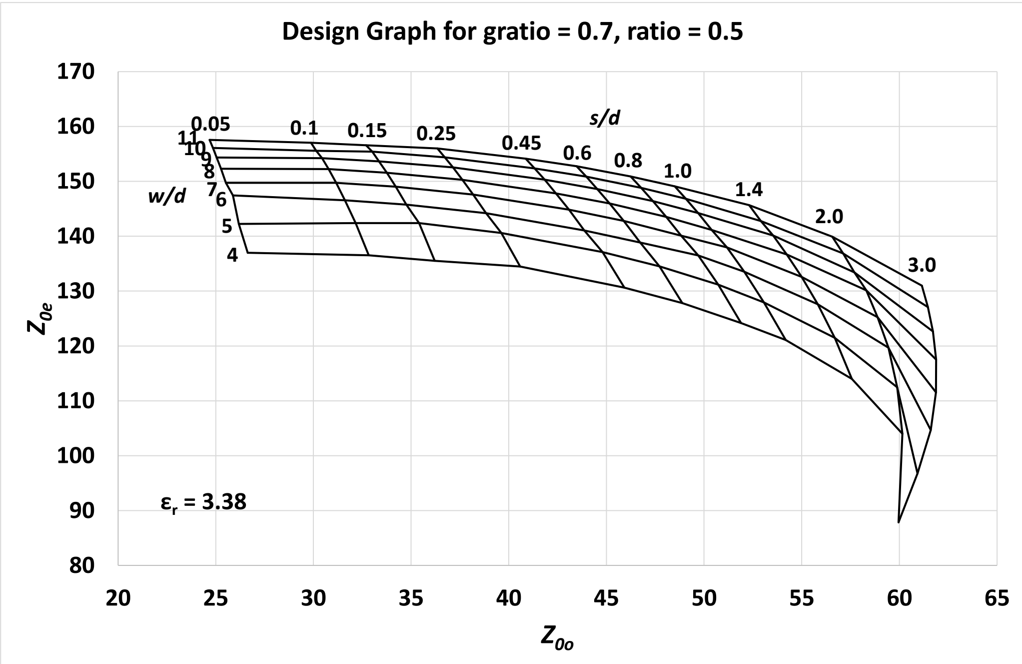
Design Graph for gratio = 0.7, ratio = 0.5
Z0e
Z0o
w/d
s/d
11
10
9
8
7
6
5
4
0.05
0.1
0.15
0.25
0.45
0.6
0.8
1.0
1.4
2.0
3.0
εr = 3.38

(d)

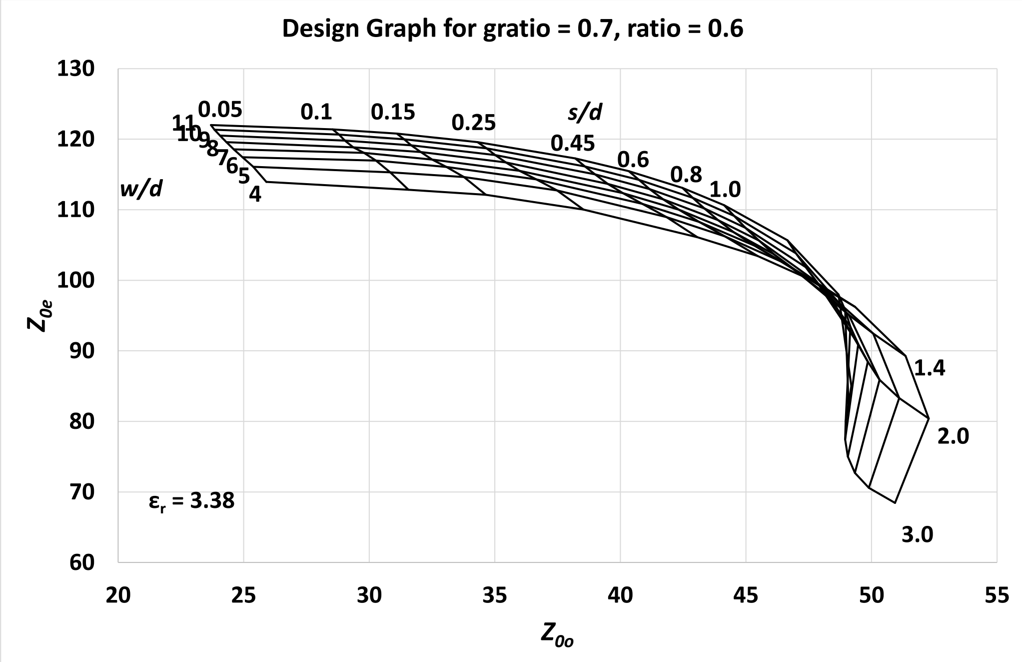
Design Graph for gratio = 0.7, ratio = 0.6
s/d
0.05
0.1
0.15
0.25
0.45
0.6
0.8
1.0
1.4
2.0
3.0
w/d
11
10
9
8
7
6
5
4
ε_r = 3.38
Z_0e
Z_0o

(e)

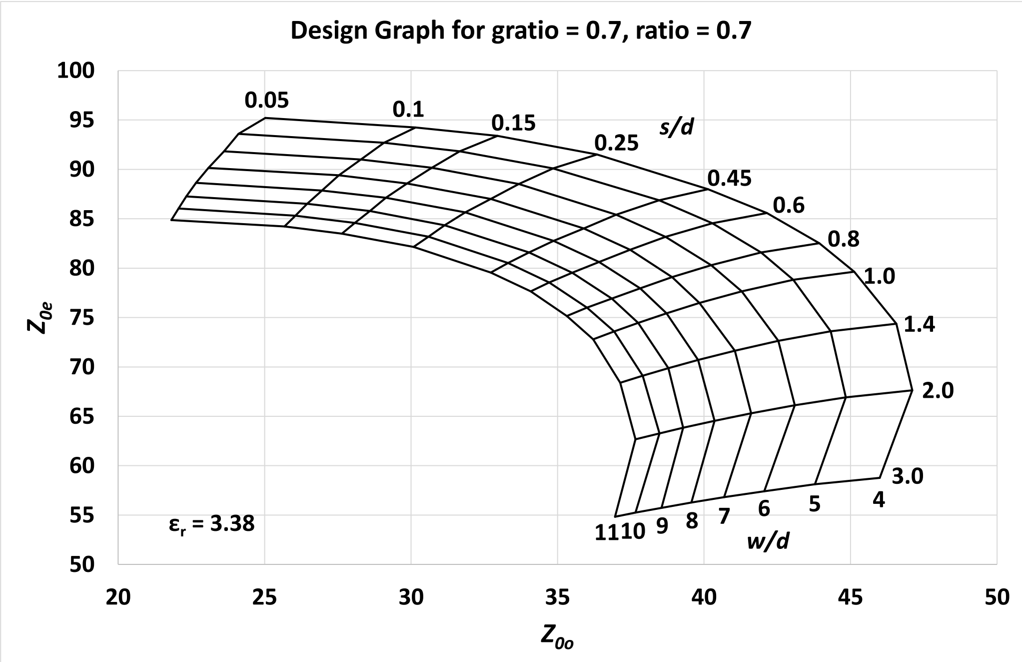
Design Graph for gratio = 0.7, ratio = 0.7
s/d
0.05
0.1
0.15
0.25
0.45
0.6
0.8
1.0
1.4
2.0
3.0
w/d
11
10
9
8
7
6
5
4
ε_r = 3.38
Z_0e
Z_0o

(f)

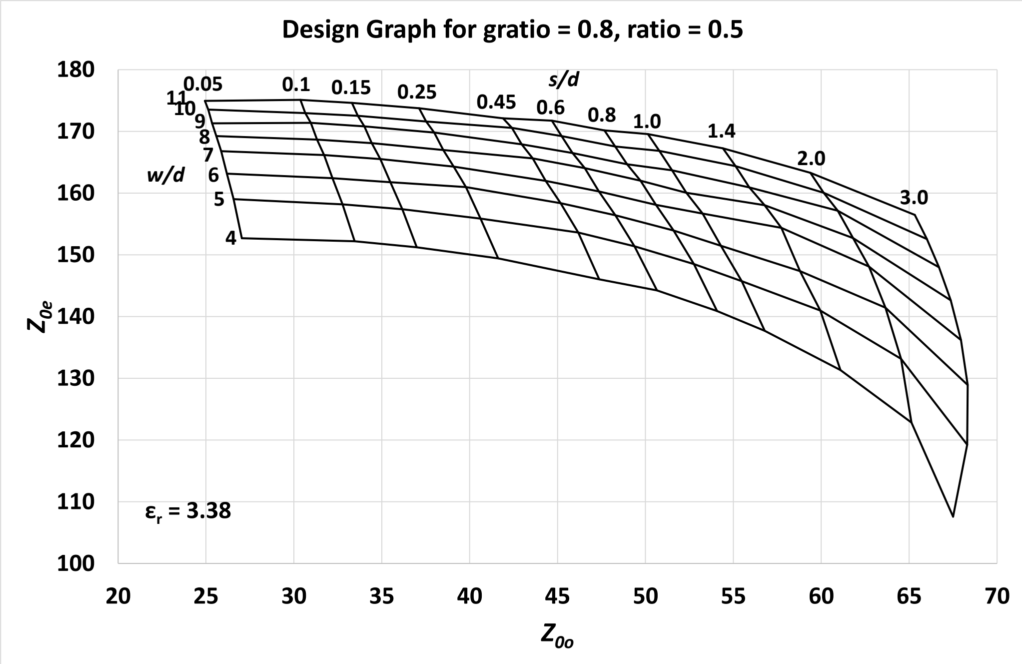

Design Graph for gratio = 0.8, ratio = 0.5
s/d
0.05 0.1 0.15 0.25 0.45 0.6 0.8 1.0 1.4 2.0 3.0
w/d
11 10 9 8 7 6 5 4
ε_r = 3.38
Z_{0e}
Z_{0o}
180 170 160 150 140 130 120 110 100
20 25 30 35 40 45 50 55 60 65 70

(g)

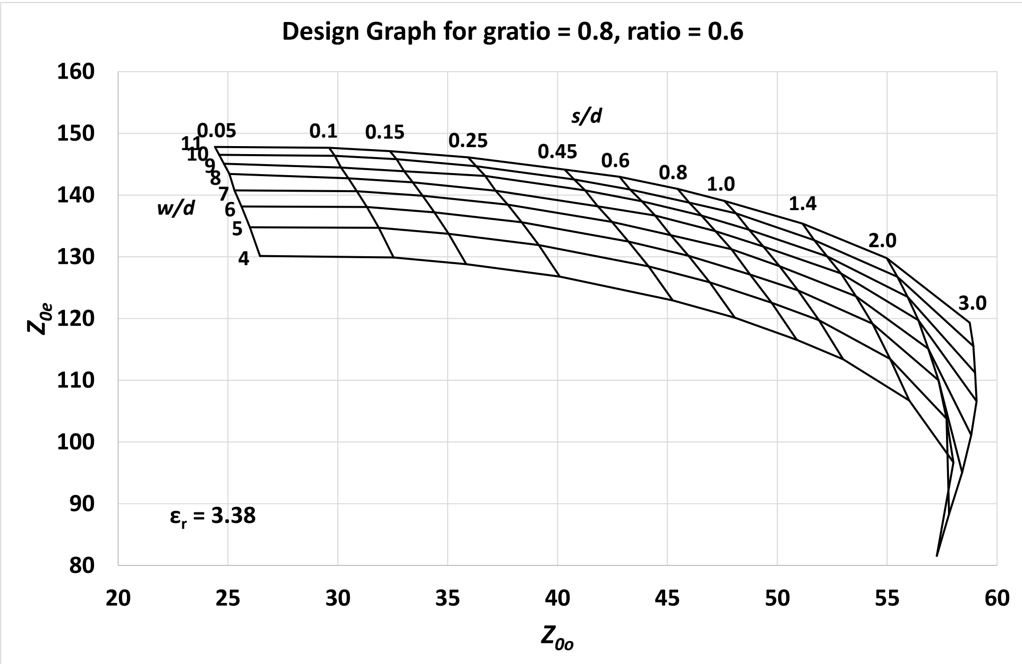

Design Graph for gratio = 0.8, ratio = 0.6
s/d
0.05 0.1 0.15 0.25 0.45 0.6 0.8 1.0 1.4 2.0 3.0
w/d
11 10 9 8 7 6 5 4
ε_r = 3.38
Z_{0e}
Z_{0o}
160 150 140 130 120 110 100 90 80
20 25 30 35 40 45 50 55 60

(h)

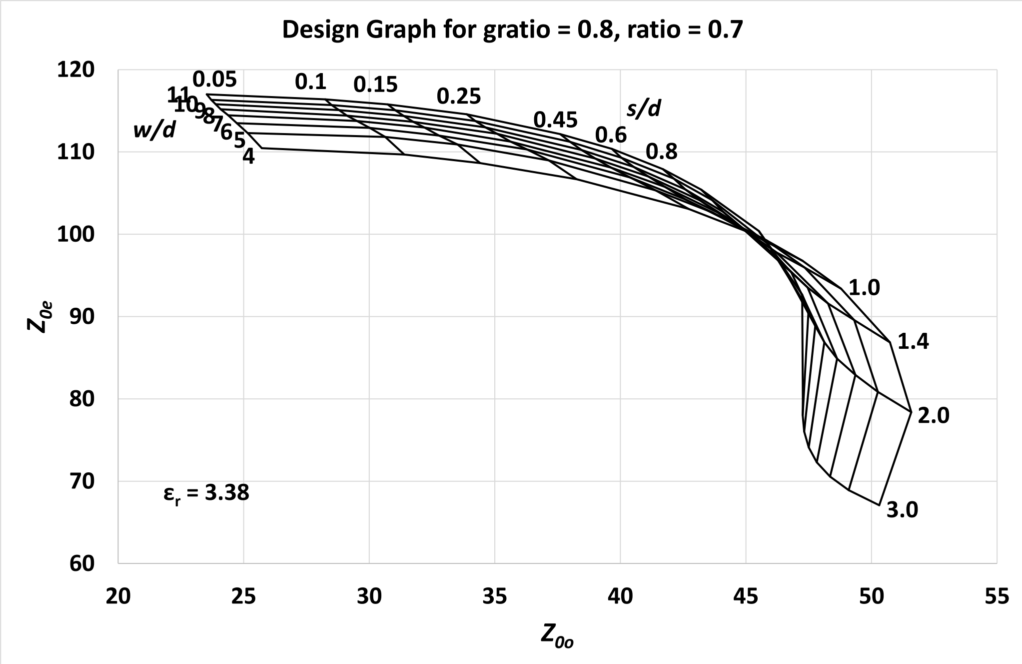

Design Graph for gratio = 0.8, ratio = 0.7
s/d
0.05
0.1
0.15
0.25
0.45
0.6
0.8
1.0
1.4
2.0
3.0
w/d
11
10
9
8
7
6
5
4
εr = 3.38
Z0e
Z0o

(i)

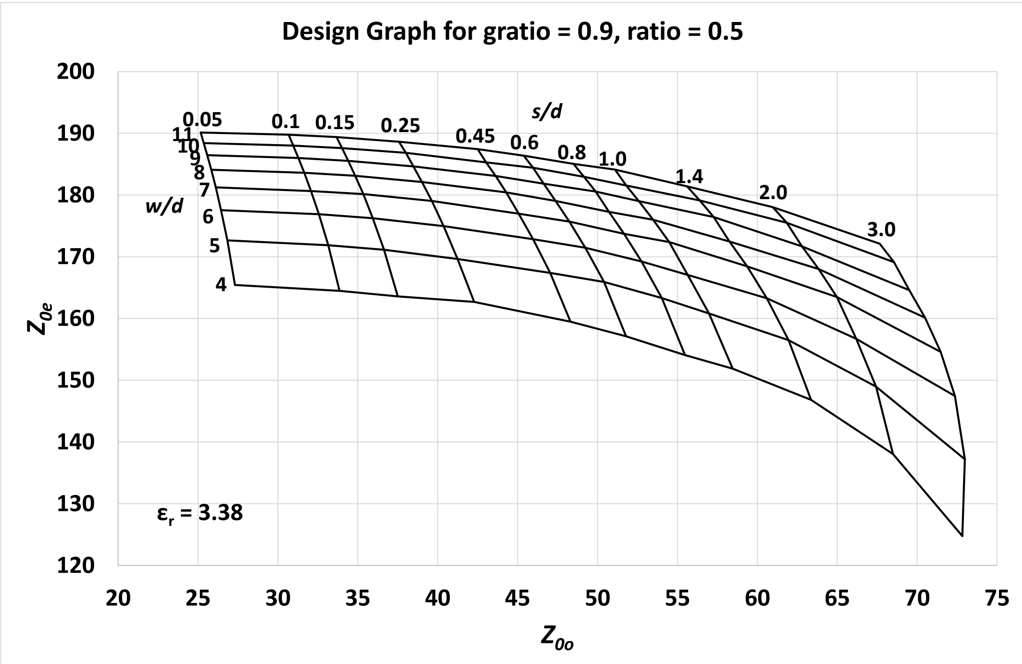

Design Graph for gratio = 0.9, ratio = 0.5
s/d
0.05
0.1
0.15
0.25
0.45
0.6
0.8
1.0
1.4
2.0
3.0
w/d
11
10
9
8
7
6
5
4
εr = 3.38
Z0e
Z0o

(j)

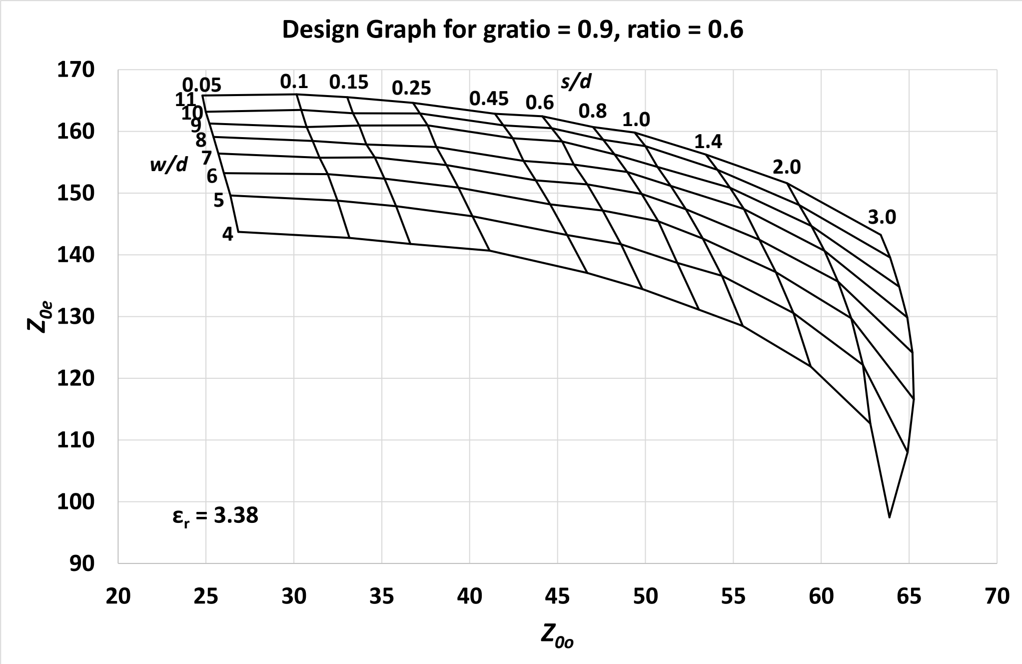
Design Graph for gratio = 0.9, ratio = 0.6
s/d
0.05
0.1
0.15
0.25
0.45
0.6
0.8
1.0
1.4
2.0
3.0
w/d
11
10
9
8
7
6
5
4
Z_{0e}
Z_{0o}
$\varepsilon_r = 3.38$
170
160
150
140
130
120
110
100
90
20 25 30 35 40 45 50 55 60 65 70

(k)

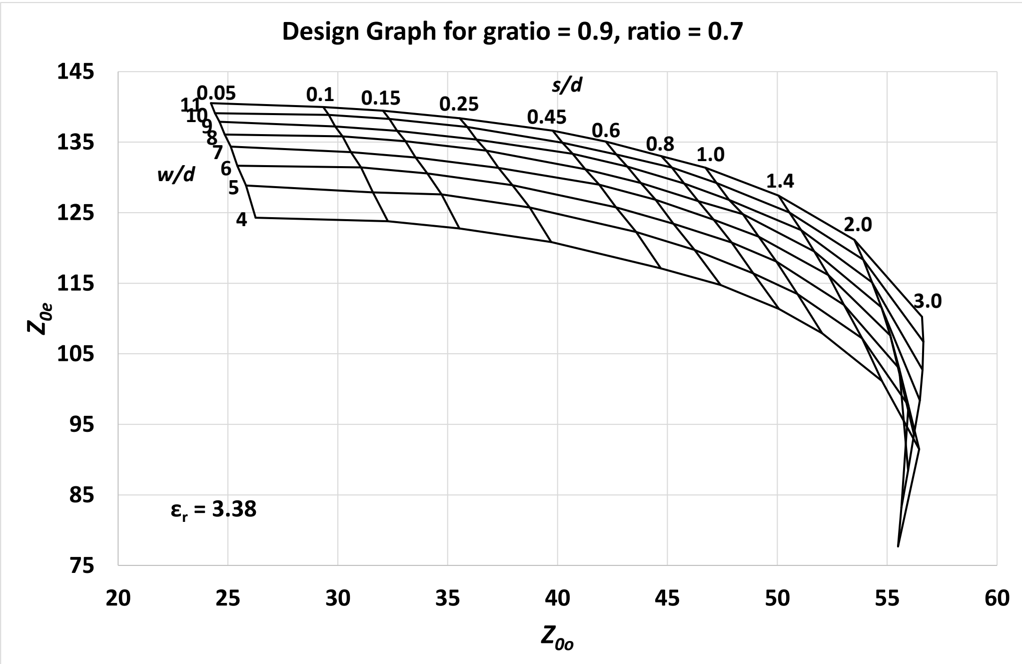
Design Graph for gratio = 0.9, ratio = 0.7
s/d
0.05
0.1
0.15
0.25
0.45
0.6
0.8
1.0
1.4
2.0
3.0
w/d
11
10
9
8
7
6
5
4
Z_{0e}
Z_{0o}
$\varepsilon_r = 3.38$
145
135
125
115
105
95
85
75
20 25 30 35 40 45 50 55 60

(l)

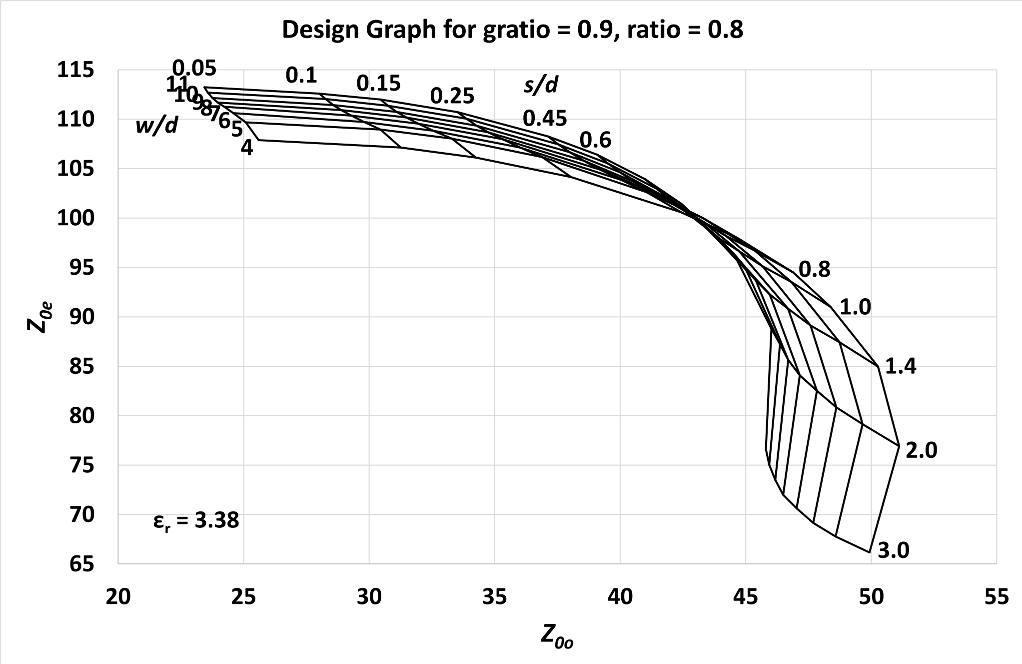
Design Graph for gratio = 0.9, ratio = 0.8
s/d
w/d
0.05
0.1
0.15
0.25
0.45
0.6
0.8
1.0
1.4
2.0
3.0
11
10
9
8
7
6
5
4
εr = 3.38
Z0e
Z0o

(m)

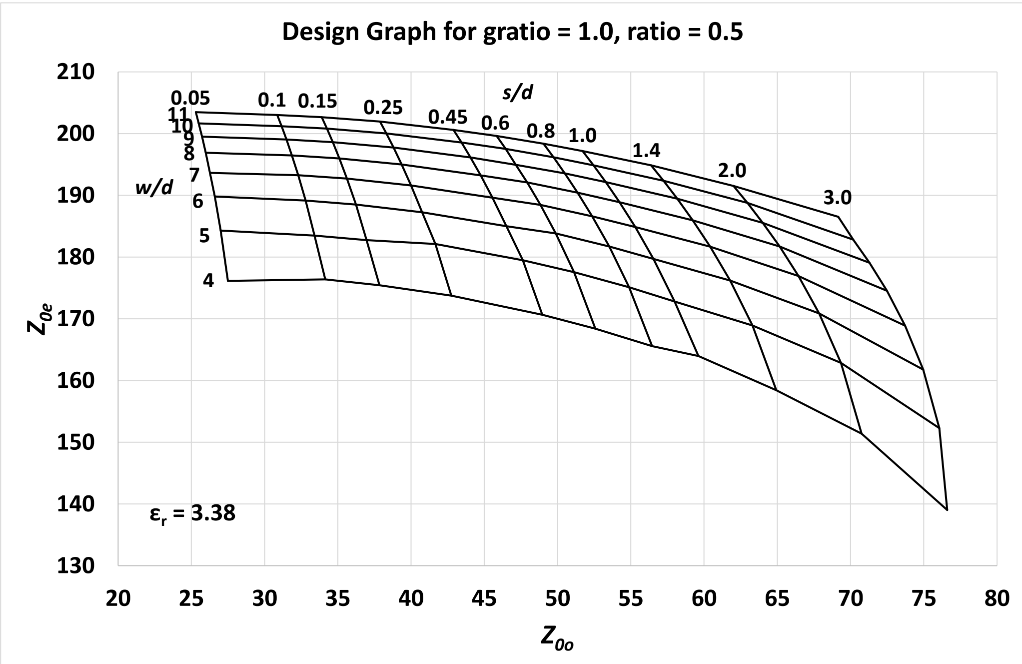
Design Graph for gratio = 1.0, ratio = 0.5
s/d
w/d
0.05
0.1
0.15
0.25
0.45
0.6
0.8
1.0
1.4
2.0
3.0
11
10
9
8
7
6
5
4
εr = 3.38
Z0e
Z0o

(n)

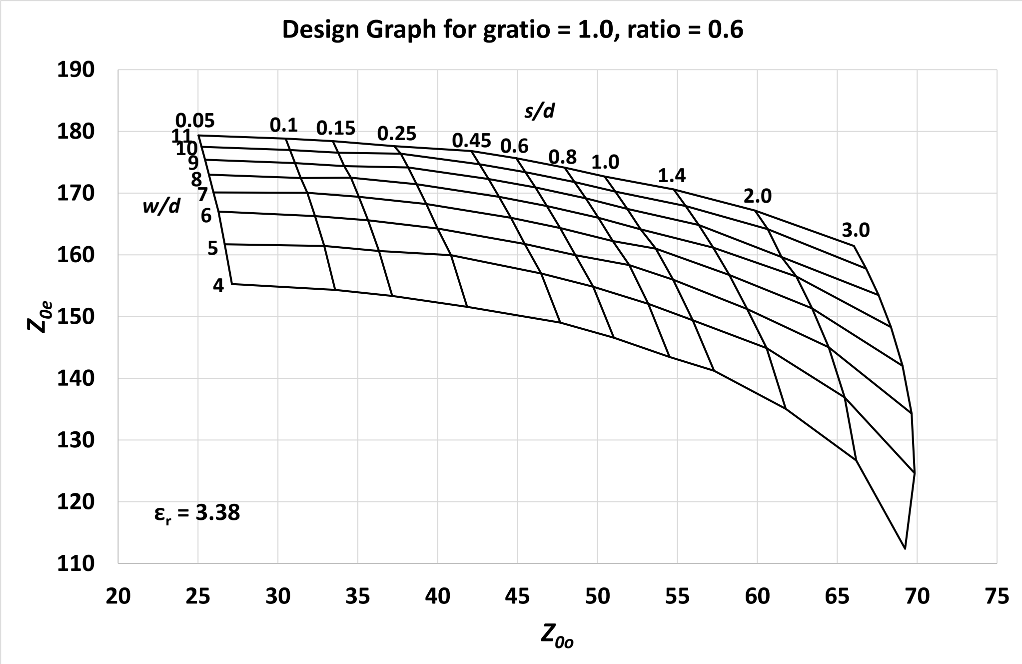
Design Graph for gratio = 1.0, ratio = 0.6
s/d
0.05
0.1
0.15
0.25
0.45
0.6
0.8
1.0
1.4
2.0
3.0
w/d
11
10
9
8
7
6
5
4
εr = 3.38
Z0e
Z0o
190
180
170
160
150
140
130
120
110
20
25
30
35
40
45
50
55
60
65
70
75

(o)

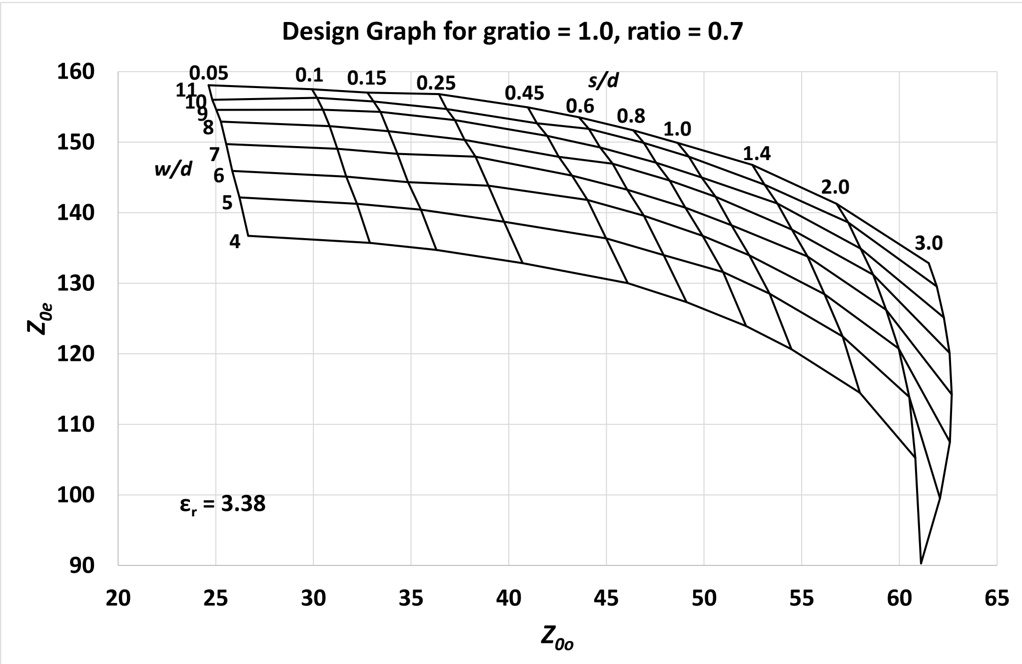
Design Graph for gratio = 1.0, ratio = 0.7
s/d
0.05
0.1
0.15
0.25
0.45
0.6
0.8
1.0
1.4
2.0
3.0
w/d
11
10
9
8
7
6
5
4
εr = 3.38
Z0e
Z0o
160
150
140
130
120
110
100
90
20
25
30
35
40
45
50
55
60
65

(p)

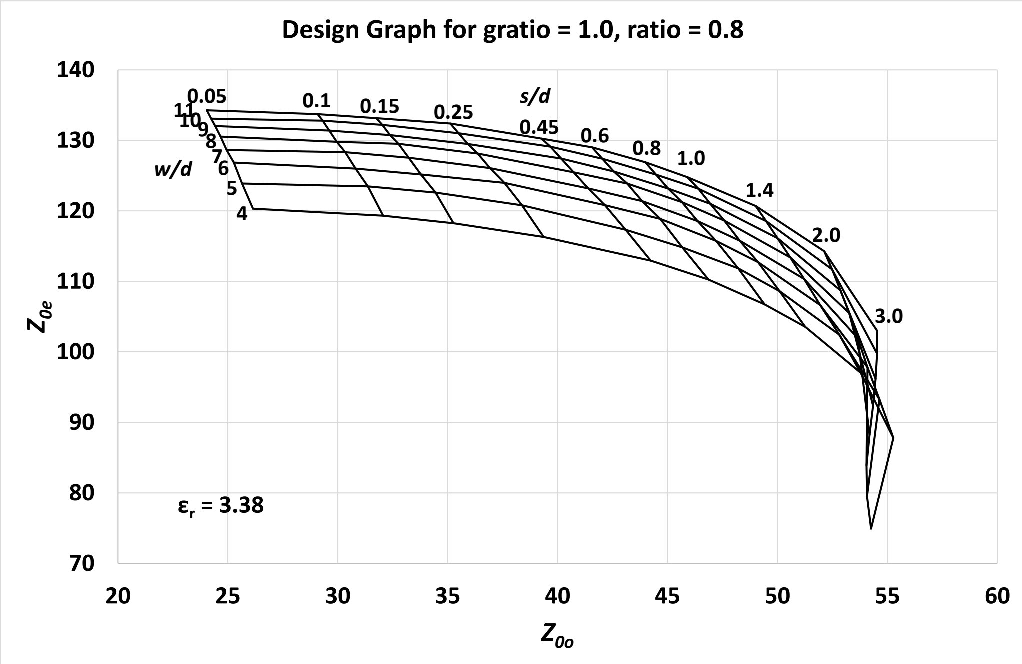

(q)

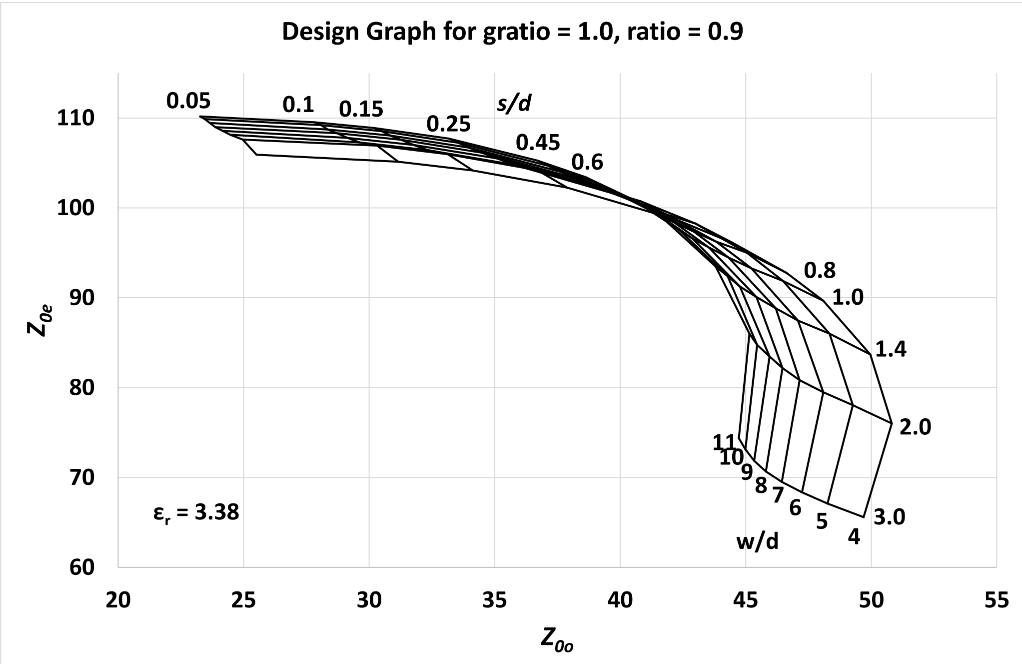

(r)

Figure 4.4: Design graphs for $\varepsilon_r = 3.38$ (a) gratio = 0.5, ratio = 0.5, (b) gratio = 0.6, ratio = 0.5, (c) gratio = 0.6, ratio = 0.6, (d) gratio = 0.7, ratio = 0.5, (e) gratio = 0.7, ratio = 0.6, (f) gratio = 0.7, ratio = 0.7, (g) gratio = 0.8, ratio = 0.5, (h) gratio = 0.8, ratio = 0.6, (i) gratio = 0.8, ratio = 0.7, (j) gratio = 0.9, ratio = 0.5, (k) gratio = 0.9, ratio = 0.6, (l) gratio = 0.9, ratio = 0.7, (m) gratio = 0.9, ratio = 0.8, (n) gratio = 1.0, ratio = 0.5, (o) gratio = 1.0, ratio = 0.6, (p) gratio = 1.0, ratio = 0.7, (q) gratio = 1.0, ratio = 0.8, and (r) gratio = 1.0, ratio = 0.9.

From the design graphs, it can be shown that there are more than one combinations of *s/d* and *w/d* to achieve the same coupling factor. Different parameter combinations, together with the thickness of the substrate, result in a different physical dimension of phase shifter. The effective wavelength at center frequency, $\lambda_{0(eff)}$ can be estimated using the equation given in Lo et al. (2017):

$$\lambda_{0(eff)} = \frac{\lambda_0}{\sqrt{\varepsilon_{eff}}} \tag{4.7}$$

where $\varepsilon_{eff} \approx \frac{1+\varepsilon_r}{2}$.

A series of simulations have been performed using parameters from the design graphs in Figure 4.3 and Figure 4.4. Figure 4.5 shows the simulated differential phase shifts for coupling factors of 4 dB, 5 dB, and 6 dB. The amount of phase shift is varied by changing the value of coupling factor, *C*. Figure 4.6 shows the relationship between the differential phase shift, (ΔΦ) and the coupling factor, *(C)* of the proposed phase shifter.

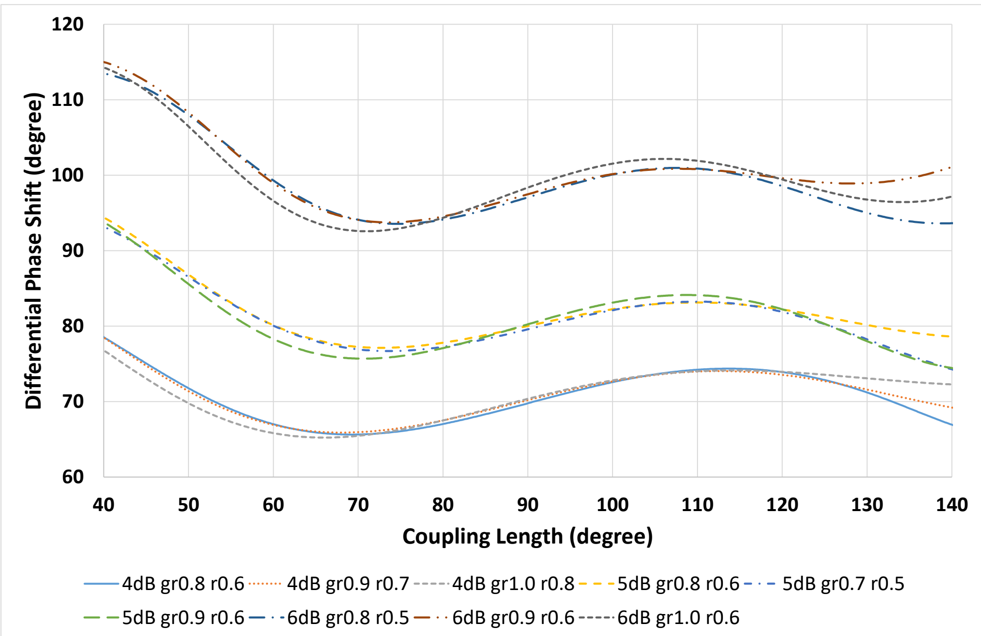

(a)

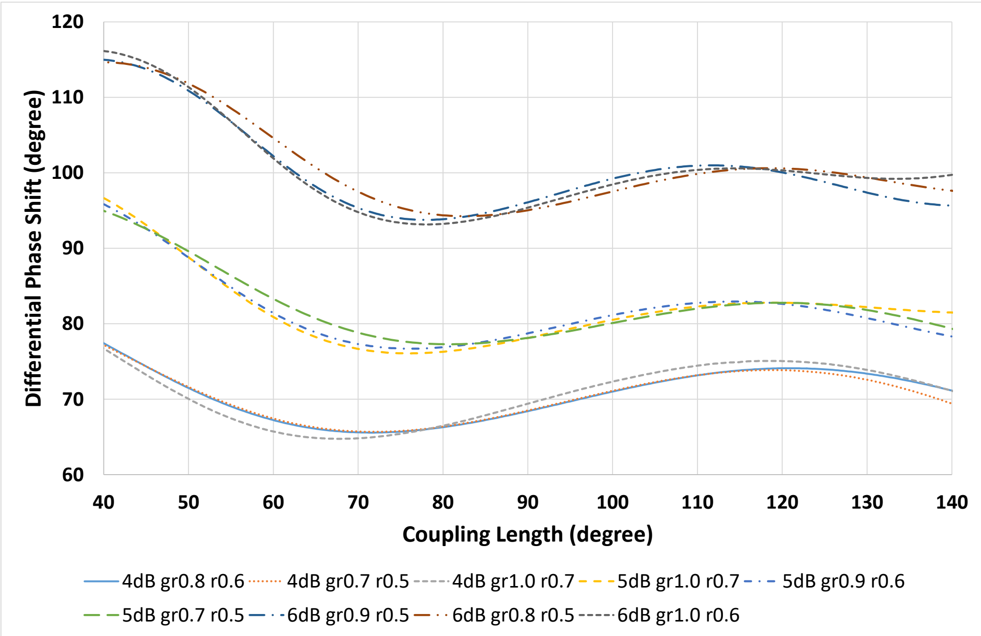

(b)

Figure 4.5: Differential phase shift for different coupling factors. (a) RT/Duroid 5880, (b) RO4003C.

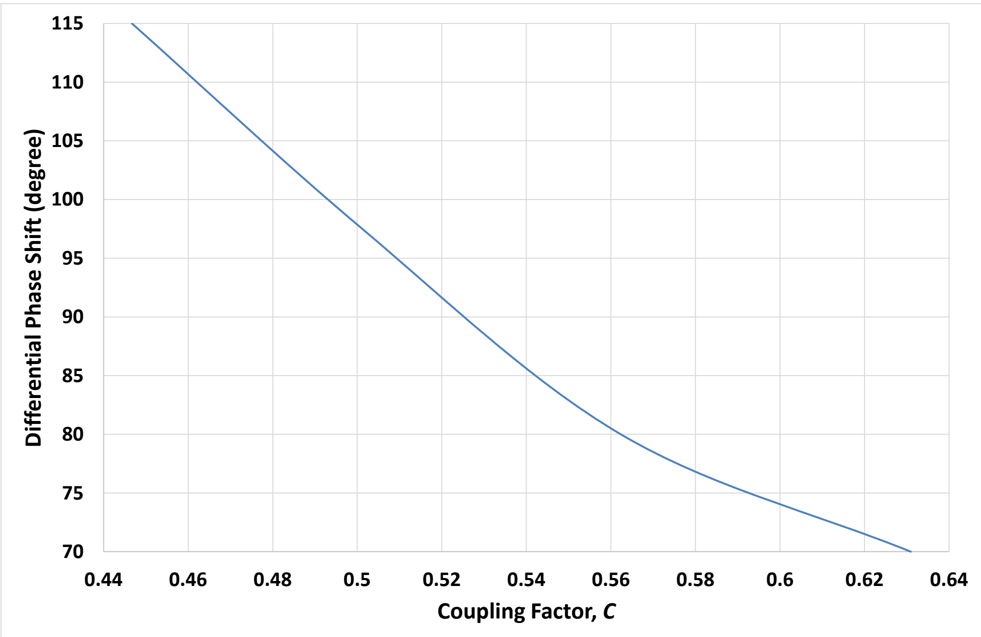

Figure 4.6: Differential phase shift ($\Delta\Phi$) for different coupling factors (C).

The coupling coefficient for a desired phase shift can be determined from Figure 4.6. At the center frequency where $\theta = 90^\circ$, Equation (4.1) reduces to:

$$Z_{i0} = \frac{Z_{0e} - Z_{0o}}{2} \tag{4.8}$$

Solving (4.8) and the expression of coupling factor, $C = \left(Z_{0e} - Z_{0o}\right)/\left(Z_{0e} + Z_{0o}\right)$, the even ($Z_{0e}$) and odd ($Z_{0o}$) mode characteristic impedances can be expressed as follows:

$$Z_{0e} = Z_{i0}\left(1/C + 1\right) \tag{4.9}$$

$$Z_{0o} = Z_{i0}\left(1/C - 1\right) \tag{4.10}$$

where Z_{i0} is the input impedance of the phase shifter at the center frequency.

The nominal value for Z_{i0} is 50 Ω. However, it can be shown from (4.1) that the impedance match bandwidth will be larger if a slightly larger Z_{i0} is used. In this project, Z_{i0} = 55 Ω is chosen. The values of Z_{0e} and Z_{0o} are calculated using (4.9) and (4.10) for different coupling factors.

Apart from minimum phase deviation around the nominal value, a phase shifter must also have low insertion loss and high return loss across the operating band. Figure 4.7 and Figure 4.8 show the simulated transmission coefficient and reflection coefficient for different values of coupling factor for the proposed design. From the figures, it can be shown that the bandwidth generally reduces with lower coupling factor, which agrees with the theoretical analysis.

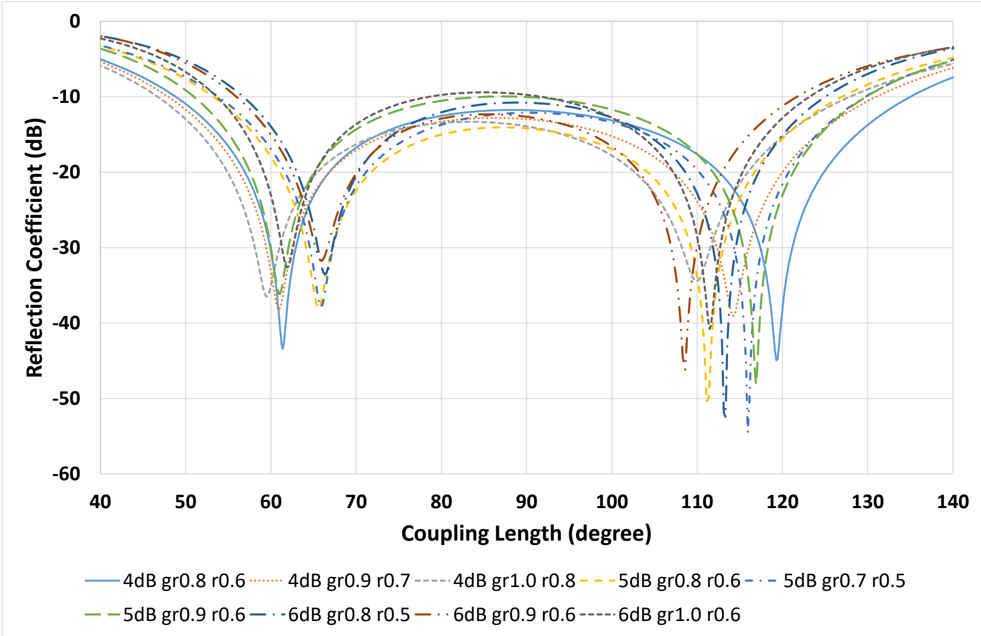

(a)

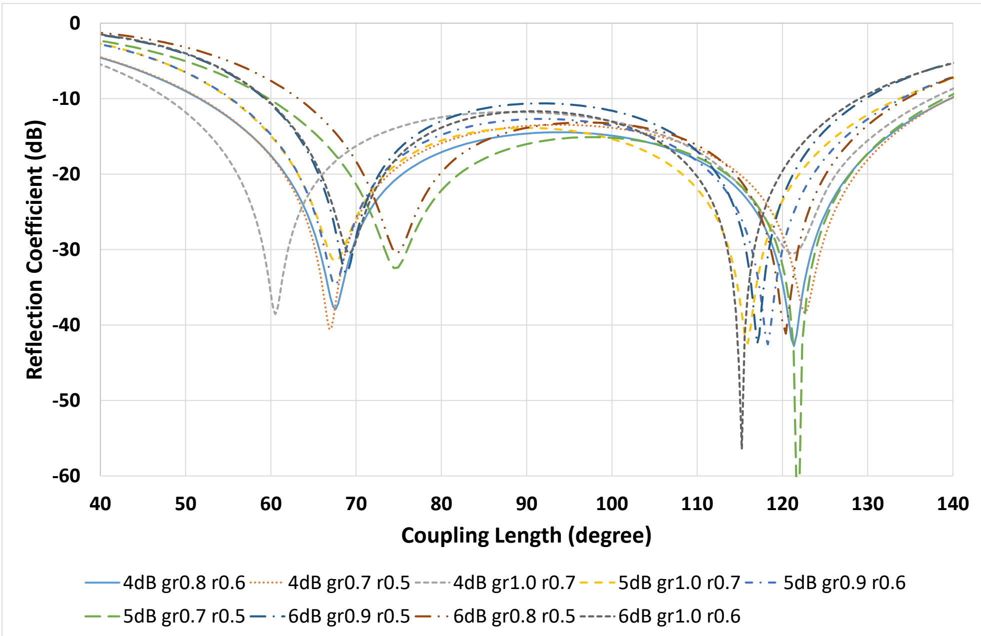

(b)

Figure 4.7: Simulated reflection coefficient (S_{11}) for (a) RT/Duroid 5880, and (b) RO4003C.

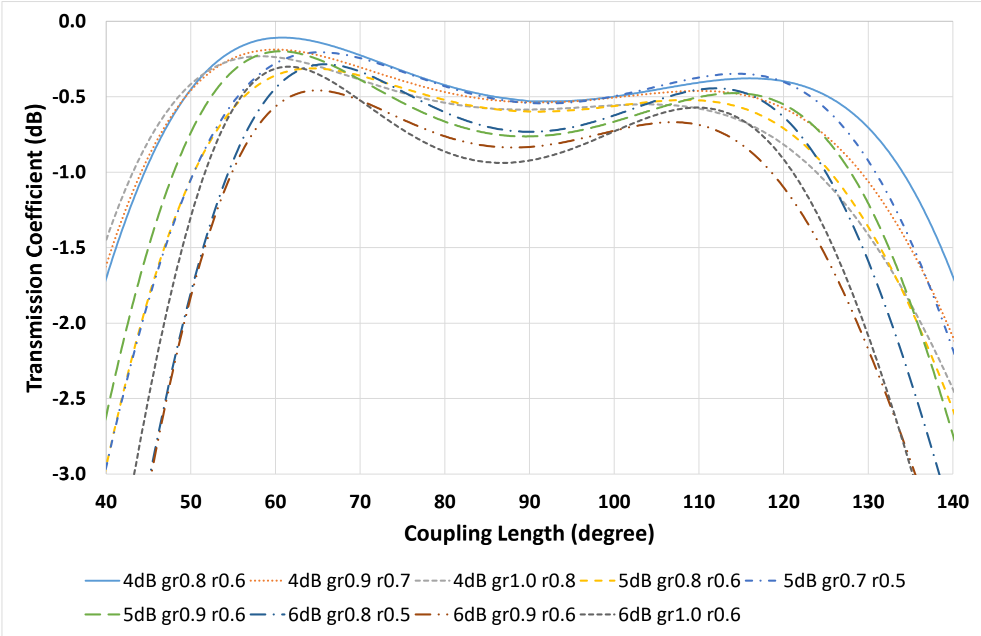

(a)

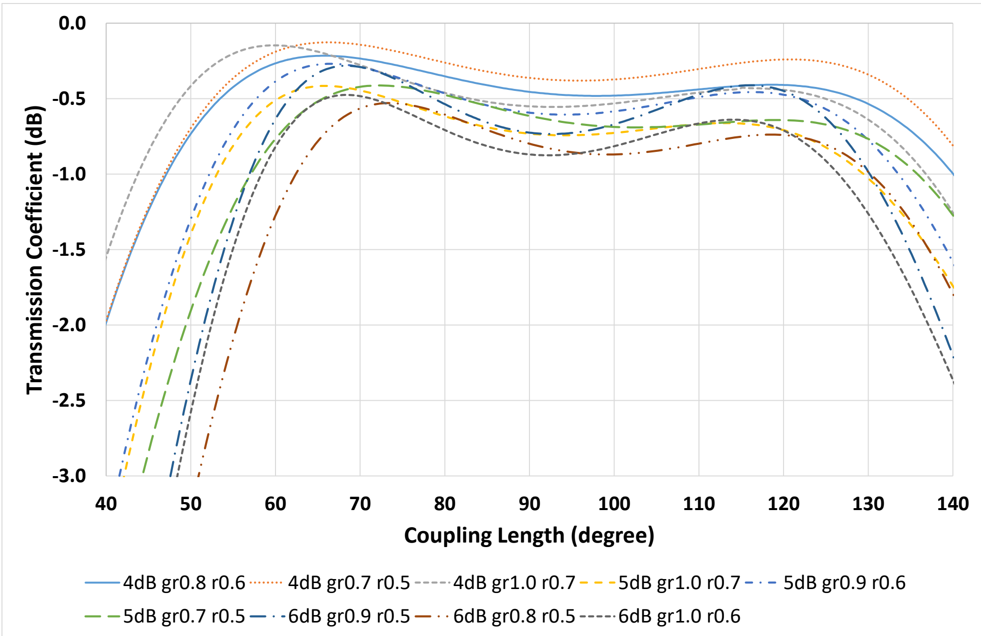

(b)

Figure 4.8: Simulated transmission coefficient (S_{21}) for (a) RT/Duroid 5880, and (b) RO4003C.

4.4 Summary of the Design Procedure for Phase Shifter

The proposed phase shifter can be designed with the following procedure:

1. Determine the coupling factor, C, for the desired phase shift using Figure 4.6.
2. Calculate the even and odd mode characteristic impedances, Z_{0e} and Z_{0o} using Equation (4.9) and Equation (4.10).
3. Using the design graphs in Figure 4.3 and Figure 4.4, find the corresponding s/d and w/d.
4. The gap width, s and the width of the semi-elliptical patches, w can be calculated from the values of s/d and w/d, where d is the thickness of the substrate.
5. The length, L of the coupler can be calculated from the axial ratio ("*ratio*") indicated on the design graph. Finally, the width of the defected ground, w_g, is calculated from the defected ground axial ratio ("*gratio*").

4.5 Results and Discussion

Using the design graphs in Figure 4.3 and Figure 4.4, the parameters for coupling factor, C = 5 dB and 6 dB are determined and shown in Table 4.1.

Table 4.1: Design parameters of phase shifters.

ε_r	s/d	w/d	d (mm)	L (mm)	w (mm)	s (mm)	w_g (mm)	C (dB)
2.2	0.209	5.575	1.575	35.123	8.781	0.329	24.586	5
2.2	0.209	5.575	0.787	17.550	4.388	0.164	12.285	5
2.2	0.574	5.440	1.575	34.272	8.568	0.904	27.418	6
2.2	0.574	5.440	0.787	17.125	4.281	0.452	13.700	6
3.38	0.418	7.110	1.524	36.119	10.836	0.637	32.507	5
3.38	0.418	7.110	0.813	19.268	5.780	0.340	17.341	5
3.38	0.890	5.415	1.524	33.010	8.252	1.356	29.709	6
3.38	0.890	5.415	0.813	17.610	4.402	0.724	15.849	6

The reflection coefficient, transmission coefficient, and differential phase shift of the proposed phase shifter are first verified using the CST Microwave Studio. The designs are fabricated on Rogers RT/Duroid 5880 and RO4003C with different substrate thicknesses and tested using a vector network analyser. The photographs of the fabricated phase shifters are shown in Figure 4.9.

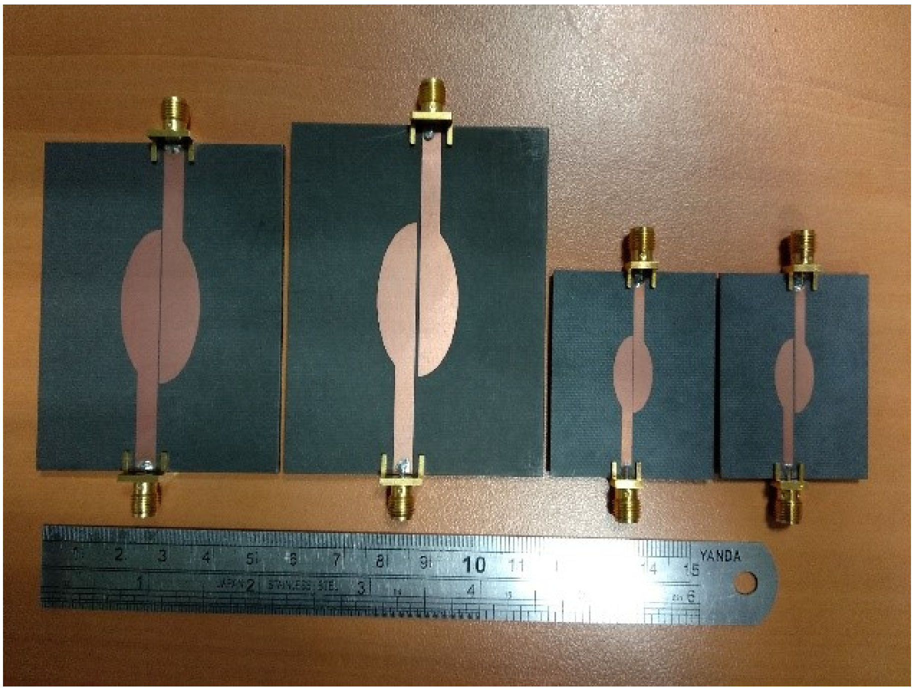

(a)

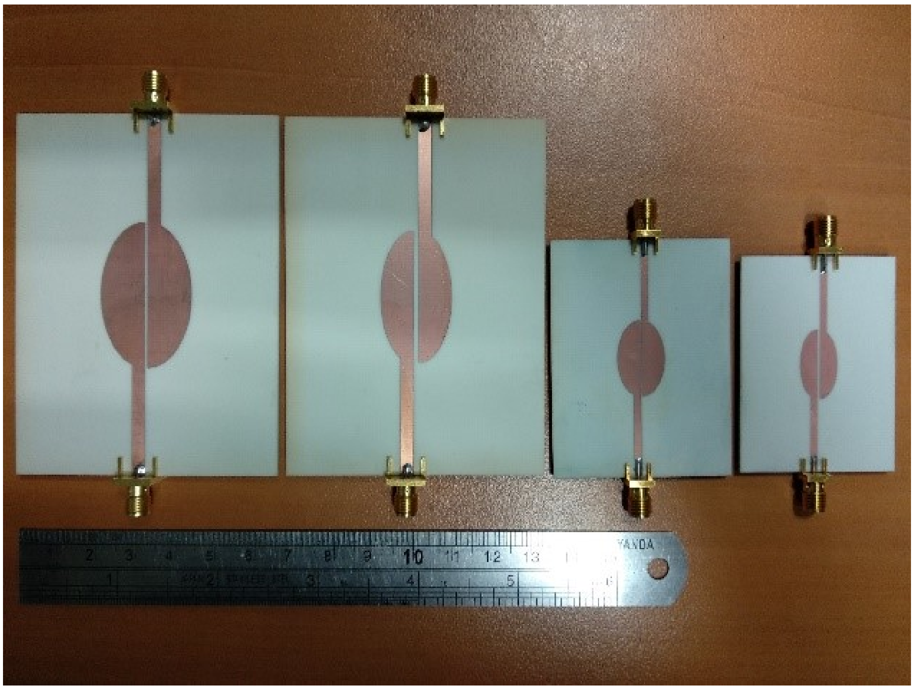

(b)

Figure 4.9: Fabricated Phase Shifters. (a) RT/Duroid 5880, (b) RO4003C.

The simulation and measurement results are shown in Figure 4.10 to Figure 4.13 .

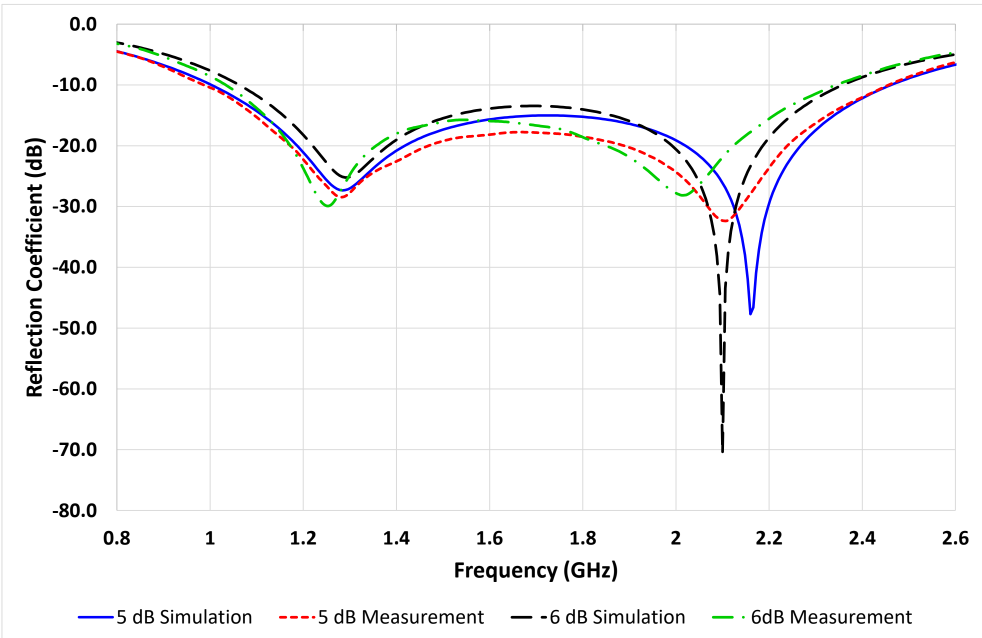

(a)

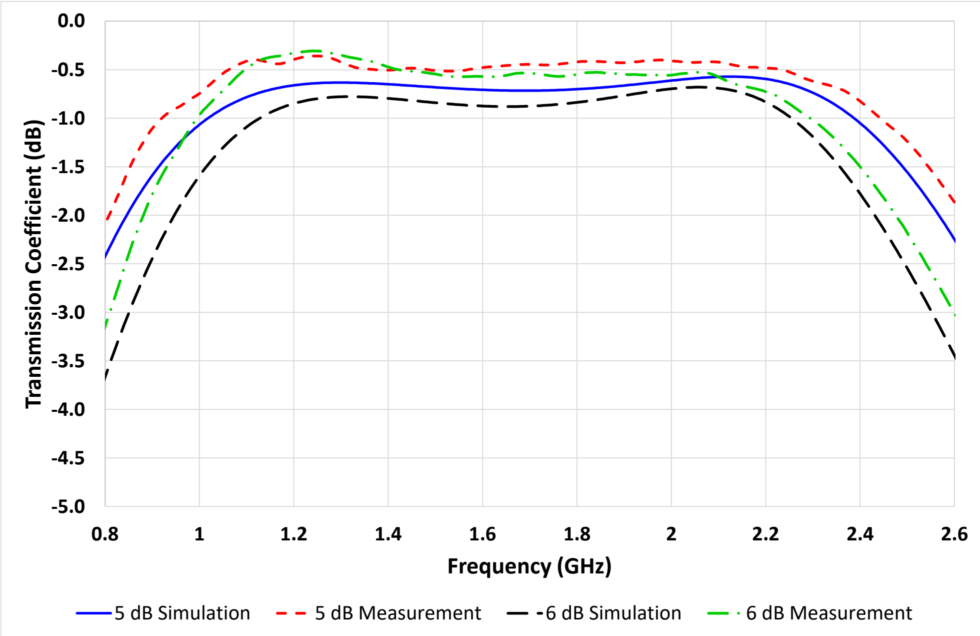

(b)

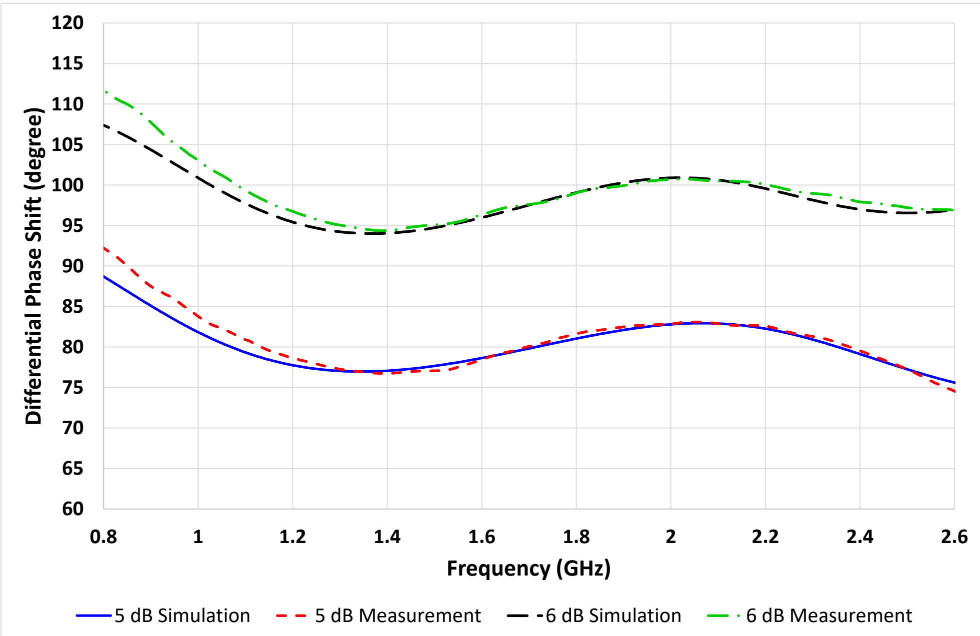

(c)

Figure 4.10: Simulation and measurement results for RT/Duroid 5880, d = 1.575mm. (a) Reflection coefficient, (b) Transmission coefficient, and (c) Differential phase shift.

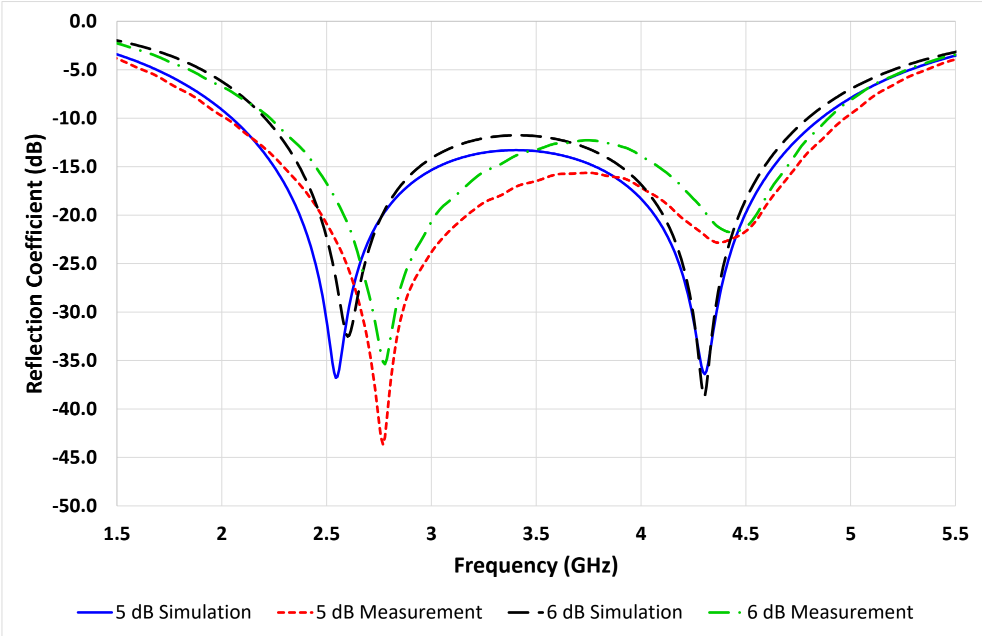

Reflection Coefficient (dB)
0.0
-5.0
-10.0
-15.0
-20.0
-25.0
-30.0
-35.0
-40.0
-45.0
-50.0
1.5
2
2.5
3
3.5
4
4.5
5
5.5
Frequency (GHz)
5 dB Simulation
5 dB Measurement
6 dB Simulation
6 dB Measurement

(a)

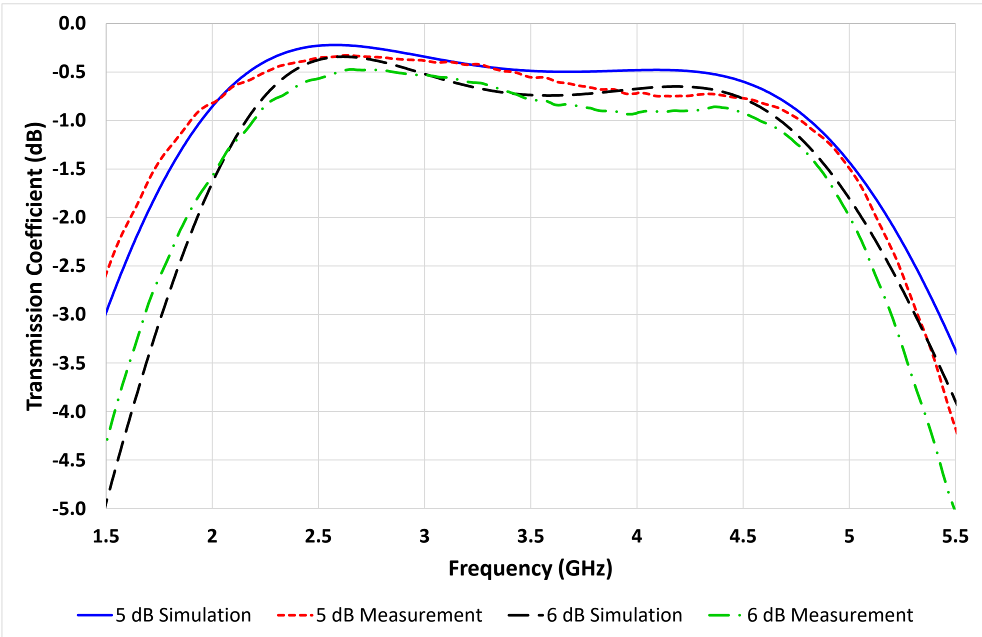

Transmission Coefficient (dB)
0.0
-0.5
-1.0
-1.5
-2.0
-2.5
-3.0
-3.5
-4.0
-4.5
-5.0
1.5
2
2.5
3
3.5
4
4.5
5
5.5
Frequency (GHz)
5 dB Simulation
5 dB Measurement
6 dB Simulation
6 dB Measurement

(b)

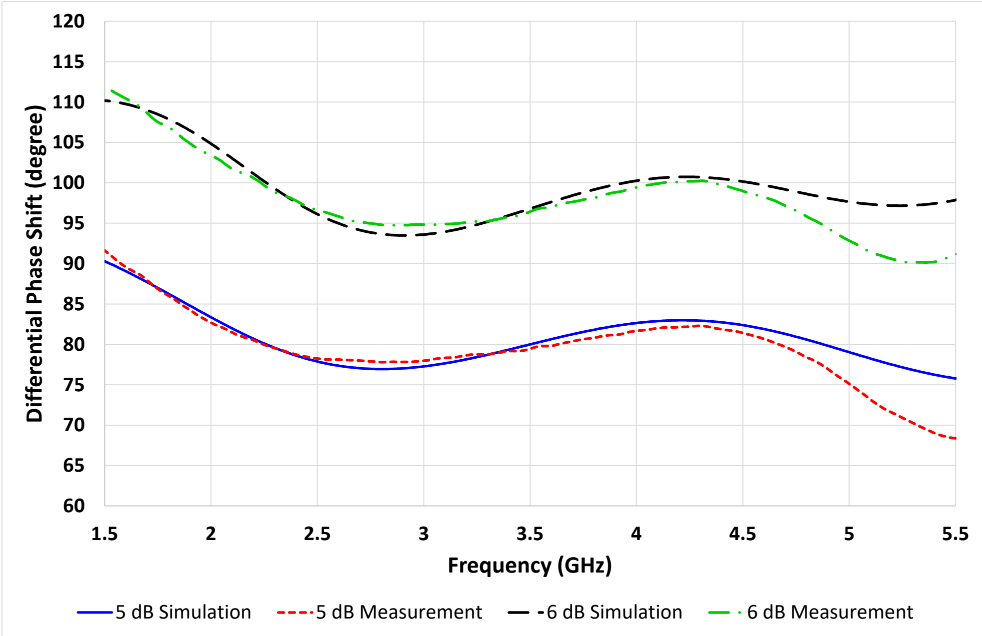

(c)

Figure 4.11: Simulation and measurement results for RT/Duroid 5880, d = 0.787mm. (a) Reflection coefficient, (b) Transmission coefficient, and (c) Differential phase shift.

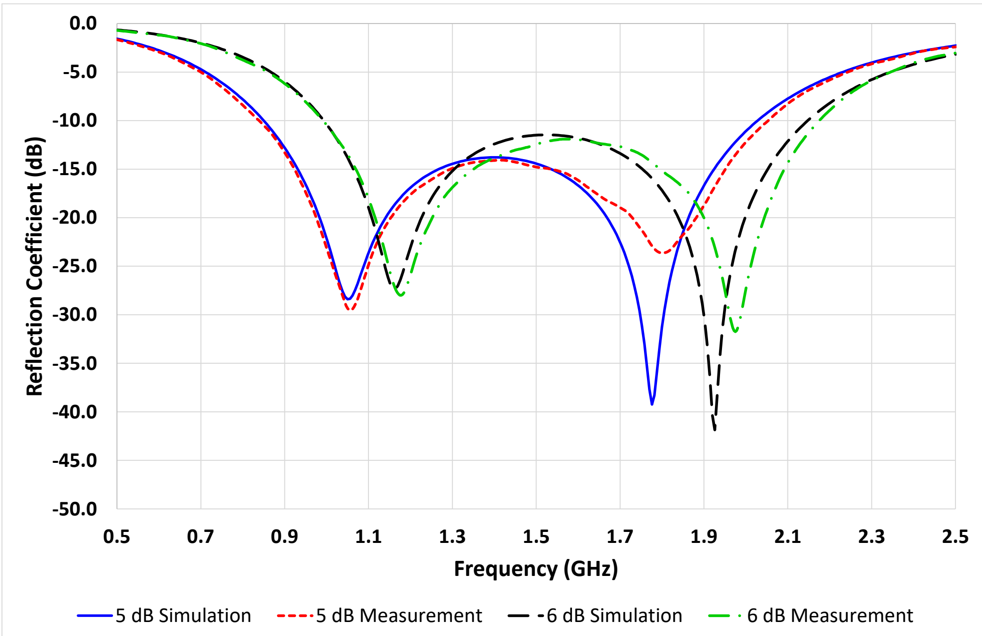

(a)

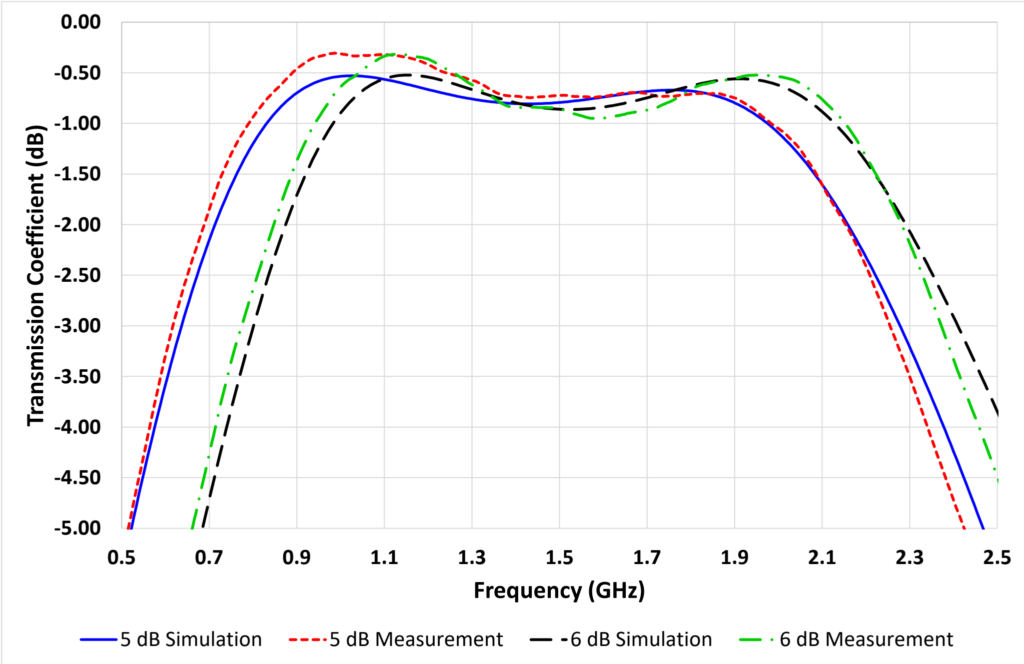

(b)

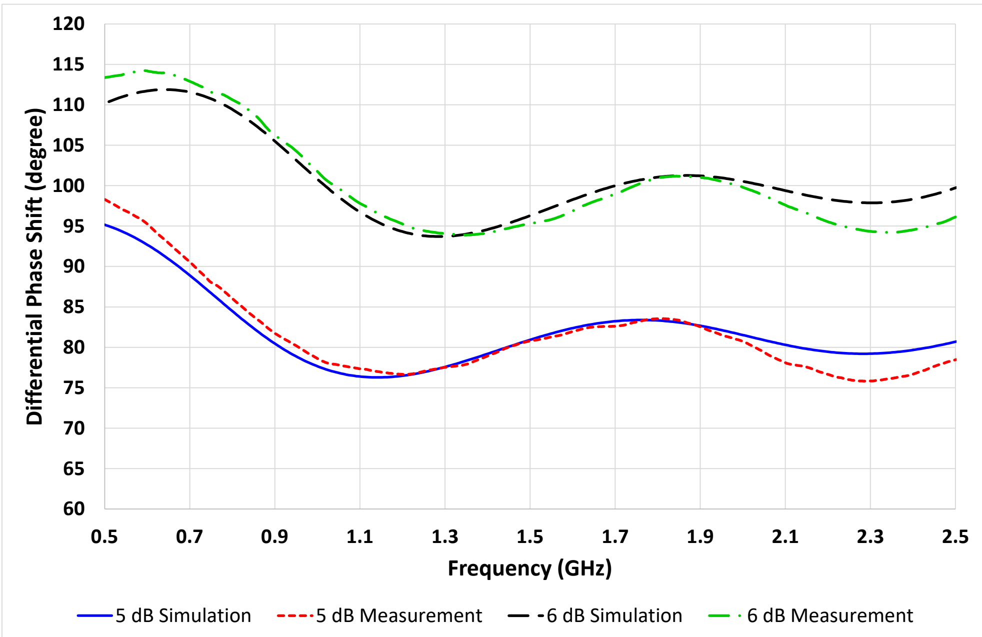

(c)

Figure 4.12: Simulation and measurement results for RO4003C, $d = 1.524$mm. (a) Reflection coefficient, (b) Transmission coefficient, and (c) Differential phase shift.

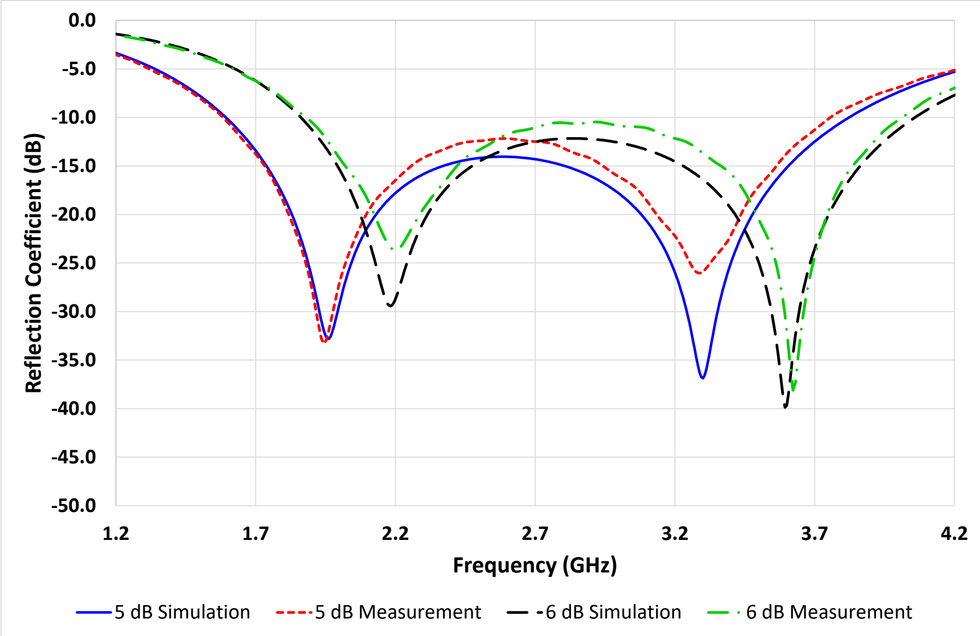

Reflection Coefficient (dB)
0.0
-5.0
-10.0
-15.0
-20.0
-25.0
-30.0
-35.0
-40.0
-45.0
-50.0
1.2
1.7
2.2
2.7
3.2
3.7
4.2
Frequency (GHz)
5 dB Simulation
5 dB Measurement
6 dB Simulation
6 dB Measurement

(a)

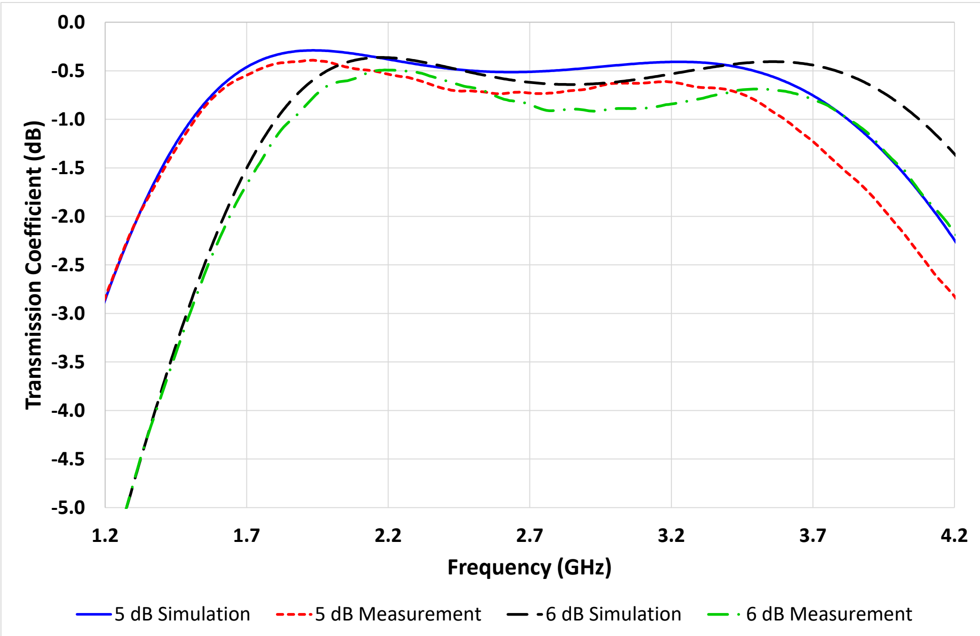

Transmission Coefficient (dB)
0.0
-0.5
-1.0
-1.5
-2.0
-2.5
-3.0
-3.5
-4.0
-4.5
-5.0
1.2
1.7
2.2
2.7
3.2
3.7
4.2
Frequency (GHz)
5 dB Simulation
5 dB Measurement
6 dB Simulation
6 dB Measurement

(b)

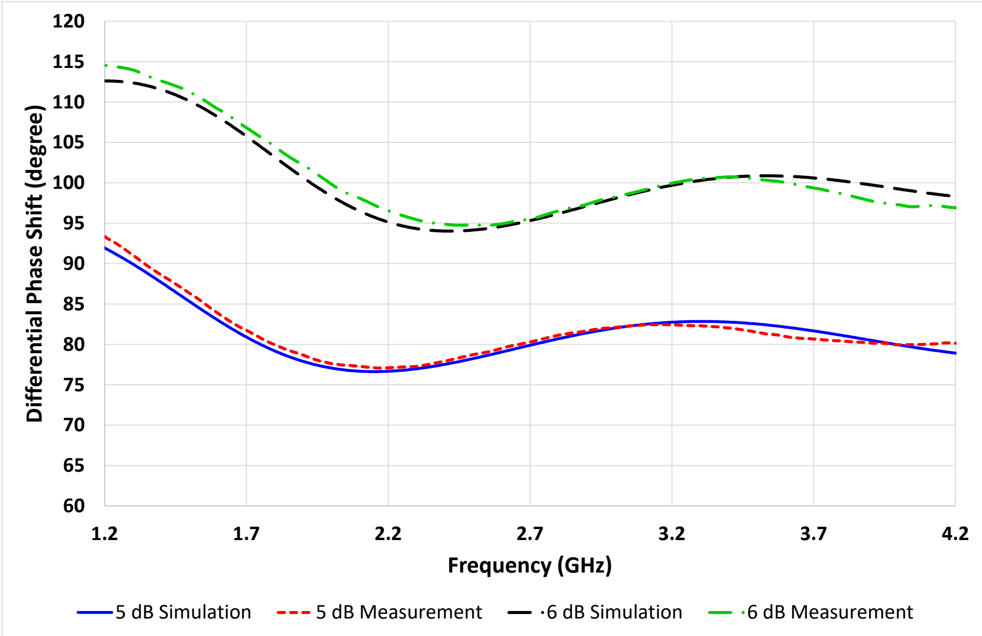

(c)

Figure 4.13: Simulation and measurement results for RO4003C, $d = 0.813$mm. (a) Reflection coefficient, (b) Transmission coefficient, and (c) Differential phase shift.

The center frequency and the bandwidth are summarized in Table 4.2 and Table 4.3.

Table 4.2: Simulated and measured center frequencies and bandwidths of the phase shifter with $\varepsilon_r = 2.2$.

	Simulation Results				Measurement Results			
Substrate thickness (mm)	1.575		0.787		1.575		0.787	
Coupling (dB)	5	6	5	6	5	6	5	6
L (mm)	35.123	34.272	17.550	17.125	35.123	34.272	17.550	17.125
Center frequency, f_c (GHz)	1.71	1.7	3.44	3.46	1.72	1.68	3.41	3.45
Bandwidth (GHz)	1.4	1.16	2.85	2.54	1.48	1.29	2.85	2.45
Bandwidth ratio	2.39	2.04	2.41	2.16	2.50	2.26	2.44	2.10
Fractional Bandwidth (%)	82.11	68.55	82.79	73.61	85.82	77.24	83.67	70.96

Table 4.3: Simulated and measured center frequencies and bandwidths of the phase shifter with $\varepsilon_r = 3.38$.

	Simulation Results				Measurement Results			
Substrate thickness (mm)	1.524		0.813		1.524		0.813	
Coupling (dB)	5	6	5	6	5	6	5	6
L (mm)	36.119	33.010	19.268	17.610	36.119	33.010	19.268	17.610
Center frequency, f_c (GHz)	1.42	1.57	2.7	2.96	1.42	1.58	2.61	2.87
Bandwidth (GHz)	1.16	1.16	2.26	2.24	1.19	1.19	2.08	2.02
Bandwidth ratio	2.38	2.18	2.44	2.22	2.43	2.21	2.33	2.08
Fractional Bandwidth (%)	81.61	74.33	83.68	75.71	83.52	75.40	79.76	70.30

From Figure 4.10 to Figure 4.13, the simulation and measurement results for all the phase shifters are closely matched. Figure 4.10 and Figure 4.11 show the simulation and measurement results for the phase shifters fabricated on RT/Duroid 5880 with coupling of 5 dB and 6 dB. Both substrate thicknesses offer similar bandwidth ratio, which are approximately 2.4 and 2.1 for coupling of 5 dB and 6 dB, respectively. The phase shifts are 80 ± 3º and 97.5 ± 3.5º for coupling of 5 dB and 6 dB, respectively. All phase shifters have return loss of better than 10 dB, and insertion loss better than 1 dB.

For the phase shifters fabricated on RO4003C with the same coupling factors, the results in Figure 4.12 and Figure 4.13 show that the bandwidth ratio are also approximately 2.4 and 2.1 for coupling of 5 dB and 6 dB, respectively. The phase shifts are 80 ± 3.5º and 97.5 ± 4º for coupling of 5 dB and 6 dB, respectively. The return losses are better than 10 dB, and the insertion losses are less than 1 dB. These results show that the proposed design exhibits wideband characteristic with low phase ripple. Generally, weaker coupling (larger air gap) results in higher insertion loss, and a lower bandwidth ratio.

A comparison between the proposed phase shifter and the edge-coupled phase shifters published in recent years is made and illustrated in Table 4.4. The proposed design offers the highest phase stability over a wide bandwidth, while maintaining low insertion loss. It also features smaller circuit size compared to phase shifter by Liu et al. (2014) and Guo et al. (2016).

Table 4.4: Comparison between the reported edge-coupled phase shifters.

Reference	Phase Shift (º)	Phase deviation (º)	Insertion Loss (dB)	Bandwidth (%)
Pu et al. (2015)	90	±3	≤ 0.9	45
Guo et al. (2006)	90	±5	≤ 1	70
Liu et al. (2014)	90	±5	≤ 1.1	105
Guo et al. (2016)	180	±8	≤ 0.6	100
This work	80	±3	≤ 1	82

4.6 Conclusion

A new design of wideband phase shifter using semi-elliptical edge-coupled structure is presented. This structure consists of two semi-elliptical lines on the top layer and an elliptical defected ground plane at the bottom layer. Sets of design graphs are formulated to facilitate the design of the phase shifter. The operating frequency and coupling are controlled by the dimension of the semi-elliptical structure and the size of the air gap. The structure is compact, simple, easy to fabricate and low cost. Both the simulation and measurement results show that the proposed design exhibits wideband characteristic with a bandwidth ratio of more than 2.4 and a phase deviation of less than 3.5º for 5 dB coupling factor. The return loss is better than 10 dB and the insertion loss is less than 1 dB.

CHAPTER 5

CONCLUSION

5.1 Summary of the Work

Directional couplers and phase shifters are widely used in microwave system such as power amplifiers, modulators, mixers, phase arrays antennas, and microwave measurement systems. Existing designs suffer from several limitations including limited bandwidth, narrow gap width between coupled lines, large circuit size, and the requirement of multilayer structure, making it difficult to be integrated onto existing circuit design.

Motivated by these limitations, a study on the design and construction of directional couplers and phase shifters is carried out. A number of designs available in the open literature are studied. A new structure which is simple, compact, easy to fabricate, and requires only two conducting layers is proposed. The design consists of two semi-elliptical patches on the top layer and an elliptical defected ground plane on the bottom layer to increase the coupling coefficient and operating bandwidth. The proposed structure is modelled as a four-port device. Two of the ports are open circuited for the case of phase shifter.

Even and odd mode analysis is carried out using commercially available electromagnetic simulation software. Sets of design graphs are formulated to facilitate the design of the directional coupler and phase shifter on substrate with dielectric constants of 2.2 and 3.38. The physical dimensions of the directional coupler and the phase shifter can be obtained using the design graphs. An approximate equation is also formulated to estimate the center frequency of the device.

The validity of the proposed designs are verified experimentally. The directional couplers and phase shifters are fabricated on substrate with different dielectric constants and thicknesses. Their performance are measured using a vector network analyser. The measurement results show good agreement with the simulation results and suggest that the proposed designs exhibit wideband performance with small coupling variation (directional coupler) and phase deviation (phase shifter). The required gap width between coupled lines for the proposed designs is much wider than the conventional microstrip design of the same coupling factor, making it more practical to realize on printed circuit board. The proposed designs also do not require multisectional coupled lines and matching networks, resulting in compact size.

5.2 Recommendation for Future Work

Additional technique to enhance the performance of the coupler and phase shifter, such as its return loss and directivity can be studied. A floating elliptical patch may also be introduced on the defected ground to reduce the odd mode impedance and increases the coupling and phase shift range. The proposed structure may be modelled and sets of mathematical equations may be formulated for the design of the proposed coupler and phase shifter.

REFERENCES

Abbosh, A.M. and Bialkowski, M.E., 2007. Design of Compact Directional Couplers for UWB Applications. *IEEE Transactions on Microwave Theory and Techniques*, 55 (2), pp. 189-194.

Abbosh A.M., 2007. Ultra-Wideband Phase Shifters. *IEEE Transactions on Microwave Theory and Techniques*, 55 (9), pp. 1935-1941.

Abbosh A.M., 2009. Analytical closed-form solutions for different configurations of parallel-coupled microstrip lines. *IET Microwaves, Antennas & Propagation*, 3 (1), pp. 137-147.

Ahn, H. and Wolff I., 2002. Asymmetric ring-hybrid phase shifters and attenuators. *IEEE Transactions on Microwave Theory and Techniques*, 50 (4), pp. 1146-1155.

Alford A., 1941. Coupled networks in radio frequency circuits. *Proceedings of the IRE*, 29, pp. 55-70.

An H., Nauwelaers B.K.J.C. and Van de Capelle A.R., 1994. Broadband microstrip antenna design with the simplified real frequency technique. *IEEE Transactions on Antennas and Propagation*, 42 (2), pp. 129-136.

Barnett E.F., Lacy P.D. and Oliver B.M., 1955. Principles of directional couplers in reciprocal systems. *Proceeding Symposium on Modern Advances in Microwave Techniques*, 14, pp. 251-268.

Chai, D., Linh M., Yim M., and Yoon G., 2003. Asymmetric Teflon-based Schiffman phase shifter. *Electronics Letters*, 39 (6), pp. 529-530.

Chang C.P., Chiu J.C., Chiu H.Y., and Wang Y.H., 2008. A 3-dB quadrature coupler using broadside-coupled coplanar waveguides. *IEEE Microwave and Wireless Components Letters*, 18 (3), pp. 191–193.

Cheng S., Jefors E., Hallbjrner P. and Rydberg A., 2006. Compact reflective microstrip phase shifter for traveling wave antenna applications. *IEEE Microwave and Wireless Components Letters*, 16 (7), pp. 413-433.

Chiu J.C., Lin J.M., Houng M.P. and Wang Y.H., 2006. PCB-compatible 3 dB coupler using microstrip-to-CPW transitions. *IEEE Microwave and Wireless Components Letters*, vol. 16 no. 6 pp. 369-371.

Cho J.H., Hwang H.Y., and Yun S.W., 2005. A design of wideband 3-dB coupler with N-section microstrip tandem structure. *IEEE Microwave and Wireless Components Letters*, 15 (2), pp. 113–115.

Cohn S.B., 1955. Shielded coupled-strip transmission line. *IRE Transactions on Microwave Theory and Techniques*, 3 (5), pp. 29-38.

Cohn S.B., 1960. Characteristic impedances of broadside-coupled strip transmission lines. *IRE Transactions on Microwave Theory and Techniques*, 8 (6), pp. 633-637.

Cohn, S.B. and Levy, R., 1984. History of Microwave Passive Components with Particular Attention to Directional Couplers. *IEEE Transactions on Microwave Theory and Techniques*, 32 (9), pp. 1046-1054.

Cristal E.G. and Young L., 1965. Theory and tables of optimum symmetrical TEM-mode coupled-transmission-line directional couplers. *IEEE Transactions on Microwave Theory and Techniques*, 13, pp. 544-558.

Dydyk M., 1990. Accurate Design of Microstrip Directional Couplers with Capacitive Compensation. *IEEE MTT-S International Microwave Symposium*, pp. 581-584.

Demyanov V.F., Malozemov V.N., 1972. Vvedeniye v Minimax. *Moscow:Nauka*, pp. 360.

Deb K., Pratap A., Agrawal S. and Meyarivan T., 2002. A fast and elitist multiobjective genetic algorithm: NSGA-II. *IEEE Transactions on Evolutionary Computation*, 6, pp. 182-197.

Edwards T.C. and Steer M.B., 2000. *Foundations of interconnect and microstrip design*, 3rd ed., Chichester: Wiley.

Eom S., 2004. Broadband 180º bit phase shifter using λ/2 coupled line and parallel λ/8 stubs. *IEEE Microwave and Wireless Components Letters*, 14 (5), pp. 228-230.

Gill P.E., Murray W. and Wright M.H., 1981. *Practical optimization*, London: Academic Press.

Guo L., Zhu H. and Abbosh A., 2016. Wideband phase shifter with wide phase range using parallel coupled lines and L-shaped networks. *IEEE Microwave and Wireless Components Letters*, 26 (8), pp. 592-594.

Guo Y., Zhang Z., and Ong L., 2006. Improved wideband Schiffman phase shifter. *IEEE Transactions on Microwave Theory and Techniques*, 54 (3), pp. 1196-1200.

Gruszczynski, S., Wincza K., and Sachse K., 2006. Design of compensated coupled-stripline 3-dB directional couplers, phase shifters, and magic-T's Part I: Single-section coupled-line circuits. *IEEE Transactions on Microwave Theory and Techniques*, 54 (11), pp. 3986-3994.

Han L., Wu K., and Chen X.P., 2009. Accurate synthesis of four-line interdigitated coupler. *IEEE Transactions on Microwave Theory and Techniques*, 57 (10), pp. 2444–2455.

Hillberg W., 1969. From approximation to exact relations for characteristic impedances. *IEEE Transactions on Microwave Theory and Techniques*, 17 (5), pp. 259-265.

Hindin H.J. and Rosenzweig A., 1968. 3-dB couplers constructed from two tandem connected 8.34-dB asymmetric couplers. *IEEE Transactions on Microwave Theory and Techniques*, vol. 19 (2), pp. 125-126.

Ho C.Y. and Moser L., 1981. Symmetrical coupler reduces phase error. *Microwaves*, pp. 82-84.

Howe, H, 1974. *Stripline Circuit Design*. Norwood: Artech House.

Jin Z., Ortiz S. and Mortazawi A., 2004. Design and performance of a new digital phase shifter at X-band. *IEEE Microwave and Wireless Components Letters*, 14 (9), pp. 428-430.

Jones E., and Bolljahn J., 1956. Coupled-strip transmission line filters and directional couplers. *IEEE Transactions on Microwave Theory and Techniques*, 4 (2), pp. 75-81.

Kajfez D., 1978. Raise Coupled Directivity with Lumped Components. *Microwaves*, 17 (3), pp.64-70.

Kajfez D., Paunovic Z. and Pavlin S., 1978. Simplified design of Lange coupler. *IEEE Transactions on Microwave Theory and Techniques*, 26 (10), pp. 806–808.

Kammler D.W., 1969. The design of discrete N-section and continuously tapered symmetrical microwave TEM directional couplers. *IEEE Transactions on Microwave Theory and Techniques*, 17 (8), pp. 577-590.

Kemp G., Hobdell J., and Biggin J.W., 1983. Ultra-wideband quadrature coupler. *Electronics Letters*, 19 (6), pp. 197–199.

Kyhl R.L., 1947. *Chapter 14: Techniques of Microwave Measurements*, New York: McGraw-Hill.

Lange J., 1969. Interdigitated strip-line quadrature hybrid. *IEEE Transactions on Microwave Theory and Techniques*, 17 (12), pp. 1150-1151.

Levy R., Lind L.F., 1968. Synthesis of symmetrical branch-guide directional couplers. *IEEE Transactions on Microwave Theory and Techniques*, 16 (2), pp. 80-89.

Levy R., 1968. Analysis and synthesis of waveguide multi-aperture directional couplers. *IEEE Transactions on Microwave Theory and Techniques*, 16 (12), pp. 995-1006.

Levy R., 1983. Improved single and multiaperture waveguide coupling theory including explanation of mutual interactions. *IEEE Transactions on Microwave Theory and Techniques*, 28, pp. 331-338.

Liu Q., Liu Y.N., Shen J.Y., Li S.L., Yu C.P. and Lu Y.H., 2014. Wideband single-layer 90° phase shifter using stepped impedance open stub and coupled-line with weak coupling. *IEEE Microwave and Wireless Components Letters*, 24 (3), pp. 176-178.

Lo Y.C. and Chung B.K., 2012. A Semi-elliptical Wideband Phase Shifter. *Progress in Electromagnetic Research Letters*, 28, pp. 91-99.

Lo Y.C., Chung B.K., and Lim E.H., 2017. A Semi-elliptical Wideband Directional Coupler. *Progress in Electromagnetic Research C*, 79, pp. 139–148.

Lomer P.D. and Crompton J.W., 1957. A new form of hybrid junction for microwave frequencies. *Proceedings of the IEE - Part B: Radio and Electronic Engineering*, 104 (15), pp. 261-264.

March S.L., 1982. Phase Velocity Compensation in Parallel-Coupled Microstrip. *IEEE MTT-S International Microwave Symposium*, pp. 410-412.

Marynowski W., Kusiek A., Walesieniuk A., and Mazur J., 2008. Investigation of broadband multilayered coupled line coupler. *2008 14th Conference on Microwave Techniques*, pp. 1-4.

Meschanov V.P., Metelnikova I.V., Tupikin V.D. and Chumaevskaya G.G., 1994. A new structure of microwave ultrawide-band differential phase shifter. *IEEE Transactions on Microwave Theory and Techniques*, 42 (5), pp. 762-765.

Minnaar, F., Coetzee J., and Joubert J., 1997. A novel ultrawideband microwave differential phase shifter. *IEEE Transactions on Microwave Theory and Techniques*, 45 (8), pp. 1249-1252.

Mongia R.K., Bahl I.J., Bhartia P. and Hong J., 2007. *RF and Microwave Coupled-line Circuits*. 2nd ed. Norwood: Artech House.

Monteath G.D., 1955. Coupled transmission lines as symmetrical directional couplers. *Proceedings of the IEE - Part B: Radio and Electronic Engineering*, 102 (3), pp. 383-392.

Mumford W.W., 1947. Directional couplers, *Proceedings of the IRE*, 35, pp. 160-165.

Oliver B.M., 1954. Directional electromagnetic couplers. *Proceedings of the IRE*, 42 (11), pp. 1686-1692.

Ou W.P., 1975. Design equations for an interdigitated directional coupler. *IEEE Transactions on Microwave Theory and Techniques*, 23 (2), pp. 253–255.

Paolino D.D., 1976. Design more accurate interdigitated couplers. *Microwaves*, pp. 34-38.

Paolino D.D., 1978. MIC Overlay Coupler Design Using Spectral Domain Techniques. *IEEE Transactions on Microwave Theory and Techniques*, 26, pp. 646-649.

Pistolkors A.A. and Neumann M.S., 1941. An instrument for direct measurement of the traveling wave coefficient in feeders. *Electrosvyaz*, IX.

Podell A., 1970. A High Directivity Microstrip Coupler Technique. *IEEE MTT-S International Microwave Symposium*, pp. 33-36.

Pozar D.M., 2011. *Microwave Engineering*. 4th ed. Chichester: Wiley.

Presser A., 1978. Interdigitated Microstrip Coupler Design. *IEEE Transactions on Microwave Theory and Techniques*, 26 (10), pp. 801-805.

Pu X.Y., Zheng S.Y., Liu J.H., Li Y.X. and Long Y.L., 2015. Novel multi-way broadband differential phase shifter with uniform reference line using coupled line structure. *IEEE Microwave and Wireless Components Letters*, 25 (3), pp. 166-168.

Quirarte J., and Starski J.P., 1991. Synthesis of Schiffman phase shifters. *IEEE Transactions on Microwave Theory and Techniques*, 39 (11), pp. 1885-1889.

Quirarte J. and Starski J.P., 1993. Novel Schiffman phase shifters. *IEEE Transactions on Microwave Theory and Techniques*, 41 (1), pp. 9-14.

Reed J., Wheeler G.J., 1956. A method of analysis of symmetrical four port networks. *IRE Transactions on Microwave Theory and Techniques*, 4 (4), pp. 246-252.

Riblet H.J., 1947. Mathematical theory of directional couplers. *Proceedings of the IRE*, 35 (11), pp. 1307-1313.

Riblet H.J., 1952. The short-slot hybrid junction. *Proceedings of the IRE*, 40, pp. 180-184.

Schiek B. and Kohler J., 1977. A method for broadband matching of microstrip differential phase shifters. *IEEE Transactions on Microwave Theory and Techniques*, 25 (8), pp. 666-671.

Schiffman B.M., 1958. A new class of broadband microwave 90-degree phase shifters. *IRE Transactions on Microwave Theory and Techniques*, 6 (2), pp. 232-237.

Schiffman B.M., 1966. Multisection microwave phase-shift network. *IEEE Transactions on Microwave Theory and Techniques*, 14 (4), pp. 209-209.

Sheleg B. and Spielman B.E., 1974. Broadband Directional Couplers Using Microstrip with Dielectric Overlays. *IEEE Transactions on Microwave Theory and Techniques*, 22 (12), pp. 1216-1220.

Shelton J.P., 1966. Impedances of offset parallel-coupled strip transmission lines. *IEEE Transactions on Microwave Theory and Techniques*, 14, pp. 7-15.

Shelton J.P. and Mosko J.A., 1966. Synthesis and design of wide-band equal-ripple TEM directional couplers and fixed phase shifters. *IEEE Transactions on Microwave Theory and Techniques*, 14 (10), pp. 462-473.

Shimizu J.K. and Jones E.M.T., 1958. Coupled-transmission-line directional couplers. *IRE Transactions on Microwave Theory and Techniques*, 6, pp. 403-410.

Sorn M., Lech R. and Mazur J., 2012. Simulation and experiment of a compact wideband 90° differential phase shifter. *IEEE Transactions on Microwave Theory and Techniques*, 60 (3), pp. 494-501.

Tanaka T., Kusoda K. and Aikawa M., 1988. Slot-coupled directional couplers on a both-sided substrate MIC and their applications. *Electronics and Communications in Japan*, 72 (3), pp. 91-99.

Tanaka T., Kusoda K., and Aikawa M., 1988. Slot-coupled directional couplers between double-sided substrate microstrip lines and their applications. *IEEE Transactions on Microwave Theory and Techniques*, 36 (12), pp. 1752–1757.

Tang C.W., Chen M.G., Lin Y.S. and Wu J.W., 2006. Broadband microstrip branch-line coupler broadband microstrip branch-line coupler. *Electronics Letters*, 42 (25), pp. 1458-1460.

Tang C.W., Tseng C.T., and Hsu K.C., 2013. Design of the Modified Planar Tandem Couplers with a Wide Passband. *IEEE Transactions on Microwave Theory and Techniques*, 61 (1), pp. 48-54.

Tang C.W., Tseng C.T. and Hsu K.C., 2014. Design of Wide Passband Microstrip Branch-Line Couplers With Multiple Sections. *IEEE Transactions on Components, Packaging and Manufacturing Technology*, 4 (7), pp. 1222-1227.

Taylor J. and Prigel, D., 1976. Wiggly phase shifters and directional couplers for radio-frequency hybrid-microcircuit applications. *IEEE Transactions on Parts, Hybrids, and Packaging*, 12 (4), pp. 317-323.

Tresselt C.P., 1966. The design and construction of broad-band high-directivity 90º couplers using nonuniform line techniques. *IEEE Transactions on Microwave Theory and Techniques*, 14, pp. 647-656.

Tresselt, C. 1968. Broad-band tapered-line phase shift networks. *IEEE Transactions on Microwave Theory and Techniques*, 16 (1), pp. 51-52.

Velazquez-Ahumada Md.C, Martel J. and Madina F., 2004. Parallel coupled microstrip filters with ground plane aperture for spurious band suppression and enhanced coupling. *IEEE Transactions on Microwave Theory and Techniques*, 52 (3), pp. 1082-1086.

Wang S. and Song L., 2016. Design and Simulation of a Kind of Wide Band Microwave Coupler with Defected Ground Structure. *IEEE International Conference on Electronic Information and Communication Technology*, pp. 462-465.

Waugh R. and LaCombe D., 1972. Unfolding the Lange coupler. *IEEE Transactions on Microwave Theory and Techniques*, 20, pp. 777-779.

Weng L.H., Guo Y.C., Shi X.W. and Chen X.Q., 2008. An Overview on Defected Ground Structure. *Progress In Electromagnetics Research B*, 7, pp. 173–189.

Wong M.F., Hanna V.F., Picon O. and Baudrand H., 1991. Analysis and design of slot-coupled directional couplers between double-sided substrate microstrip lines. *IEEE Transactions on Microwave Theory and Techniques*, 29 (12), pp. 2123-2129.

Wu Y., Sun W., Leung S.W., Diao Y., Chan K.H., and Siu Y.M., 2013. Single-Layer Microstrip High-Directivity Coupled-Line Coupler with Tight Coupling. *IEEE Transactions on Microwave Theory and Techniques*, 61 (2), pp. 746-753.

Yeung L.K., 2011. A compact dual-band 90º coupler with coupled-line sections. *IEEE Transactions on Microwave Theory and Techniques*, 59 (9), pp. 2227-2232.

Yeung S.H., Chan W.S., Ng K.T. and Man K.F., 2012. Computational optimization algorithms for antennas and RF/microwave circuit designs: An overview. *IEEE Transactions on Industrial Informatics*, 8 (2), pp. 216-227.

Yeung S.H., Mei Z., Sarkar T.K. and Salazar-Palma M., 2013. Design and testing of a single-layer microstrip ultrawideband 90° differential phase shifter. *IEEE Microwave and Wireless Components Letters*, 23 (3), pp. 122-124.

Yeung S.H., Xue Q. and Man K.F., 2012. Broadband 90º Differential Phase Shifter Constructed Using a Pair of Multisection Radial Line Stubs. *IEEE Transactions on Microwave Theory and Techniques*, 60 (9), pp. 2760-2767.

Zheng S.Y., Chan W.S. and Man K.F., 2010. Broadband Phase Shifter Using Loaded Transmission Line. *IEEE Microwave and Wireless Components Letters*, 20 (9), pp. 498-500.

LIST OF PUBLICATIONS

1. **Lo Y.C.**, Chung B.K., 2012. A semi-elliptical wideband phase shifter. *Progress In Electromagnetics Research Letters*, 28, pp.91-99.
2. **Lo Y.C.**, Chung B. K. and Lim E.H., 2017. A semi-elliptical wideband directional coupler. *Progress In Electromagnetics Research C, Progress In Electromagnetics Research,* 79, pp 139-148.
3. **Lo Y.C.**, Chung B.K., and Lim E.H., 2019. Design of wideband phase shifter with edge-coupled semi-elliptical lines. *IET Microwaves, Antennas & Propagation* (under review).

APPENDIX A

The fort-port configuration of parallel coupled TEM transmission lines can be analyzed by connecting matched terminations, Z_0 at ports 2, 3, and 4. The circuit is driven from a 2V source which also has an impedance of Z_0, as shown in Figure A.1.

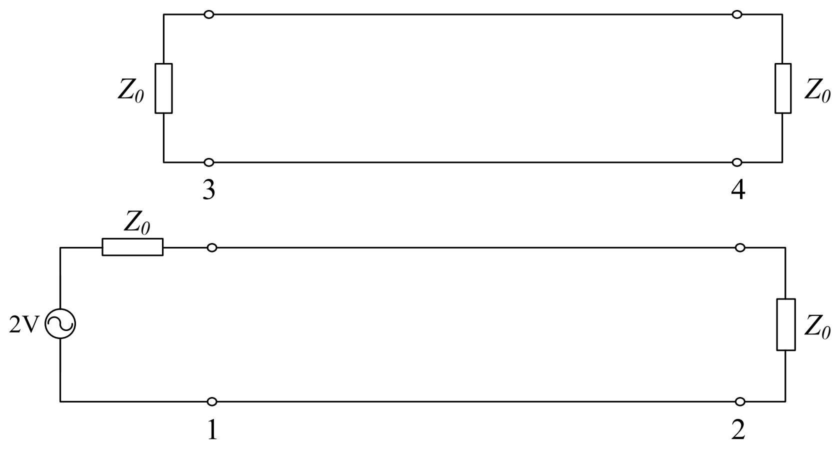

Figure A.1: Terminated parallel-coupled transmission lines.

The analysis is applied to TEM mode, where the even and odd mode characteristic impedances appear and the phase velocities for both modes are the same. For propagation that is not strictly TEM, the basic impedance relationships and the principle frequency dependence of voltage ratios can still be applied quite accurately.

The parallel-coupled transmission lines in Figure A.1 may be analyzed by considering even mode excitation first, followed by odd mode excitation, and finally combining the results. Figure A.2 shows the equivalent circuits for the coupled lines under even and odd mode excitation. The transmission lines are assumed to be lossless so that the propagation constant, γ is reduced to phase constant, $j\beta$ only.

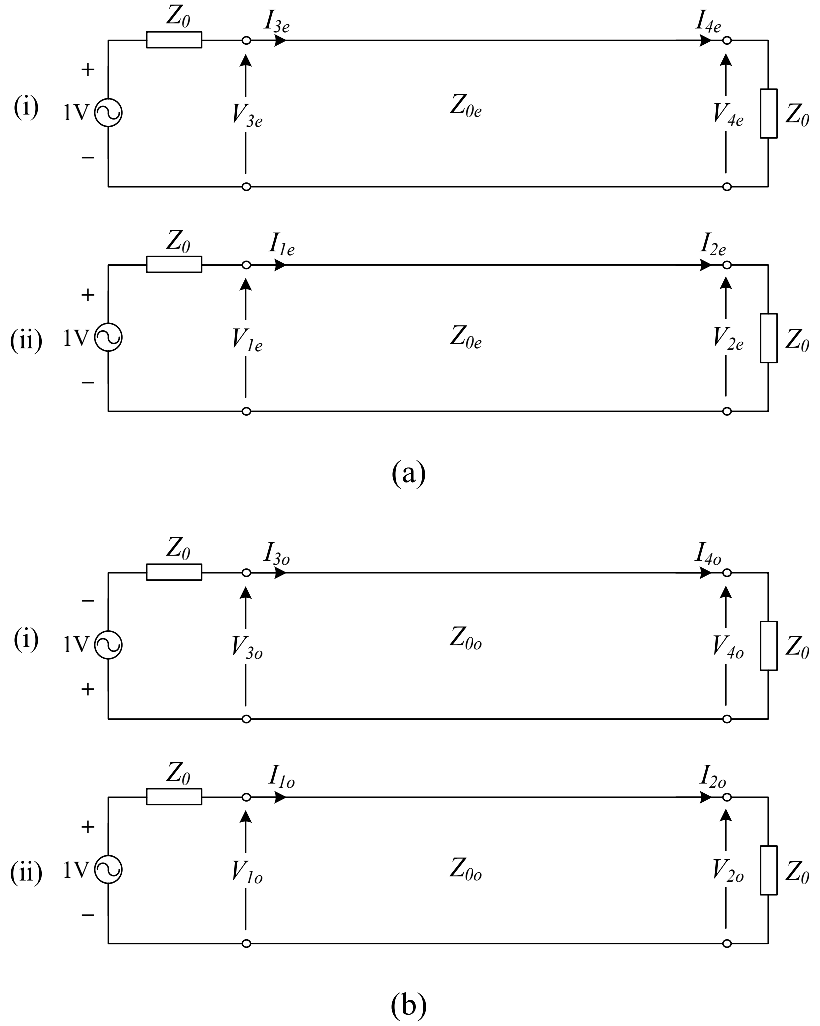

Figure A.2: Equivalent circuits for the parallel-coupled transmission lines. (a) Even mode excitation, and (b) Odd mode excitation.

Only two of the circuits (Figure A.2(a)(ii) and Figure A.2(b)(ii)) need to be solved since the structure is physically symmetrical. For even mode, $I_{1e} = I_{3e}$, $I_{2e} = I_{4e}$, $V_{1e} = V_{3e}$ and $V_{2e} = V_{4e}$, while for odd mode, $I_{1o} = -I_{3o}$, $I_{2o} = -I_{4o}$, $V_{1o} = -V_{3o}$, and $V_{2o} = -V_{4o}$. The total voltages and currents are a superposition of the even and odd mode solutions, which can be given as:

$$V_1 = V_{1e} + V_{1o} \qquad\qquad I_1 = I_{1e} + I_{1o} \qquad\qquad \text{(A.1a)}$$

$$V_2 = V_{2e} + V_{2o} \qquad I_2 = I_{2e} + I_{2o} \tag{A.1b}$$

$$V_3 = V_{3e} + V_{3o} = V_{1e} - V_{1o} \qquad I_3 = I_{3e} + I_{3o} = I_{1e} - I_{1o} \tag{A.1c}$$

$$V_4 = V_{4e} + V_{4o} = V_{2e} - V_{2o} \qquad I_4 = I_{4e} + I_{4o} = I_{2e} - I_{2o} \tag{A.1d}$$

Using the *ABCD* matrix, the voltage and current relationship can be expressed as:

$$\begin{bmatrix} V_{1e} \\ I_{1e} \end{bmatrix} = \begin{bmatrix} \cos\theta & jZ_{0e}\sin\theta \\ jY_{0e}\sin\theta & \cos\theta \end{bmatrix} \begin{bmatrix} V_{2e} \\ I_{2e} \end{bmatrix} \tag{A.2}$$

$$\begin{bmatrix} V_{1o} \\ I_{1o} \end{bmatrix} = \begin{bmatrix} \cos\theta & jZ_{0o}\sin\theta \\ jY_{0o}\sin\theta & \cos\theta \end{bmatrix} \begin{bmatrix} V_{2o} \\ I_{2o} \end{bmatrix} \tag{A.3}$$

Applying the conditions $V_{2e} = Z_0 I_{2e}$, $V_{2o} = Z_0 I_{2o}$, $V_{1e} + I_{1e}Z_0 = 1$, and $V_{1o} + I_{1o}Z_0 = 1$, the following voltage and current expressions are obtained:

$$V_{1e} = \frac{Z_{0e}Z_0\cos\theta + jZ_{0e}^2\sin\theta}{2Z_{0e}Z_0\cos\theta + j\left(Z_{0e}^2 + Z_0^2\right)\sin\theta} \tag{A.4}$$

$$I_{1e} = \frac{Z_{0e}\cos\theta + jZ_0\sin\theta}{2Z_{0e}Z_0\cos\theta + j\left(Z_{0e}^2 + Z_0^2\right)\sin\theta} \tag{A.5}$$

$$V_{2e} = \frac{Z_{0e}Z_0}{2Z_{0e}Z_0\cos\theta + j\left(Z_{0e}^2 + Z_0^2\right)\sin\theta} \tag{A.6}$$

$$I_{2e} = \frac{Z_{0e}}{2Z_{0e}Z_0\cos\theta + j\left(Z_{0e}^2 + Z_0^2\right)\sin\theta} \tag{A.7}$$

$$V_{1o} = \frac{Z_{0o}Z_0\cos\theta + jZ_{0o}^2\sin\theta}{2Z_{0o}Z_0\cos\theta + j\left(Z_{0o}^2 + Z_0^2\right)\sin\theta} \tag{A.8}$$

$$I_{1o} = \frac{Z_{0o}\cos\theta + jZ_0\sin\theta}{2Z_{0o}Z_0\cos\theta + j\left(Z_{0o}^2 + Z_0^2\right)\sin\theta} \tag{A.9}$$

$$V_{2o} = \frac{Z_{0o}Z_0}{2Z_{0o}Z_0\cos\theta + j\left(Z_{0o}^2 + Z_0^2\right)\sin\theta} \tag{A.10}$$

$$I_{2o} = \frac{Z_{0o}}{2Z_{0o}Z_0 \cos\theta + j\left(Z_{0o}^2 + Z_0^2\right)\sin\theta} \quad \text{(A.11)}$$

The input impedance of port 1, Z_{in} can be expressed as:

$$Z_{in} = \frac{V_1}{I_1} = \frac{V_{1e} + V_{1o}}{I_{1e} + I_{1o}} \quad \text{(A.12)}$$

Let

$$D_e = 2Z_{0e}Z_0 \cos\theta + j\left(Z_{0e}^2 + Z_0^2\right)\sin\theta \quad \text{(A.13)}$$

and

$$D_o = 2Z_{0o}Z_0 \cos\theta + j\left(Z_{0o}^2 + Z_0^2\right)\sin\theta \quad \text{(A.14)}$$

Equation (A.12) can be written as:

$$Z_{in} = \frac{Z_0\left(Z_{0o}D_e + Z_{0e}D_o\right)\cos\theta + j\left(Z_{0o}^2 D_e + Z_{0e}^2 D_o\right)\sin\theta}{\left(Z_{0o}D_e + Z_{0e}D_o\right)\cos\theta + jZ_0\left(D_e + D_o\right)\sin\theta} \quad \text{(A.15)}$$

In order for all ports to be matched, Z_{in} = Z_0. The condition will be satisfied if:

$$Z_0^2\left(D_e + D_o\right) = Z_{0o}^2 D_e + Z_{0e}^2 D_o \quad \text{(A.16)}$$

Substituting (A.13) and (A.14) into (A.16),

$$\begin{aligned} &2Z_0^3\left(Z0e + Z0o\right)\cos\theta + j\left(Z_{0e}^2 Z_0^2 + Z_{0o}^2 Z_0^2 + 2Z_0^4\right)\sin\theta \\ &\quad = 2Z_{0e}Z_{0o}Z_0\left(Z_{0e} + Z_{0o}\right)\cos\theta + j\left(Z_{0e}^2 Z_0^2 + Z_{0o}^2 Z_0^2 + 2Z_{0e}^2 Z_{0o}^2\right)\sin\theta \end{aligned} \quad \text{(A.17)}$$

Therefore,

$$Z_0^2 = Z_{0e} + Z_{0o} \quad \text{(A.18)}$$

Substituting (A.18) into (A.4) to (A.11),

$$V_{1e} = \frac{Z_0 \cos\theta + jZ_{0e}\sin\theta}{2Z_0 \cos\theta + j\left(Z_{0e} + Z_{0o}\right)\sin\theta} \quad \text{(A.19)}$$

$$I_{1e} = \frac{\cos\theta + j\left(Z_{0o}/Z_0\right)\sin\theta}{2Z_0\cos\theta + j\left(Z_{0e} + Z_{0o}\right)\sin\theta} \tag{A.20}$$

$$V_{2e} = \frac{Z_0}{2Z_0\cos\theta + j\left(Z_{0e} + Z_{0o}\right)\sin\theta} \tag{A.21}$$

$$I_{2e} = \frac{1}{2Z_0\cos\theta + j\left(Z_{0e} + Z_{0o}\right)\sin\theta} \tag{A.22}$$

$$V_{1o} = \frac{Z_0\cos\theta + jZ_{0o}\sin\theta}{2Z_0\cos\theta + j\left(Z_{0e} + Z_{0o}\right)\sin\theta} \tag{A.23}$$

$$I_{1o} = \frac{\cos\theta + j\left(Z_{0e}/Z_0\right)\sin\theta}{2Z_0\cos\theta + j\left(Z_{0e} + Z_{0o}\right)\sin\theta} \tag{A.24}$$

$$V_{2o} = \frac{Z_0}{2Z_0\cos\theta + j\left(Z_{0e} + Z_{0o}\right)\sin\theta} \tag{A.25}$$

$$I_{2o} = \frac{1}{2Z_0\cos\theta + j\left(Z_{0e} + Z_{0o}\right)\sin\theta} \tag{A.26}$$

The total voltages and currents can be obtained by substituting (A.19) to (A.26) into (A.1):

$$V_1 = \frac{2Z_0\cos\theta + j\left(Z_{0e} + Z_{0o}\right)\sin\theta}{2Z_0\cos\theta + j\left(Z_{0e} + Z_{0o}\right)\sin\theta} = 1 \tag{A.27}$$

$$I_1 = \frac{2\cos\theta + j\left(Z_{0e} + Z_{0o}\right)/Z_0\sin\theta}{2Z_0\cos\theta + j\left(Z_{0e} + Z_{0o}\right)\sin\theta} = \frac{1}{Z_0} \tag{A.28}$$

$$V_2 = \frac{2Z_0}{2Z_0\cos\theta + j\left(Z_{0e} + Z_{0o}\right)\sin\theta} \tag{A.29}$$

$$I_2 = \frac{2}{2Z_0\cos\theta + j\left(Z_{0e} + Z_{0o}\right)\sin\theta} \tag{A.30}$$

$$V_3 = \frac{j\left(Z_{0e} - Z_{0o}\right)\sin\theta}{2Z_0\cos\theta + j\left(Z_{0e} + Z_{0o}\right)\sin\theta} \tag{A.31}$$

$$I_3 = \frac{j\left(Z_{0o} - Z_{0e}\right)/Z_0 \sin\theta}{2Z_0 \cos\theta + j\left(Z_{0e} + Z_{0o}\right)\sin\theta} \quad \text{(A.32)}$$

$$V_4 = \frac{0}{2Z_0 \cos\theta + j\left(Z_{0e} + Z_{0o}\right)\sin\theta} = 0 \quad \text{(A.33)}$$

$$I_4 = \frac{0}{2Z_0 \cos\theta + j\left(Z_{0e} + Z_{0o}\right)\sin\theta} = 0 \quad \text{(A.34)}$$

If the coupling coefficient, C is defined by:

$$C = \frac{Z_{0e} - Z_{0o}}{Z_{0e} + Z_{0o}} \quad \text{(A.35)}$$

Using equation (A.18) and (A.35), the voltages at each port can be re-written as:

$$V_1 = 1 \quad \text{(A.36)}$$

$$V_2 = \frac{\sqrt{1-C^2}}{\sqrt{1-C^2}\cos\theta + j\sin\theta} \quad \text{(A.37)}$$

$$V_3 = \frac{jC\sin\theta}{\sqrt{1-C^2}\cos\theta + j\sin\theta} \quad \text{(A.38)}$$

$$V_4 = 0 \quad \text{(A.39)}$$

For $\theta = \pi/2$, the length of the coupled structure is $\lambda/4$ long. Equation (A.37) and (A.38) can be reduced to

$$V_2 = -j\sqrt{1-C^2} \quad \text{(A.40)}$$

$$V_3 = C \quad \text{(A.41)}$$

APPENDIX B

The input impedance and the two-port Z-parameter of the open-circuited coupled line is given by D. M. Pozar (2011):

$$Z_i = \frac{\sqrt{\left(Z_{0e} - Z_{0o}\right)^2 - \left(Z_{0e} + Z_{0o}\right)^2 \cos^2\theta}}{2\sin\theta} \tag{B.1}$$

$$\begin{bmatrix} Z_{11} & Z_{21} \\ Z_{21} & Z_{22} \end{bmatrix} = \frac{-j}{2}\begin{bmatrix} (Z_{0e} + Z_{0o})\cot\beta l & (Z_{0e} - Z_{0o})\csc\beta l \\ (Z_{0e} - Z_{0o})\csc\beta l & (Z_{0e} + Z_{0o})\cot\beta l \end{bmatrix} \tag{B.2}$$

From (B.2),

$$Z_{11} = -\frac{j}{2}\left(Z_{0e} + Z_{0o}\right)\cot\theta \tag{B.3}$$

$$Z_{21} = -\frac{j}{2}\left(Z_{0e} - Z_{0o}\right)\frac{1}{\sin\theta} \tag{B.4}$$

The Z-parameters can be converted to S-parameters using the conversion formulas:

$$S_{11} = \frac{\left(Z_{11} - Z_0\right)\left(Z_{22} + Z_0\right) - Z_{12}Z_{21}}{\left(Z_{11} + Z_0\right)\left(Z_{22} + Z_0\right) - Z_{12}Z_{21}} \tag{B.5}$$

$$S_{21} = \frac{2Z_{21}Z_0}{\left(Z_{11} + Z_0\right)\left(Z_{22} + Z_0\right) - Z_{12}Z_{21}} \tag{B.6}$$

For the proposed structure, $Z_{11} = Z_{22}$ and $Z_{12} = Z_{21}$. Therefore, the reflection coefficient, S_{11} is given by:

$$S_{11} = \frac{\left(Z_{11}^2 - Z_0^2\right) - Z_{21}^2}{\left(Z_{11} + Z_0\right)^2 - Z_{21}^2}$$

$$=\frac{-\frac{\left(Z_{0e}+Z_{0o}\right)^2\cos^2\theta}{4\sin^2\theta}-\frac{\left(Z_{0e}-Z_{0o}\right)^2}{4}+\frac{\left(Z_{0e}-Z_{0o}\right)^2}{4\sin^2\theta}}{-\frac{\left(Z_{0e}+Z_{0o}\right)^2\cos^2\theta}{4\sin^2\theta}+\frac{\left(Z_{0e}-Z_{0o}\right)^2}{4}+\frac{\left(Z_{0e}-Z_{0o}\right)^2}{4\sin^2\theta}-j\frac{\left(Z_{0e}-Z_{0o}\right)\left(Z_{0e}+Z_{0o}\right)}{2}\frac{\cos\theta}{\sin\theta}}$$

$$=\frac{-\cos^2\theta-C^2\sin^2\theta+C^2}{C^2\sin^2\theta-\cos^2\theta+C^2-j2C\cos\theta\sin\theta}$$

$$=\frac{\left(1-C^2\right)\cos^2\theta}{\cos^2\theta-\left(1+\sin^2\theta\right)C^2+j2C\cos\theta\sin\theta} \tag{B.7}$$

From (B.6), the transmission coefficient, S_{21} can be expressed as:

$$S_{21}=\frac{2Z_{21}Z_0}{\left(Z_{11}+Z_0\right)\left(Z_{11}+Z_0\right)-Z_{21}^2}$$

$$=\frac{-j\frac{Z_0\left(Z_{0e}-Z_{0o}\right)}{\sin\theta}}{Z_0^2-j\frac{Z_0\left(Z_{0e}+Z_{0o}\right)\cos\theta}{\sin\theta}-\frac{\left(Z_{0e}+Z_{0o}\right)^2\cos^2\theta}{4\sin^2\theta}+\frac{\left(Z_{0e}-Z_{0o}\right)^2}{4\sin^2\theta}}$$

$$=\frac{-j\frac{\left(Z_{0e}-Z_{0o}\right)^2}{2\sin\theta}}{\frac{\left(Z_{0e}-Z_{0o}\right)^2}{4}-\frac{\left(Z_{0e}+Z_{0o}\right)^2\cos^2\theta}{4\sin^2\theta}+\frac{\left(Z_{0e}-Z_{0o}\right)^2}{4\sin^2\theta}-j\frac{\left(Z_{0e}-Z_{0o}\right)\left(Z_{0e}+Z_{0o}\right)\cos\theta}{2\sin\theta}}$$

$$=\frac{-j2C^2\sin\theta}{C^2\sin^2\theta-\cos^2\theta+C^2-j2C\cos\theta\sin\theta}$$

$$=\frac{j2C^2\sin\theta}{\cos^2\theta-\left(1+\sin^2\theta\right)C^2+j2C\cos\theta\sin\theta} \tag{B.8}$$

Base on Equation (B.8), the phase shift, $\angle S_{21}=\Phi$ is given by:

$$\Phi=90^o-\tan^{-1}\left(\frac{2C\cos\theta\sin\theta}{\cos^2\theta-\left(1+\sin^2\theta\right)C^2}\right) \tag{B.9}$$